NASA-CR-200529

THE OHIO STATE UNIVERSITY

Material Measurements Using Groundplane Apertures

K. Komisarek, A. Dominek and N. Wang

The Ohio State University

ElectroScience Laboratory

Department of Electrical Engineering
Columbus, Ohio 43212

Technical Report 731507-1
Grant No. NAG3-1785
October 1995

National Aeronautics and Space Administration
Lewis Research Center
21000 Brookpark Rd.
Cleveland, OH 44135

NOTICES

When Government drawings, specifications, or other data are used for any purpose other than in connection with a definitely related Government procurement operation, the United States Government thereby incurs no responsibility nor any obligation whatsoever, and the fact that the Government may have formulated, furnished, or in any way supplied the said drawings, specifications, or other data, is not to be regarded by implication or otherwise as in any manner licensing the holder or any other person or corporation, or conveying any rights or permission to manufacture, use, or sell any patented invention that may in any way be related thereto.

50272-101

REPORT DOCUMENTATION PAGE	1. REPORT NO.	2.	3. Recipient's Accession No.

4. Title and Subtitle

Material Measurements Using Groundplane Apertures

5. Report Date

October 1995

6.

7. Author(s)

K. Komisarek, A. Dominek and N. Wang

8. Performing Org. Rept. No.

731507-1

9. Performing Organization Name and Address

The Ohio State University
ElectroScience Laboratory
1320 Kinnear Road
Columbus, OH 43212

10. Project/Task/Work Unit No.

11. Contract(C) or Grant(G) No.

(C)

(G) NAG3-1785

12. Sponsoring Organization Name and Address

NASA Lewis Research Center
21000 Brookpark Rd.
Cleveland, OH 44135

13. Report Type/Period Covered

Technical Report

14.

15. Supplementary Notes

16. Abstract (Limit: 200 words)

A technique for material parameter determination using an aperture in a groundplane is studied. The material parameters are found by relating the measured reflected field in the aperture to a numerical model. Two apertures are studied which can have a variety of different material configurations covering the aperture. The aperture cross-sections studied are rectangular and coaxial. The material configurations involved combinations of single layer and dual layers with or without a resistive exterior resistive sheet. The resistivity of the resistive sheet can be specified to simulate a PEC backing ($0\Omega/\square$) to a free space backing ($\infty\Omega/\square$). Numerical parameter studies and measurements were performed to assess the feasibility of the technique.

17. Document Analysis a. Descriptors

MATERIALS
MEASUREMENT
MICROWAVE

b. Identifiers/Open-Ended Terms

c. COSATI Field/Group

18. Availability Statement	19. Security Class (This Report) Unclassified	21. No. of Pages 92
	20. Security Class (This Page) Unclassified	22. Price

(See ANSI-Z39.18) *See Instructions on Reverse* OPTIONAL FORM 272 (4-77)
Department of Commerce

Contents

List of Figures

List of Tables

Chapter 1

Introduction

The electromagnetic behavior of an ordinary isotropic, linear, homogeneous material is completely specified by the complex constitutive parameters, or the permittivity and the permeability, of the material. The permittivity and the permeability of the material are denoted as ϵ and μ. If these constitutive material parameters are unknown, they must be determined before any electromagnetic problem involving the material can be solved.

The literature is rich with a variety of techniques to determine these constitutive parameters [1, 2]. Of these techniques, one appears to be very practical to determine the permittivity of a non-magnetic material which would naturally be in a slab form. This technique relates the reflection coefficient of an aperture in a material coated groundplane. This technique is not new and was first used by [4, 5] and by any other in recent times [6, 7, 8].

Unlike the closed form parameter determination using reflection and transmission waveguide measurements [9], a numerical search has to be performed between measured and calculated values for this aperture technique. A Newton-Raphson iteration scheme is often used using the complex reflection coefficient if the material is lossy. For cases when the material is lossless, the magnitude or the phase of the reflection coefficient is sufficient to make a parameter determination.

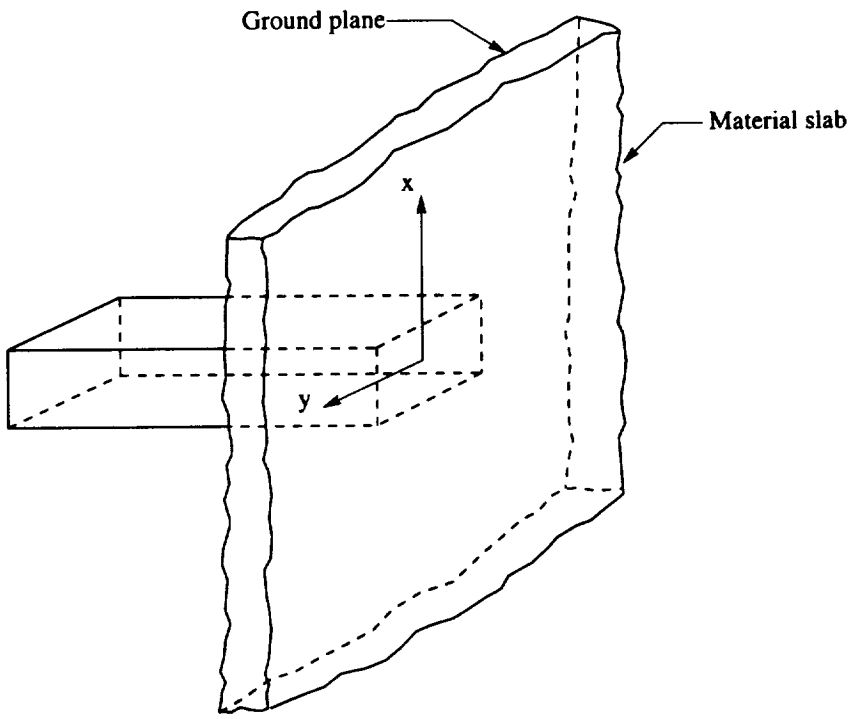

Figure 1.1: Rectangular aperture

The parameter determination using an aperture technique as several advantages over other techniques. This technique is convenient for planar samples since minimal sample preparation is required and is non-destructive. Errors resulting from poor sample shape (waveguide air gaps) are eliminated Additionally, the phase reference plane is exactly determined by the groundplane surface unlike in waveguide measurements where the possibility of some shift always exists. Phase reference stability is very important in the determination of large permittivity values.

The work in this report expands the technique to include additional reflection coefficient expressions for different material configurations and apertures. The apertures of intersect are the rectangular and coaxial apertures as shown in Figures 1.1 and 1.2. The coaxial aperture is of interest due to the potential of broader bandwidth measurements, especially at lower frequencies. It should be noted that a commercial

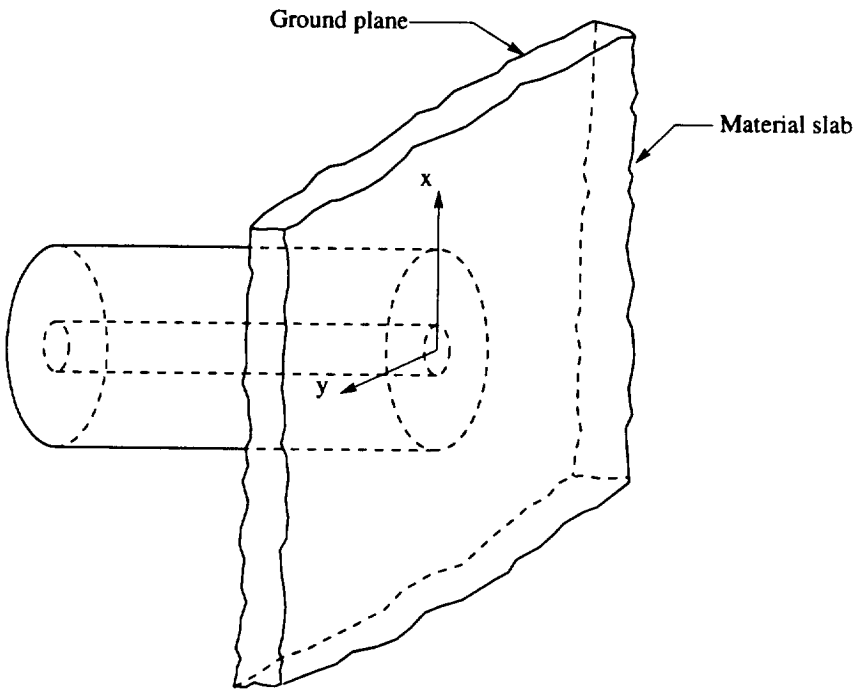

Figure 1.2: Coaxial aperture

coaxial probe is available but the software often used with it does not account for sample thickness [10].

The material configurations presented and studied in this report are shown in Figures 1.3 and 1.4. This material configurations allows for the study of material-groundplane air gaps, PEC (perfect electric conductor) backed samples, sheet resistivity determination and the equivalence of sheet resistivity modeling with lossy material layers of finite thickness.

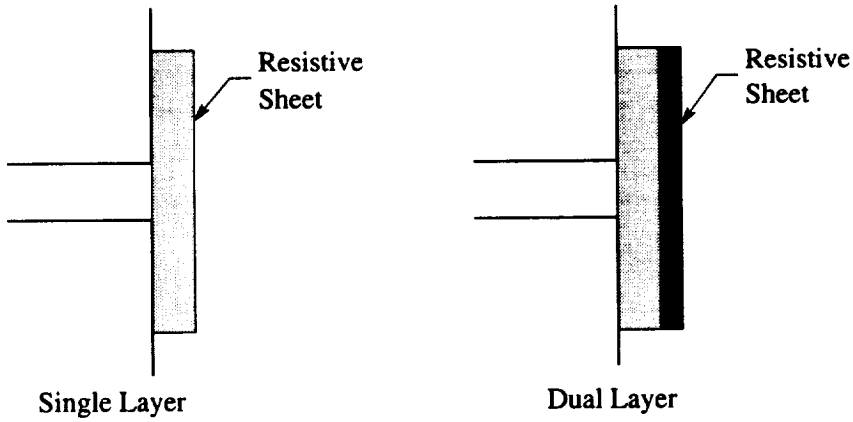

Figure 1.3: Rectangular aperture

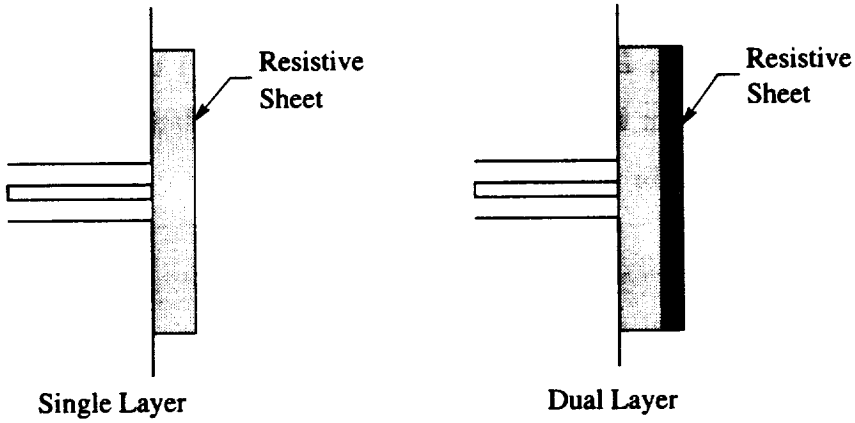

Figure 1.4: Coaxial aperture

Chapter 2

Numerical Model

The numerical model upon which the permittivity de-embedding procedure is based is developed in this chapter. The functionals in the de-embedding procedure are based on the reflection coefficient of the rectangular or coaxial aperture, covered by a dielectric slab/resistive or PEC sheet configuration. The reflection coefficient is computed from the aperture admittance. The derivation of the aperture admittance for both aperture shapes is based upon the rectangular aperture work of Rudduck [12]. In each of the two sections to follow, the basic derivation of the rectangular or coaxial aperture admittance is presented, followed by the specifics for the various dielectric slab/resistive or PEC sheet configurations under investigation.

2.1 Rectangular Aperture

The admittance of a rectangular aperture is developed here. The analysis involves representing the fields external to the aperture in terms of the Fourier integral of their plane wave spectra. The aperture admittance is obtained by using a variational assumption for the aperture total field distribution and matching the boundary conditions for the various dielectric slab/resistive or PEC sheet configurations under study.

The analysis starts with the representation of the electric vector potential $\mathbf{F}$ in terms of the rectangular electric scalar potentials ϕ and ψ:

$$\mathbf{F}_{0,1,2} = \phi_{0,1,2}\hat{\mathbf{x}} + \psi_{0,1,2}\hat{\mathbf{y}}. \tag{2.1}$$

Referring to Figure 2.1, it can be seen that the potentials are functions of x, y, and z, defined only for $z \geq 0$. The subscript 1 refers to Region 1, the dielectric slab in contact with the groundplane. The subscript 2 refers to Region 2, a second dielectric slab which may be on the first dielectric slab. The free space region above the dielectric slab(s) is denoted as Region 0 and all quantities associated with that region possess the subscript 0. The scalar potentials are solutions to the scalar wave equation

$$(\nabla^2 + k_{0,1,2}^2)\left\{ \begin{array}{c} \psi_{0,1,2} \\ \phi_{0,1,2} \end{array} \right\}, \tag{2.2}$$

where the wavenumbers $k_{0,1,2}$ are given by

$$k_0^2 = \omega^2 \mu_0 \epsilon_0, \tag{2.3}$$

for Region 0, and

$$k_{1,2}^2 = \omega^2 \mu_0 \epsilon_{1,2} = k_0^2 \epsilon_{r_{1,2}}, \tag{2.4}$$

for Regions 1 and 2. In general the relative permittivities $\epsilon_{r_{1,2}}$ are complex, representing possible losses in the slabs.

The scalar potentials can be expressed in terms of their plane-wave spectra. In Regions 1 and 2, the total spectra are comprised of the incident and reflected spectra, respectively denoted by I and R. In Region 0, the total spectra are each comprised of one transmitted spectrum, denoted by T. Thus the plane wave spectral representation of the scalar potentials in Region 1 are given by

$$\begin{aligned} \psi_1(x,y,z) \;=\; & \frac{1}{(2\pi)^2} \int_{-\infty}^{\infty} \int_{-\infty}^{\infty} \left[I_{\psi_1}(k_x,k_y) e^{-jk_{z_1}z} + R_{\psi_1}(k_x,k_y) e^{+jk_{z_1}z} \right] \\ & e^{-jk_x x} e^{-jk_y y} dk_x dk_y \end{aligned} \tag{2.5}$$

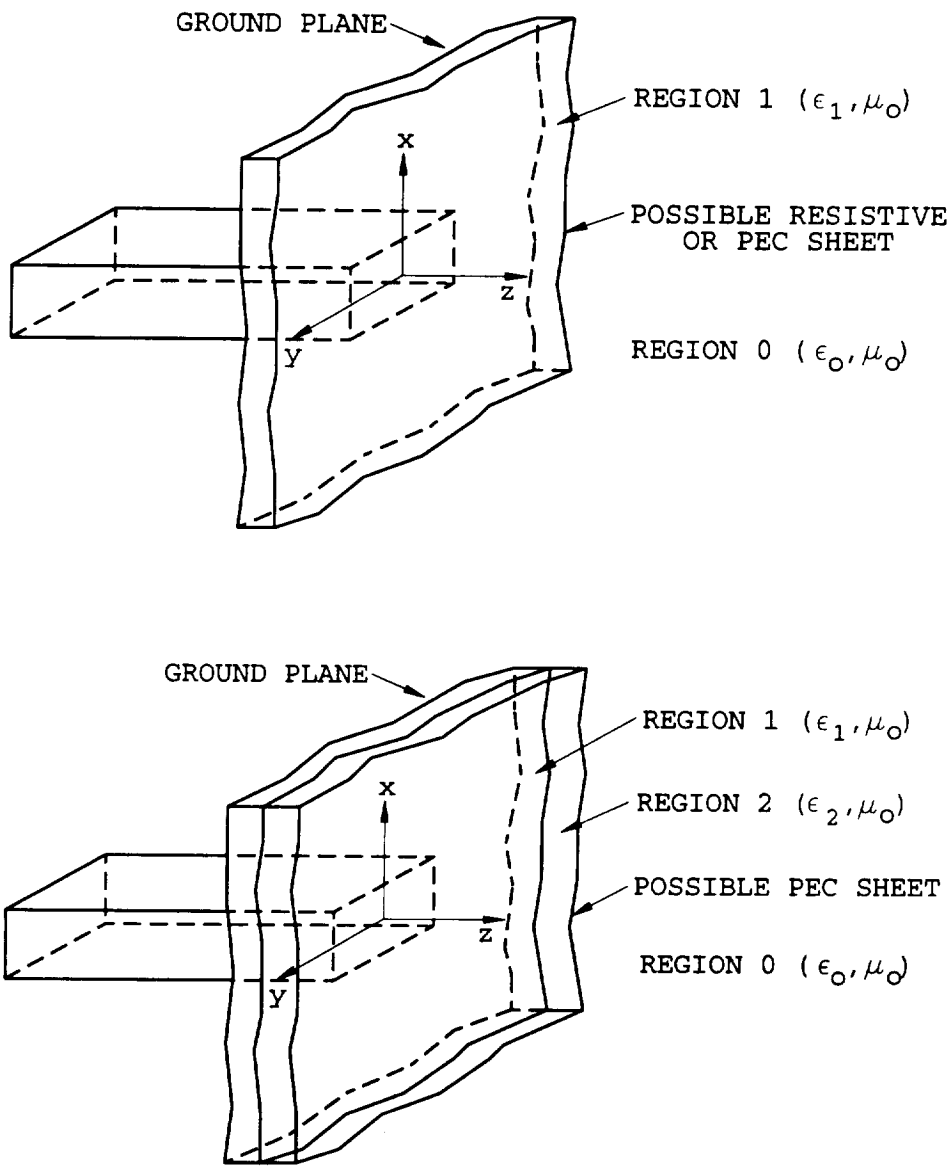

Figure 2.1: Dielectric slab/resistive sheet configurations on rectangular aperture groundplane.

and

$$\phi_1(x,y,z) = \frac{1}{(2\pi)^2}\int_{-\infty}^{\infty}\int_{-\infty}^{\infty}\left[I_{\phi_1}(k_x,k_y)e^{-jk_{z_1}z} + R_{\phi_1}(k_x,k_y)e^{+jk_{z_1}z}\right] e^{-jk_xx}e^{-jk_yy}dk_xdk_y; \tag{2.6}$$

in Region 2 by

$$\psi_2(x,y,z) = \frac{1}{(2\pi)^2}\int_{-\infty}^{\infty}\int_{-\infty}^{\infty}\left[I_{\psi_2}(k_x,k_y)e^{-jk_{z_2}z} + R_{\psi_2}(k_x,k_y)e^{+jk_{z_2}z}\right] e^{-jk_xx}e^{-jk_yy}dk_xdk_y \tag{2.7}$$

and

$$\phi_2(x,y,z) = \frac{1}{(2\pi)^2}\int_{-\infty}^{\infty}\int_{-\infty}^{\infty}\left[I_{\phi_2}(k_x,k_y)e^{-jk_{z_2}z} + R_{\phi_2}(k_x,k_y)e^{+jk_{z_2}z}\right] e^{-jk_xx}e^{-jk_yy}dk_xdk_y; \tag{2.8}$$

and in Region 0 by

$$\psi_0(x,y,z) = \frac{1}{(2\pi)^2}\int_{-\infty}^{\infty}\int_{-\infty}^{\infty}T_{\psi_0}(k_x,k_y)e^{-jk_{z_0}z}e^{-jk_xx}e^{-jk_yy}dk_xdk_y \tag{2.9}$$

and

$$\phi_0(x,y,z) = \frac{1}{(2\pi)^2}\int_{-\infty}^{\infty}\int_{-\infty}^{\infty}T_{\phi_0}(k_x,k_y)e^{-jk_{z_0}z}e^{-jk_xx}e^{-jk_yy}dk_xdk_y. \tag{2.10}$$

The propagation constants are given by

$$k_{z_{0,1,2}} = \pm\sqrt{k_{0,1,2}^2 - k_x^2 - k_y^2}, \tag{2.11}$$

where the sign is chosen so that the radiation condition is satisfied. Thus the sign for each propagation constant is chosen so that

$$\Re(k_{z_{0,1,2}}) \geq 0 \tag{2.12}$$

and

$$\Im(k_{z_{0,1,2}}) \leq 0. \tag{2.13}$$

From vector potential theory, the electric and magnetic fields are related to the electric vector potential by

$$\mathbf{E} = -\nabla \times \mathbf{F} \tag{2.14}$$

and

$$\mathbf{H} = \frac{1}{j\omega\mu_0}\left[k_{0,1,2}^2\mathbf{F} + \nabla(\nabla \cdot \mathbf{F})\right]. \tag{2.15}$$

Therefore the rectangular components of the electric and magnetic fields in Region 1 are given by

$$\begin{aligned} E_{x_1}(x,y,z) &= \frac{1}{(2\pi)^2}\int_{-\infty}^{\infty}\int_{-\infty}^{\infty}\left[-jk_{z_1}I_{\psi_1}e^{-jk_{z_1}z} + jk_{z_1}R_{\psi_1}e^{jk_{z_1}z}\right] \\ &\quad e^{-jk_x x}e^{-jk_y y}dk_x dk_y, \end{aligned} \tag{2.16}$$

$$\begin{aligned} E_{y_1}(x,y,z) &= \frac{1}{(2\pi)^2}\int_{-\infty}^{\infty}\int_{-\infty}^{\infty}\left[jk_{z_1}I_{\phi_1}e^{-jk_{z_1}z} - jk_{z_1}R_{\phi_1}e^{jk_{z_1}z}\right] \\ &\quad e^{-jk_x x}e^{-jk_y y}dk_x dk_y, \end{aligned} \tag{2.17}$$

$$\begin{aligned} H_{x_1}(x,y,z) &= \frac{1}{(2\pi)^2}\int_{-\infty}^{\infty}\int_{-\infty}^{\infty}\left\{\frac{k_1^2 - k_x^2}{j\omega\mu_0}\left[I_{\phi_1}e^{-jk_{z_1}z} + R_{\phi_1}e^{jk_{z_1}z}\right] - \right. \\ &\quad \left.\frac{k_x k_y}{j\omega\mu_0}\left[I_{\psi_1}e^{-jk_{z_1}z} + R_{\psi_1}e^{jk_{z_1}z}\right]\right\}e^{-jk_x x}e^{-jk_y y}dk_x dk_y, \end{aligned} \tag{2.18}$$

and

$$\begin{aligned} H_{y_1}(x,y,z) &= \frac{1}{(2\pi)^2}\int_{-\infty}^{\infty}\int_{-\infty}^{\infty}\left\{\frac{k_1^2 - k_y^2}{j\omega\mu_0}\left[I_{\psi_1}e^{-jk_{z_1}z} + R_{\psi_1}e^{jk_{z_1}z}\right] - \right. \\ &\quad \left.\frac{k_x k_y}{j\omega\mu_0}\left[I_{\phi_1}e^{-jk_{z_1}z} + R_{\phi_1}e^{jk_{z_1}z}\right]\right\}e^{-jk_x x}e^{-jk_y y}dk_x dk_y; \end{aligned} \tag{2.19}$$

in Region 2 by

$$\begin{aligned} E_{x_2}(x,y,z) &= \frac{1}{(2\pi)^2}\int_{-\infty}^{\infty}\int_{-\infty}^{\infty}\left[-jk_{z_2}I_{\psi_2}e^{-jk_{z_2}z} + jk_{z_2}R_{\psi_2}e^{jk_{z_2}z}\right] \\ &\quad e^{-jk_x x}e^{-jk_y y}dk_x dk_y, \end{aligned} \tag{2.20}$$

$$\begin{aligned} E_{y_2}(x,y,z) &= \frac{1}{(2\pi)^2}\int_{-\infty}^{\infty}\int_{-\infty}^{\infty}\left[jk_{z_2}I_{\phi_2}e^{-jk_{z_2}z} - jk_{z_2}R_{\phi_2}e^{jk_{z_2}z}\right] \\ &\quad e^{-jk_x x}e^{-jk_y y}dk_x dk_y, \end{aligned} \tag{2.21}$$

$$H_{x_2}(x,y,z) = \frac{1}{(2\pi)^2}\int_{-\infty}^{\infty}\int_{-\infty}^{\infty}\left\{\frac{k_2^2-k_x^2}{j\omega\mu_0}\left[I_{\phi_2}e^{-jk_{z_2}z}+R_{\phi_2}e^{jk_{z_2}z}\right]-\frac{k_xk_y}{j\omega\mu_0}\left[I_{\psi_2}e^{-jk_{z_2}z}+R_{\psi_2}e^{jk_{z_2}z}\right]\right\}e^{-jk_xx}e^{-jk_yy}dk_xdk_y, \quad (2.22)$$

and

$$H_{y_2}(x,y,z) = \frac{1}{(2\pi)^2}\int_{-\infty}^{\infty}\int_{-\infty}^{\infty}\left\{\frac{k_2^2-k_y^2}{j\omega\mu_0}\left[I_{\psi_2}e^{-jk_{z_2}z}+R_{\psi_2}e^{jk_{z_2}z}\right]-\frac{k_xk_y}{j\omega\mu_0}\left[I_{\phi_2}e^{-jk_{z_2}z}+R_{\phi_2}e^{jk_{z_2}z}\right]\right\}e^{-jk_xx}e^{-jk_yy}dk_xdk_y; \quad (2.23)$$

and in Region 0 by

$$E_{x_0}(x,y,z) = \frac{1}{(2\pi)^2}\int_{-\infty}^{\infty}\int_{-\infty}^{\infty}-jk_{z_0}T_{\psi_0}e^{-jk_{z_0}z}e^{-jk_xx}e^{-jk_yy}dk_xdk_y, \quad (2.24)$$

$$E_{y_0}(x,y,z) = \frac{1}{(2\pi)^2}\int_{-\infty}^{\infty}\int_{-\infty}^{\infty}jk_{z_0}T_{\phi_0}e^{-jk_{z_0}z}e^{-jk_xx}e^{-jk_yy}dk_xdk_y, \quad (2.25)$$

$$H_{x_0}(x,y,z) = \frac{1}{(2\pi)^2}\int_{-\infty}^{\infty}\int_{-\infty}^{\infty}\left[\frac{k_0^2-k_x^2}{j\omega\mu_0}T_{\phi_0}-\frac{k_xk_y}{j\omega\mu_0}T_{\psi_0}\right]e^{-jk_{z_0}z}e^{-jk_xx}e^{-jk_yy}dk_xdk_y, \quad (2.26)$$

and

$$H_{y_0}(x,y,z) = \frac{1}{(2\pi)^2}\int_{-\infty}^{\infty}\int_{-\infty}^{\infty}\left[\frac{k_0^2-k_y^2}{j\omega\mu_0}T_{\psi_0}-\frac{k_xk_y}{j\omega\mu_0}T_{\phi_0}\right]e^{-jk_{z_0}z}e^{-jk_xx}e^{-jk_yy}dk_xdk_y. \quad (2.27)$$

Note that in the above the k_x, k_y functional dependence is dropped from the spectra and are understood.

The solution to the fields can be obtained by satisfying the boundary conditions at the groundplane/dielectric slab interface and other interfaces present in the dielectric slab/resistive sheet configurations if the total fields in the aperture are known. However, the total fields in the aperture are not known, since they consist of an infinite sum of waveguide modes with unknown coefficients. In order to find the coefficients, a Moment Method solution can be set up in a manner similar to

that which has been performed for the coaxial aperture case [11]. For the purposes of this investigation a simple variational solution will be used [3]. The variational solution consists of the assumption of a form for the aperture electric field whereby first-order deviations of the assumed field from the exact field will be manifested as second-order errors in the admittance. The electric field is assumed to be of the form of the dominant TE_{10} mode. This aperture field assumption works well in the case where the waveguide dimensions are such that all higher-order modes are evanescent [12]. In such a case any deviations of calculated admittance values from measurements are attributed to the exclusion of higher-order modes.

Thus the total electric field in the plane $z = 0$ is assumed to be

$$\mathbf{E}(x,y,0) = \mathbf{e}_0 = \begin{cases} \sqrt{\frac{2}{ab}} \cos\frac{\pi y}{b}\hat{\mathbf{x}} & , \quad \text{in the aperture} \\ \mathbf{0} & , \quad \text{outside the aperture} \end{cases}, \tag{2.28}$$

where the factor $\sqrt{\frac{2}{ab}}$ normalizes the electric field so that

$$\int_{-\infty}^{\infty}\int_{-\infty}^{\infty} \mathbf{E}(x,y,0)\cdot\mathbf{E}(x,y,0)dxdy = 1. \tag{2.29}$$

Referring back to Figure 2.1, it can be seen that b is the length of the longer edge of the waveguide, and a is the length of the shorter waveguide edge.

The rectangular waveguide aperture admittance, Y_a, is given by

$$\begin{aligned} Y_a &= \frac{\int_{-\infty}^{\infty}\int_{-\infty}^{\infty} \mathbf{E}(x,y,0)\times\mathbf{H}(x,y,0)dxdy}{\left|\int_{-\infty}^{\infty}\int_{-\infty}^{\infty} \mathbf{E}(x,y,0)\cdot\mathbf{e}_0 dxdy\right|^2} \\ &= \int_{-\infty}^{\infty}\int_{-\infty}^{\infty} E_{x_1}(x,y,0)H_{y_1}(x,y,0)dxdy. \end{aligned} \tag{2.30}$$

Evaluation of (2.30) is accomplished through the use of Parseval's Theorem in two dimensions in a rectangular coordinate system:

$$\int_{-\infty}^{\infty}\int_{-\infty}^{\infty} E_{x_1}H_{y_1}\,dxdy = \frac{1}{(2\pi)^2}\int_{-\infty}^{\infty}\int_{-\infty}^{\infty} \mathcal{E}_{x_1}\mathcal{H}_{y_1}\,dk_x dk_y, \tag{2.31}$$

where $\mathcal{E}_{x_1}$ and $\mathcal{H}_{y_1}$ are the Fourier transforms of E_{x_1} and H_{y_1}, at $z = 0$. These transforms can be found from (2.16) and (2.19) and are given by

$$\mathcal{E}_{x_1}(k_x,k_y) = jk_{z_1}\left[-I_{\psi_1} + R_{\psi_1}\right] \tag{2.32}$$

and

$$\mathcal{H}_{y_1}(k_x,k_y)=\frac{1}{j\omega\mu_0}\left[(k_1^2-k_y^2)(I_{\psi_1}+R_{\psi_1})-k_xk_y(I_{\phi_1}+R_{\phi_1})\right]. \tag{2.33}$$

Thus the aperture admittance can be written as

$$\begin{aligned}Y_a &= \frac{1}{(2\pi)^2}\int_{-\infty}^{\infty}\int_{-\infty}^{\infty}\{jk_{z_1}[-I_{\psi_1}+R_{\psi_1}]\}\\ &\quad\left\{\frac{1}{j\omega\mu_0}\left[(k_1^2-k_y^2)(I_{\psi_1}+R_{\psi_1})-k_xk_y(I_{\phi_1}+R_{\phi_1})\right]\right\}dk_xdk_y.\end{aligned} \tag{2.34}$$

The unknown quantities in (2.34) are the incident and reflected spectra of Region 1. The boundary condition of continuous tangential electric field at $z=0$ for each pair of spectral values (k_x,k_y) gives the relationships between the Region 1 incident and reflected spectra as

$$-jk_{z_1}\left[I_{\psi_1}-R_{\psi_1}\right]=4\pi\sqrt{\frac{2b}{a}}\frac{\sin\left(\frac{k_xa}{2}\right)\cos\left(\frac{k_yb}{2}\right)}{k_x(\pi^2-k_y^2b^2)}=f \tag{2.35}$$

and

$$jk_{z_1}\left[I_{\phi_1}-R_{\phi_1}\right]=0, \tag{2.36}$$

where the Fourier transform of the aperture electric field is denoted by f for the sake of brevity. The substitution of (2.35) and (2.36) into (2.34) yields

$$Y_a=\frac{1}{(2\pi)^2}\int_{-\infty}^{\infty}\int_{-\infty}^{\infty}\left\{\frac{1}{j\omega\mu_0}\left[(k_1^2-k_y^2)(2I_{\psi_1}-\frac{jf}{k_{z_1}})-2k_xk_yI_{\phi_1}\right]\right\}fdk_xdk_y. \tag{2.37}$$

In order to make the numerical evaluation of the admittance more convenient, the following change of variables is made:

$$k_x=k_0\beta\cos\alpha \tag{2.38}$$

and

$$k_y=k_0\beta\sin\alpha. \tag{2.39}$$

Therefore the aperture admittance can be written as

$$\begin{aligned}Y_a &= \frac{-Y_0}{(2\pi)^2}\int_0^{\infty}\int_0^{2\pi}\left[\left(\epsilon_{r_1}-\beta^2\sin^2\alpha\right)\left(2k_0^2I_{\psi_1}-\frac{jfk_0}{\sqrt{\epsilon_{r_1}-\beta^2}}\right)\right.\\ &\quad\left.-2\beta^2\sin\alpha\cos\alpha k_0^2I_{\phi_1}\right]jfk_0\beta d\alpha d\beta,\end{aligned} \tag{2.40}$$

where Y_0 is the admittance of free space. In order to use the aperture admittance in the calculation of the reflection coefficient, it must first be normalized with respect to the TE_{10} mode waveguide admittance:

$$Y_n = \frac{Y_a}{Y_g} = \frac{Y_a}{Y_0\sqrt{1-\left(\frac{\lambda_g}{2b}\right)^2}}, \tag{2.41}$$

where λ_g is the wavelength in the waveguide. Thus, the reflection coefficient of the rectangular waveguide aperture is given by

$$\Gamma = \frac{1-Y_n}{1+Y_n}. \tag{2.42}$$

A few items about the integration in (2.40) must be stated. The β integration is performed along the path in the complex β plane shown in Figure 2.2. The

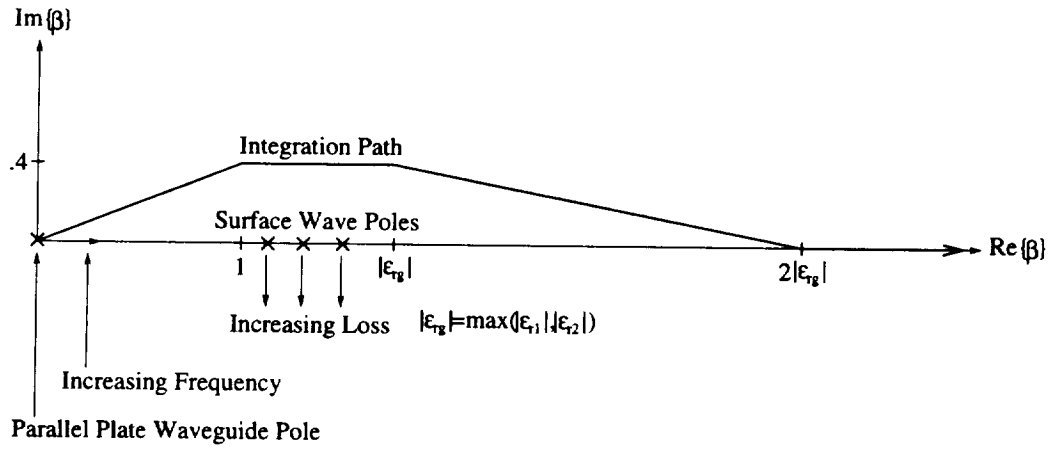

Figure 2.2: Integration path in the complex β plane, with surface wave poles and parallel plate waveguide pole (PEC sheet backed cases only).

integration path is deformed from the real axis so as to avoid surface wave poles. Surface wave poles can occur on the real axis when there is at least one lossless dielectric layer in any of the five configurations of Figure 2.1. These poles occur in the interval $1 \leq \beta \leq \epsilon_r$, where ϵ_r is the greater of the two real relative permittivities, or is the only real relative permittivity. Loss in the dielectric layer(s) causes the layer(s) surface wave poles to move below the real axis. The integration path starts at $\beta = 0$, goes to $1.0 + j0.4$, then to $|\epsilon_{rg}| + j0.4$, $2|\epsilon_{rg}|$, and then $\infty + j0$. This integration

path was determined experimentally and found to work well. The integration path crosses no poles during its deformation from the real axis, so no residues need to be computed and included in the integral.

If there is a PEC sheet present, an additional complication occurs when the frequency is high enough to excite one or more parallel plate waveguide modes. A mode manifests itself as a pole in the complex β plane by appearing at $\beta = 0$ at the cutoff frequency, and then moves along the positive real axis as the frequency increases. No provision has been included in the codes for this contingency, since the codes are to be used only at frequencies where there are no propagating parallel plate waveguide modes.

However, the solution for the reflection coefficient is by no means complete. The aperture admittance is still dependent on the unknown incident spectra I_{ψ_1} and I_{ϕ_1}, which are dependent on the boundary conditions given by the particular dielectric slab/resistive or PEC sheet configuration in contact with the aperture ground plane. The following subsections give the derivation of I_{ψ_1} and I_{ϕ_1} for the five configurations under investigation.

2.1.1 Two Dielectric Layers - Free Space Backed

Figure 2.3 shows two dielectric layers, free space backed, on a rectangular aperture groundplane. The width of the first layer is d_1, and the width of the second layer is $d_2 - d_1$. The incident spectra I_{ψ_1} and I_{ϕ_1} are determined by the enforcement of the boundary conditions at the three interfaces at $z = 0$, d_1, and d_2. The boundary condition enforcement occurs at each set (k_x, k_y) of spectral frequencies. The enforcement of boundary conditions results in a system of linear equations with the spectra as unknowns to be solved. The boundary conditions with their resulting equations are listed here:

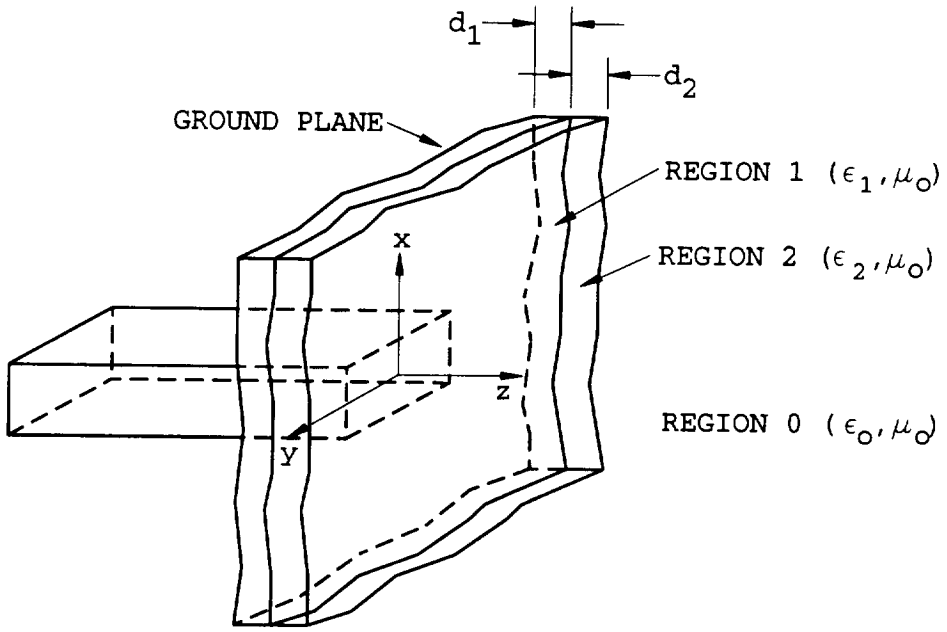

Figure 2.3: Two dielectric layers, free space backed on a rectangular aperture ground-plane.

The boundary condition of continuous tangential electric field across the interface at $z = 0$ gives the following two equations:

$$-jk_{z_1} I_{\psi_1} + jk_{z_1} R_{\psi_1} = f, \tag{2.43}$$

$$jk_{z_1} I_{\phi_1} - jk_{z_1} R_{\phi_1} = 0. \tag{2.44}$$

The boundary condition of continuous tangential electric field across the interface at $z = d_1$ gives the following two equations:

$$-jk_{z_1} I_{\psi_1} e^{-jk_{z_1} d_1} + jk_{z_1} R_{\psi_1} e^{jk_{z_1} d_1} = -jk_{z_2} I_{\psi_2} e^{-jk_{z_2} d_1} + jk_{z_2} R_{\psi_2} e^{jk_{z_2} d_1}, \tag{2.45}$$

$$jk_{z_1} I_{\phi_1} e^{-jk_{z_1} d_1} - jk_{z_1} R_{\phi_1} e^{jk_{z_1} d_1} = jk_{z_2} I_{\phi_2} e^{-jk_{z_2} d_1} - jk_{z_2} R_{\phi_2} e^{jk_{z_2} d_1}. \tag{2.46}$$

The boundary condition of continuous tangential magnetic field across the interface at $z = d_1$ gives the following two equations:

$$\begin{aligned}(k_1^2 - k_x^2)\left[I_{\phi_1} e^{-jk_{z_1} d_1} + R_{\phi_1} e^{jk_{z_1} d_1}\right] - k_x k_y \left[I_{\psi_1} e^{-jk_{z_1} d_1} + R_{\psi_1} e^{jk_{z_1} d_1}\right] &= \\ (k_2^2 - k_x^2)\left[I_{\phi_2} e^{-jk_{z_2} d_1} + R_{\phi_2} e^{jk_{z_2} d_1}\right] - k_x k_y \left[I_{\psi_2} e^{-jk_{z_2} d_1} + R_{\psi_2} e^{jk_{z_2} d_1}\right] &,\end{aligned} \tag{2.47}$$

$$(k_1^2 - k_y^2)\left[I_{\psi_1} e^{-jk_{z_1}d_1} + R_{\psi_1} e^{jk_{z_1}d_1}\right] - k_x k_y \left[I_{\phi_1} e^{-jk_{z_1}d_1} + R_{\phi_1} e^{jk_{z_1}d_1}\right] =$$
$$(k_2^2 - k_y^2)\left[I_{\psi_2} e^{-jk_{z_2}d_1} + R_{\psi_2} e^{jk_{z_2}d_1}\right] - k_x k_y \left[I_{\phi_2} e^{-jk_{z_2}d_1} + R_{\phi_2} e^{jk_{z_2}d_1}\right] \quad . \quad (2.48)$$

The boundary condition of continuous tangential electric field across the interface at $z = d_2$ gives the following two equations:

$$-jk_{z_2} I_{\psi_2} e^{-jk_{z_2}d_2} + jk_{z_2} R_{\psi_2} e^{jk_{z_2}d_2} = -jk_{z_0} T_{\psi_0} e^{-jk_{z_0}d_2}, \quad (2.49)$$
$$jk_{z_2} I_{\phi_2} e^{-jk_{z_2}d_2} - jk_{z_2} R_{\phi_2} e^{jk_{z_2}d_2} = jk_{z_0} T_{\phi_0} e^{-jk_{z_0}d_2}. \quad (2.50)$$

The boundary condition of continuous tangential magnetic field across the interface at $z = d_2$ gives the following two equations:

$$(k_2^2 - k_x^2)\left[I_{\phi_2} e^{-jk_{z_2}d_2} + R_{\phi_2} e^{jk_{z_2}d_2}\right] - k_x k_y \left[I_{\psi_2} e^{-jk_{z_2}d_2} + R_{\psi_2} e^{jk_{z_2}d_2}\right] =$$
$$(k_0^2 - k_x^2) T_{\phi_0} e^{-jk_{z_0}d_2} - k_x k_y T_{\psi_0} e^{-jk_{z_0}d_2} \quad , \quad (2.51)$$

$$(k_2^2 - k_y^2)\left[I_{\psi_2} e^{-jk_{z_2}d_2} + R_{\psi_2} e^{jk_{z_2}d_2}\right] - k_x k_y \left[I_{\phi_2} e^{-jk_{z_2}d_2} + R_{\phi_2} e^{jk_{z_2}d_2}\right] =$$
$$(k_0^2 - k_y^2) T_{\psi_0} e^{-jk_{z_0}d_2} - k_x k_y T_{\phi_0} e^{-jk_{z_0}d_2} \quad . \quad (2.52)$$

These ten linear equations in the ten unknown spectra form this matrix equation:

$$\begin{bmatrix}
z_{11} & 0 & -z_{11} & 0 & 0 & 0 & 0 & 0 & 0 & 0 \\
0 & -z_{11} & 0 & z_{11} & 0 & 0 & 0 & 0 & 0 & 0 \\
z_{31} & 0 & z_{33} & 0 & z_{35} & 0 & z_{37} & 0 & 0 & 0 \\
0 & z_{31} & 0 & z_{33} & 0 & z_{35} & 0 & z_{37} & 0 & 0 \\
z_{51} & z_{52} & z_{53} & z_{54} & z_{55} & z_{56} & z_{57} & z_{58} & 0 & 0 \\
z_{61} & z_{51} & z_{63} & z_{53} & z_{65} & z_{55} & z_{67} & z_{57} & 0 & 0 \\
0 & 0 & 0 & 0 & z_{75} & 0 & z_{77} & 0 & z_{79} & 0 \\
0 & 0 & 0 & 0 & 0 & z_{75} & 0 & z_{77} & 0 & z_{79} \\
0 & 0 & 0 & 0 & z_{95} & z_{96} & z_{97} & z_{98} & z_{99} & z_{9A} \\
0 & 0 & 0 & 0 & z_{A5} & z_{95} & z_{A7} & z_{97} & z_{A9} & z_{99}
\end{bmatrix}
\begin{bmatrix}
I_{\psi_1} \\ I_{\phi_1} \\ R_{\psi_1} \\ R_{\phi_1} \\ I_{\psi_2} \\ I_{\phi_2} \\ R_{\psi_2} \\ R_{\phi_2} \\ T_{\psi_0} \\ T_{\phi_0}
\end{bmatrix}
=
\begin{bmatrix}
f \\ 0 \\ 0 \\ 0 \\ 0 \\ 0 \\ 0 \\ 0 \\ 0 \\ 0
\end{bmatrix}
, \quad (2.53)$$

where

$$
\begin{aligned}
z_{11} &= -jk_{z_1}, & z_{65} &= -(k_2^2 - k_y^2)e^{-jk_{z_2}d_1},\\
z_{31} &= -jk_{z_1}e^{-jk_{z_1}d_1}, & z_{67} &= -(k_2^2 - k_y^2)e^{+jk_{z_2}d_1},\\
z_{33} &= jk_{z_1}e^{+jk_{z_1}d_1}, & z_{75} &= -jk_{z_2}e^{-jk_{z_2}d_2},\\
z_{35} &= jk_{z_2}e^{-jk_{z_2}d_1}, & z_{77} &= jk_{z_2}e^{+jk_{z_2}d_2},\\
z_{37} &= -jk_{z_2}e^{+jk_{z_2}d_1}, & z_{79} &= jk_{z_0}e^{-jk_{z_0}d_2},\\
z_{51} &= -k_xk_ye^{-jk_{z_1}d_1}, & z_{95} &= -k_xk_ye^{-jk_{z_2}d_2},\\
z_{52} &= (k_1^2 - k_x^2)e^{-jk_{z_1}d_1}, & z_{96} &= (k_2^2 - k_x^2)e^{-jk_{z_2}d_2},\\
z_{53} &= -k_xk_ye^{+jk_{z_1}d_1}, & z_{97} &= -k_xk_ye^{+jk_{z_2}d_2},\\
z_{54} &= (k_1^2 - k_x^2)e^{+jk_{z_1}d_1}, & z_{98} &= (k_2^2 - k_x^2)e^{+jk_{z_2}d_2},\\
z_{55} &= k_xk_ye^{-jk_{z_2}d_1}, & z_{99} &= k_xk_ye^{-jk_{z_0}d_2},\\
z_{56} &= -(k_2^2 - k_x^2)e^{-jk_{z_2}d_1}, & z_{9A} &= -(k_0^2 - k_x^2)e^{-jk_{z_0}d_2},\\
z_{57} &= k_xk_ye^{+jk_{z_2}d_1}, & z_{A5} &= (k_2^2 - k_y^2)e^{-jk_{z_2}d_2},\\
z_{58} &= -(k_2^2 - k_x^2)e^{+jk_{z_2}d_1}, & z_{A7} &= (k_2^2 - k_y^2)e^{+jk_{z_2}d_2},\\
z_{61} &= (k_1^2 - k_y^2)e^{-jk_{z_1}d_1}, & z_{A9} &= -(k_0^2 - k_y^2)e^{-jk_{z_0}d_2}.\\
z_{63} &= (k_1^2 - k_y^2)e^{+jk_{z_1}d_1},
\end{aligned}
\tag{2.54}
$$

Note that the hexadecimal number A is used in the place of the subscript 10 for the sake of simplicity. The matrix equation of (2.53) can be reduced into a four equation system in the four unknowns I_{ψ_2}, I_{ϕ_2}, R_{ψ_2}, and R_{ϕ_2}. These four unknowns have a simple relationship to the desired unknowns I_{ψ_1} and I_{ϕ_1}. Thus the solution for the spectra I_{ψ_1} and I_{ϕ_1} is given by

$$
\begin{bmatrix}
Z_{11} & Z_{12} & Z_{13} & Z_{14}\\
Z_{21} & Z_{11} & Z_{23} & Z_{13}\\
Z_{31} & Z_{32} & Z_{33} & Z_{34}\\
Z_{41} & Z_{31} & Z_{43} & Z_{33}
\end{bmatrix}
\begin{bmatrix}
I_{\psi_2}\\ I_{\phi_2}\\ R_{\psi_2}\\ R_{\phi_2}
\end{bmatrix}
=
\begin{bmatrix}
V_1\\ V_2\\ 0\\ 0
\end{bmatrix},
\tag{2.55}
$$

where

$$
Z_{11} = k_xk_y\left[1 - j\frac{k_{z_2}}{k_{z_1}}\cot(k_{z_1}d_1)\right]e^{-jk_{z_2}d_1},
\tag{2.56}
$$

$$Z_{12} = \left[(k_x^2 - k_2^2) - j\frac{k_{z_2}}{k_{z_1}}(k_x^2 - k_1^2)\cot(k_{z_1}d_1)\right] e^{-jk_{z_2}d_1}, \quad (2.57)$$

$$Z_{13} = k_x k_y \left[1 + j\frac{k_{z_2}}{k_{z_1}}\cot(k_{z_1}d_1)\right] e^{+jk_{z_2}d_1}, \quad (2.58)$$

$$Z_{14} = \left[(k_x^2 - k_2^2) + j\frac{k_{z_2}}{k_{z_1}}(k_x^2 - k_1^2)\cot(k_{z_1}d_1)\right] e^{+jk_{z_2}d_1}, \quad (2.59)$$

$$Z_{21} = \left[(k_y^2 - k_2^2) - j\frac{k_{z_2}}{k_{z_1}}(k_y^2 - k_1^2)\cot(k_{z_1}d_1)\right] e^{-jk_{z_2}d_1}, \quad (2.60)$$

$$Z_{23} = \left[(k_y^2 - k_2^2) + j\frac{k_{z_2}}{k_{z_1}}(k_y^2 - k_1^2)\cot(k_{z_1}d_1)\right] e^{+jk_{z_2}d_1}, \quad (2.61)$$

$$Z_{31} = k_x k_y \left[\frac{k_{z_2}}{k_{z_0}} - 1\right] e^{-jk_{z_2}d_2}, \quad (2.62)$$

$$Z_{32} = \left[(k_x^2 - k_0^2)\frac{k_{z_2}}{k_{z_0}} - (k_x^2 - k_2^2)\right] e^{-jk_{z_2}d_2}, \quad (2.63)$$

$$Z_{33} = -k_x k_y \left[\frac{k_{z_2}}{k_{z_0}} + 1\right] e^{+jk_{z_2}d_2}, \quad (2.64)$$

$$Z_{34} = -\left[(k_x^2 - k_0^2)\frac{k_{z_2}}{k_{z_0}} + (k_x^2 - k_2^2)\right] e^{+jk_{z_2}d_2}, \quad (2.65)$$

$$Z_{41} = \left[(k_y^2 - k_0^2)\frac{k_{z_2}}{k_{z_0}} - (k_y^2 - k_2^2)\right] e^{-jk_{z_2}d_2}, \quad (2.66)$$

$$Z_{43} = -\left[(k_y^2 - k_0^2)\frac{k_{z_2}}{k_{z_0}} + (k_y^2 - k_2^2)\right] e^{+jk_{z_2}d_2}, \quad (2.67)$$

$$V_1 = \frac{k_x k_y}{k_{z_1}}(\cot(k_{z_1}d_1) - j)e^{+jk_{z_1}d_1} f, \quad (2.68)$$

$$V_2 = \frac{(k_y^2 - k_1^2)}{k_{z_1}}(\cot(k_{z_1}d_1) - j)e^{+jk_{z_1}d_1} f, \quad (2.69)$$

and

$$I_{\psi_1} = \frac{(k_{z_2}/k_{z_1})}{2j\sin(k_{z_1}d_1)}\left(e^{+jk_{z_2}d_1}R_{\psi_2} - e^{-jk_{z_2}d_1}I_{\psi_2}\right) + \frac{[\cot(k_{z_1}d_1) + j]f}{2k_{z_1}}, \quad (2.70)$$

$$I_{\phi_1} = \frac{(k_{z_2}/k_{z_1})}{2j\sin(k_{z_1}d_1)}\left(e^{+jk_{z_2}d_1}R_{\phi_2} - e^{-jk_{z_2}d_1}I_{\phi_2}\right). \quad (2.71)$$

Note that the substitution of variables in (2.38) and (2.39) is needed in (2.56)-(2.71) for the purposes of computation of the aperture admittance.

2.1.2 Two Dielectric Layers - PEC Sheet Backed

Figure 2.4 shows two dielectric layers, PEC sheet backed, on a rectangular aperture groundplane. The width of the first layer is d_1, and the width of the second layer is $d_2 - d_1$. The PEC sheet is located at $z = d_2$. The incident spectra I_{ψ_1} and I_{ϕ_1} are determined by the enforcement of the boundary conditions at the three interfaces at $z = 0$, d_1, and d_2. The boundary condition enforcement occurs at each set (k_x, k_y) of spectral frequencies. The enforcement of boundary conditions results in a system of linear equations with the spectra as unknowns to be solved. The boundary conditions and resulting equations at $z = 0$ and $z = d_1$ are the same as for the free space backed case of 2.1.1.

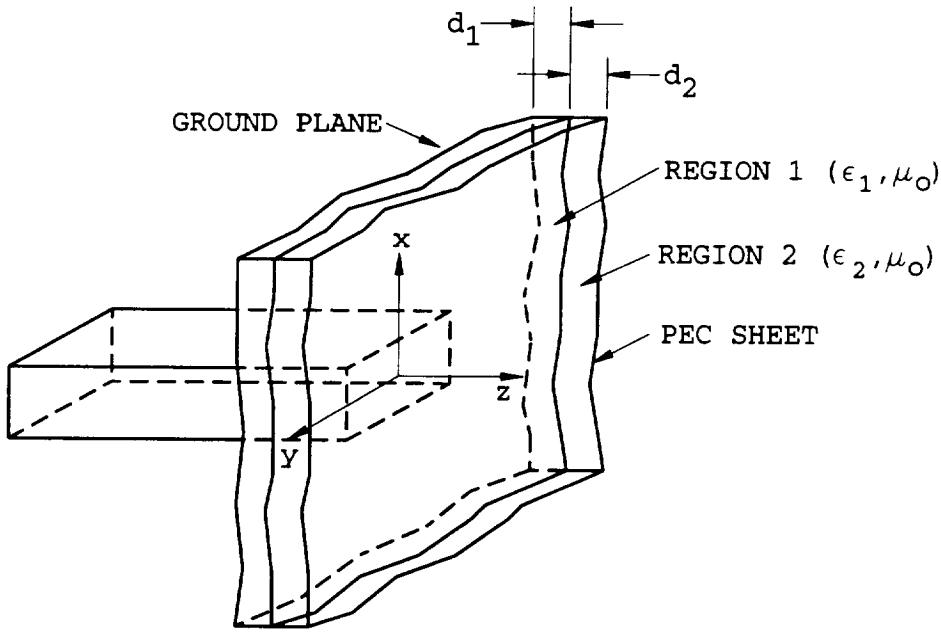

Figure 2.4: Two dielectric layers, PEC sheet backed on a rectangular aperture groundplane.

The boundary condition at $z = d_2$ is that of vanishing tangential electric field, which produces the two equations:

$$-jk_{z_2} I_{\psi_2} e^{-jk_{z_2} d_2} + jk_{z_2} R_{\psi_2} e^{jk_{z_2} d_2} = 0, \tag{2.72}$$

$$jk_{z_2} I_{\phi_2} e^{-jk_{z_2} d_2} - jk_{z_2} R_{\phi_2} e^{jk_{z_2} d_2} = 0. \tag{2.73}$$

(2.43)-(2.48), (2.72), and (2.73) form a linear system of eight equations in eight unknown spectra, given by the matrix equation:

$$\begin{bmatrix} z_{11} & 0 & -z_{11} & 0 & 0 & 0 & 0 & 0 \\ 0 & -z_{11} & 0 & z_{11} & 0 & 0 & 0 & 0 \\ z_{31} & 0 & z_{33} & 0 & z_{35} & 0 & z_{37} & 0 \\ 0 & z_{31} & 0 & z_{33} & 0 & z_{35} & 0 & z_{37} \\ z_{51} & z_{52} & z_{53} & z_{54} & z_{55} & z_{56} & z_{57} & z_{58} \\ z_{61} & z_{51} & z_{63} & z_{53} & z_{65} & z_{55} & z_{67} & z_{57} \\ 0 & 0 & 0 & 0 & z_{75} & 0 & z_{77} & 0 \\ 0 & 0 & 0 & 0 & 0 & z_{75} & 0 & z_{77} \end{bmatrix} \begin{bmatrix} I_{\psi_1} \\ I_{\phi_1} \\ R_{\psi_1} \\ R_{\phi_1} \\ I_{\psi_2} \\ I_{\phi_2} \\ R_{\psi_2} \\ R_{\phi_2} \end{bmatrix} = \begin{bmatrix} f \\ 0 \\ 0 \\ 0 \\ 0 \\ 0 \\ 0 \\ 0 \end{bmatrix}, \tag{2.74}$$

where

$$\begin{aligned} z_{11} &= -jk_{z_1}, & z_{56} &= -(k_2^2 - k_x^2)e^{-jk_{z_2}d_1}, \\ z_{31} &= -jk_{z_1}e^{-jk_{z_1}d_1}, & z_{57} &= k_xk_ye^{+jk_{z_2}d_1}, \\ z_{33} &= jk_{z_1}e^{+jk_{z_1}d_1}, & z_{58} &= -(k_2^2 - k_x^2)e^{+jk_{z_2}d_1}, \\ z_{35} &= jk_{z_2}e^{-jk_{z_2}d_1}, & z_{61} &= (k_1^2 - k_y^2)e^{-jk_{z_1}d_1}, \\ z_{37} &= -jk_{z_2}e^{+jk_{z_2}d_1}, & z_{63} &= (k_1^2 - k_y^2)e^{+jk_{z_1}d_1}, \\ z_{51} &= -k_xk_ye^{-jk_{z_1}d_1}, & z_{65} &= -(k_2^2 - k_y^2)e^{-jk_{z_2}d_1}, \\ z_{52} &= (k_1^2 - k_x^2)e^{-jk_{z_1}d_1}, & z_{67} &= -(k_2^2 - k_y^2)e^{+jk_{z_2}d_1}, \\ z_{53} &= -k_xk_ye^{+jk_{z_1}d_1}, & z_{75} &= -jk_{z_2}e^{-jk_{z_2}d_2}. \\ z_{54} &= (k_1^2 - k_x^2)e^{+jk_{z_1}d_1}, & z_{77} &= jk_{z_2}e^{+jk_{z_2}d_2}. \\ z_{55} &= k_xk_ye^{-jk_{z_2}d_1}, \end{aligned} \tag{2.75}$$

The matrix equation of (2.74) can be reduced into a two equation system in the two unknowns I_{ψ_2} and I_{ϕ_2}. These two unknowns have a simple relationship to the desired unknowns I_{ψ_1} and I_{ϕ_1}. Thus the solution for the spectra I_{ψ_1} and I_{ϕ_1} is given by

$$I_{\psi_2} = \frac{V_1Z_{11} - V_2Z_{12}}{Z_{11}^2 - Z_{12}Z_{21}}, \tag{2.76}$$

$$I_{\phi_2} = \frac{V_2Z_{11} - V_1Z_{21}}{Z_{11}^2 - Z_{12}Z_{21}}, \tag{2.77}$$

where

$$Z_{11} = k_x k_y \left[\left(1 - j \frac{k_{z_2}}{k_{z_1}} \cot(k_{z_1} d_1) \right) e^{-jk_{z_2} d_1} + \left(1 + j \frac{k_{z_2}}{k_{z_1}} \cot(k_{z_1} d_1) \right) e^{+jk_{z_2} d_1} e^{-2jk_{z_2} d_2} \right], \quad (2.78)$$

$$Z_{12} = \left[(k_x^2 - k_2^2) - j(k_x^2 - k_1^2) \frac{k_{z_2}}{k_{z_1}} \cot(k_{z_1} d_1) \right] e^{-jk_{z_2} d_1} + \left[(k_x^2 - k_2^2) + j(k_x^2 - k_1^2) \frac{k_{z_2}}{k_{z_1}} \cot(k_{z_1} d_1) \right] e^{+jk_{z_2} d_1} e^{-2jk_{z_2} d_2}, \quad (2.79)$$

$$Z_{21} = \left[(k_y^2 - k_2^2) - j(k_y^2 - k_1^2) \frac{k_{z_2}}{k_{z_1}} \cot(k_{z_1} d_1) \right] e^{-jk_{z_2} d_1} + \left[(k_y^2 - k_2^2) + j(k_y^2 - k_1^2) \frac{k_{z_2}}{k_{z_1}} \cot(k_{z_1} d_1) \right] e^{+jk_{z_2} d_1} e^{-2jk_{z_2} d_2}, \quad (2.80)$$

$$V_1 = \frac{k_x k_y}{k_{z_1}} (\cot(k_{z_1} d_1) - j) e^{+jk_{z_1} d_1} f, \quad (2.81)$$

$$V_2 = \frac{(k_y^2 - k_1^2)}{k_{z_1}} (\cot(k_{z_1} d_1) - j) e^{+jk_{z_1} d_1} f, \quad (2.82)$$

and

$$I_{\psi_1} = \frac{(k_{z_2}/k_{z_1})}{2j \sin(k_{z_1} d_1)} \left(e^{-2jk_{z_2} d_2} e^{+jk_{z_2} d_1} - e^{-jk_{z_2} d_1} \right) I_{\psi_2} + \frac{[\cot(k_{z_1} d_1) + j] f}{2k_{z_1}}, \quad (2.83)$$

$$I_{\phi_1} = \frac{(k_{z_2}/k_{z_1})}{2j \sin(k_{z_1} d_1)} \left(e^{-2jk_{z_2} d_2} e^{+jk_{z_2} d_1} - e^{-jk_{z_2} d_1} \right) I_{\phi_2}. \quad (2.84)$$

Note that the substitution of variables in (2.38) and (2.39) is needed in (2.78)-(2.84) for the purposes of computation of the aperture admittance.

2.1.3 One Dielectric Layer - Resistive Sheet Backed

Figure 2.5 shows one dielectric layer, resistive sheet backed, on a rectangular aperture groundplane. The width of the single layer is d_1. The resistive sheet is located at $z = d_1$. The incident spectra I_{ψ_1} and I_{ϕ_1} are determined by the enforcement of the boundary conditions at the two interfaces at $z = 0$ and d_1. The boundary condition enforcement occurs at each set (k_x, k_y) of spectral frequencies. The enforcement of boundary conditions results in a system of linear equations with the spectra as

unknowns to be solved. The boundary conditions and resulting equations at $z = 0$ and are the same as for the free space backed case of 2.1.1.

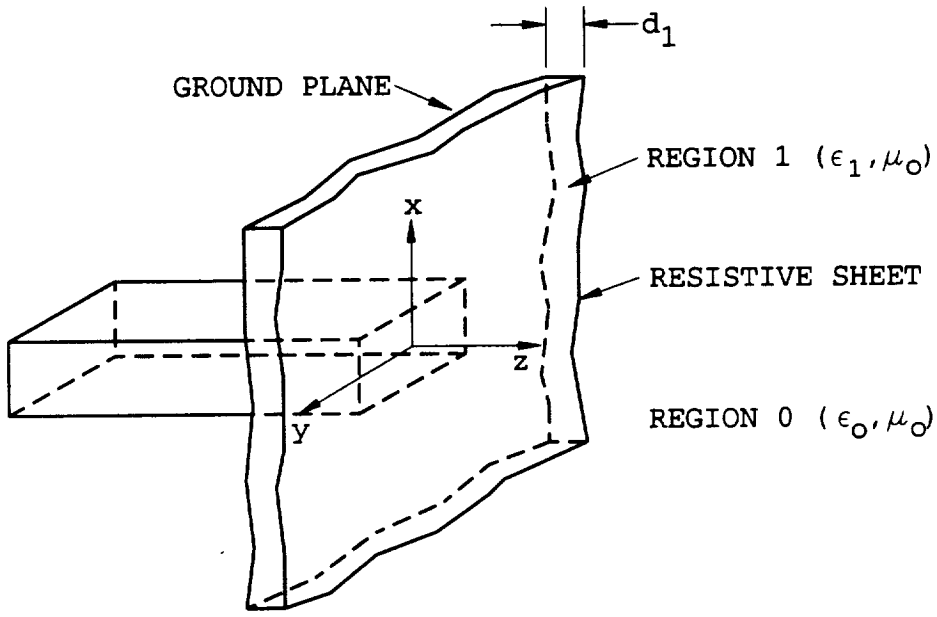

Figure 2.5: One dielectric layer, resistive sheet backed on a rectangular aperture groundplane.

The resistive boundary conditions that the electric and magnetic fields obey at $z = d_1$ are

$$\hat{\mathbf{z}} \times (\mathbf{E}_0 - \mathbf{E}_1) = \mathbf{0} \tag{2.85}$$

$$\hat{\mathbf{z}} \times \hat{\mathbf{z}} \times \mathbf{E} = -R\hat{\mathbf{z}} \times (\mathbf{H}_0 - \mathbf{H}_1) \tag{2.86}$$

(2.85) gives rise to these two equations:

$$-jk_{z_1} I_{\psi_1} e^{-jk_{z_1} d_1} + jk_{z_1} R_{\psi_1} e^{jk_{z_1} d_1} = -jk_{z_0} T_{\psi_0} e^{-jk_{z_0} d_1}, \tag{2.87}$$

$$jk_{z_1} I_{\phi_1} e^{-jk_{z_1} d_1} - jk_{z_1} R_{\phi_1} e^{jk_{z_1} d_1} = jk_{z_0} T_{\phi_0} e^{-jk_{z_0} d_1}. \tag{2.88}$$

(2.86) gives rise to these two equations:

$$-jk_{z_0} T_{\psi_0} e^{-jk_{z_0} d_1} = R\left\{\frac{k_1^2 - k_y^2}{j\omega\mu_0}\left[I_{\psi_1} e^{-jk_{z_1} d_1} + R_{\psi_1} e^{jk_{z_1} d_1}\right]\right.$$

$$
\begin{aligned}
& -\frac{k_x k_y}{j\omega\mu_0}\left[I_{\phi_1}e^{-jk_{z_1}d_1}+R_{\phi_1}e^{jk_{z_1}d_1}\right] \\
& -\left[\frac{k_0^2-k_y^2}{j\omega\mu_0}T_{\psi_0}-\frac{k_x k_y}{j\omega\mu_0}T_{\phi_0}\right]e^{-jk_{z_0}d_1}\Bigg\}, \qquad (2.89)
\end{aligned}
$$

$$
\begin{aligned}
jk_{z_0}T_{\phi_0}e^{-jk_{z_0}d_1} = R\Bigg\{ & \left[\frac{k_0^2-k_x^2}{j\omega\mu_0}T_{\phi_0}-\frac{k_x k_y}{j\omega\mu_0}T_{\psi_0}\right]e^{-jk_{z_0}d_1} \\
& -\frac{k_1^2-k_x^2}{j\omega\mu_0}\left[I_{\phi_1}e^{-jk_{z_1}d_1}+R_{\phi_1}e^{jk_{z_1}d_1}\right] \\
& +\frac{k_x k_y}{j\omega\mu_0}\left[I_{\psi_1}e^{-jk_{z_1}d_1}+R_{\psi_1}e^{jk_{z_1}d_1}\right]\Bigg\}. \qquad (2.90)
\end{aligned}
$$

(2.43), (2.44), and (2.87)-(2.90) form a linear system of six equations in six unknown spectra, given by the matrix equation:

$$
\begin{bmatrix}
z_{11} & 0 & -z_{11} & 0 & 0 & 0 \\
0 & -z_{11} & 0 & z_{11} & 0 & 0 \\
z_{31} & 0 & z_{33} & 0 & z_{35} & 0 \\
0 & z_{31} & 0 & z_{33} & 0 & z_{35} \\
z_{51} & z_{52} & z_{53} & z_{54} & z_{55} & z_{56} \\
-z_{52} & z_{62} & -z_{54} & z_{64} & -z_{56} & z_{66}
\end{bmatrix}
\begin{bmatrix} I_{\psi_1} \\ I_{\phi_1} \\ R_{\psi_1} \\ R_{\phi_1} \\ T_{\psi_0} \\ T_{\phi_0} \end{bmatrix}
=
\begin{bmatrix} f \\ 0 \\ 0 \\ 0 \\ 0 \\ 0 \end{bmatrix}, \qquad (2.91)
$$

where

$$
\begin{aligned}
z_{11} &= -jk_{z_1}, & z_{54} &= -R\tfrac{k_x k_y}{j\omega\mu_0}e^{+jk_{z_1}d_1}, \\
z_{31} &= -jk_{z_1}e^{-jk_{z_1}d_1}, & z_{55} &= j\left[k_{z_0}+R\tfrac{(k_0^2-k_y^2)}{\omega\mu_0}\right]e^{-jk_{z_0}d_1}, \\
z_{33} &= jk_{z_1}e^{+jk_{z_1}d_1}, & z_{56} &= R\tfrac{k_x k_y}{j\omega\mu_0}e^{-jk_{z_0}d_1}, \\
z_{35} &= jk_{z_0}e^{-jk_{z_0}d_1}, & z_{62} &= -R\tfrac{(k_1^2-k_x^2)}{j\omega\mu_0}e^{-jk_{z_1}d_1}, \qquad (2.92) \\
z_{51} &= R\tfrac{(k_1^2-k_y^2)}{j\omega\mu_0}e^{-jk_{z_1}d_1}, & z_{64} &= -R\tfrac{(k_1^2-k_x^2)}{j\omega\mu_0}e^{+jk_{z_1}d_1}, \\
z_{52} &= -R\tfrac{k_x k_y}{j\omega\mu_0}e^{-jk_{z_1}d_1}, & z_{66} &= -j\left[k_{z_0}+R\tfrac{(k_0^2-k_x^2)}{\omega\mu_0}\right]e^{-jk_{z_0}d_1}. \\
z_{53} &= R\tfrac{(k_1^2-k_y^2)}{j\omega\mu_0}e^{+jk_{z_1}d_1}, &&
\end{aligned}
$$

The matrix equation of (2.91) can be reduced into a two equation system in the two desired unknowns I_{ψ_1} and I_{ϕ_1}. Thus the solution for the spectra I_{ψ_1} and I_{ϕ_1} is given by

$$
I_{\psi_1} = \frac{V_1 Z_{22} - V_2 Z_{12}}{Z_{11}Z_{22} - Z_{12}^2}, \qquad (2.93)
$$

$$I_{\phi_1} = \frac{V_2 Z_{11} - V_1 Z_{12}}{Z_{11} Z_{22} - Z_{12}^2}, \tag{2.94}$$

where

$$Z_{11} = 2R\frac{(k_1^2 - k_y^2)}{j\omega\mu_0}\cos(k_{z_1} d_1) + 2\left(1 + R\frac{(k_0^2 - k_y^2)}{k_{z_0}\omega\mu_0}\right) k_{z_1}\sin(k_{z_1} d_1), \tag{2.95}$$

$$Z_{12} = -2R\frac{k_x k_y}{j\omega\mu_0}\left(\cos(k_{z_1} d_1) + j\frac{k_{z_1}}{k_{z_0}}\sin(k_{z_1} d_1)\right), \tag{2.96}$$

$$Z_{22} = -2R\frac{(k_1^2 - k_x^2)}{j\omega\mu_0}\cos(k_{z_1} d_1) - 2\left(1 + R\frac{(k_0^2 - k_x^2)}{k_{z_0}\omega\mu_0}\right) k_{z_1}\sin(k_{z_1} d_1), \tag{2.97}$$

$$V_1 = \left[1 + \frac{R}{\omega\mu_0}\left(\frac{(k_0^2 - k_y^2)}{k_{z_0}} + \frac{(k_1^2 - k_y^2)}{k_{z_1}}\right)\right] e^{+jk_{z_1} d_1} f, \tag{2.98}$$

$$V_2 = \frac{R k_x k_y}{\omega\mu_0}\left(\frac{1}{k_{z_0}} + \frac{1}{k_{z_1}}\right) e^{+jk_{z_1} d_1} f. \tag{2.99}$$

Note that the substitution of variables in (2.38) and (2.39) is needed in (2.95)-(2.99) for the purposes of computation of the aperture admittance.

2.1.4 One Dielectric Layer - Free Space Backed

Figure 2.6 shows one dielectric layer, free space backed, on a rectangular aperture groundplane. The width of the single layer is d_1. The incident spectra I_{ψ_1} and I_{ϕ_1} are determined by the enforcement of the boundary conditions at the two interfaces at $z = 0$ and d_1. The boundary condition enforcement occurs at each set (k_x, k_y) of spectral frequencies. The enforcement of boundary conditions results in a system of linear equations with the spectra as unknowns to be solved. The boundary conditions and resulting equations at $z = 0$ and are the same as for the free space backed case of 2.1.1. The boundary conditions on the electric field at $z = d_1$ are the same as for the resistive sheet backed case of 2.1.3, that of continuous tangential electric field.

The boundary conditions on the magnetic field at $z = d_1$ is that of continuous tangential magnetic field, giving the following two equations:

$$(k_1^2 - k_x^2)\left[I_{\phi_1} e^{-jk_{z_1} d_1} + R_{\phi_1} e^{jk_{z_1} d_1}\right] - k_x k_y \left[I_{\psi_1} e^{-jk_{z_1} d_1} + R_{\psi_1} e^{jk_{z_1} d_1}\right] = (k_0^2 - k_x^2) T_{\phi_0} e^{-jk_{z_0} d_1} - k_x k_y T_{\psi_0} e^{-jk_{z_0} d_1}, \tag{2.100}$$

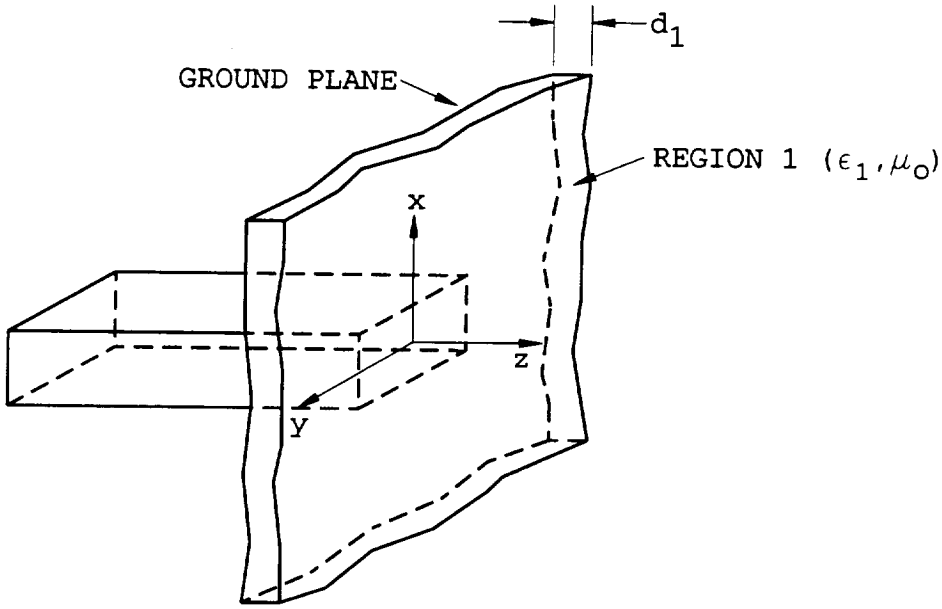

Figure 2.6: One dielectric layer, free space backed on a rectangular aperture groundplane.

$$(k_1^2 - k_y^2)\left[I_{\psi_1} e^{-jk_{z_1}d_1} + R_{\psi_1} e^{jk_{z_1}d_1}\right] - k_x k_y \left[I_{\phi_1} e^{-jk_{z_1}d_1} + R_{\phi_1} e^{jk_{z_1}d_1}\right] =$$
$$(k_0^2 - k_y^2) T_{\psi_0} e^{-jk_{z_0}d_1} - k_x k_y T_{\phi_0} e^{-jk_{z_0}d_1} \quad . \quad (2.101)$$

(2.43), (2.44), (2.87), (2.88), (2.100), and (2.101) form a linear system of six equations in six unknown spectra, given by the matrix equation:

$$\begin{bmatrix} z_{11} & 0 & -z_{11} & 0 & 0 & 0 \\ 0 & -z_{11} & 0 & z_{11} & 0 & 0 \\ z_{31} & 0 & z_{33} & 0 & z_{35} & 0 \\ 0 & z_{31} & 0 & z_{33} & 0 & z_{35} \\ z_{51} & z_{52} & z_{53} & z_{54} & z_{55} & z_{56} \\ z_{61} & z_{51} & z_{63} & z_{53} & z_{65} & z_{55} \end{bmatrix} \begin{bmatrix} I_{\psi_1} \\ I_{\phi_1} \\ R_{\psi_1} \\ R_{\phi_1} \\ T_{\psi_0} \\ T_{\phi_0} \end{bmatrix} = \begin{bmatrix} f \\ 0 \\ 0 \\ 0 \\ 0 \\ 0 \end{bmatrix}, \quad (2.102)$$

where

$$
\begin{aligned}
z_{11} &= -jk_{z_1}, & z_{54} &= (k_1^2 - k_x^2)e^{+jk_{z_1}d_1}, \\
z_{31} &= -jk_{z_1}e^{-jk_{z_1}d_1}, & z_{55} &= k_x k_y e^{-jk_{z_0}d_1}, \\
z_{33} &= jk_{z_1}e^{+jk_{z_1}d_1}, & z_{56} &= -(k_0^2 - k_x^2)e^{-jk_{z_0}d_1}, \\
z_{35} &= jk_{z_0}e^{-jk_{z_0}d_1}, & z_{61} &= (k_1^2 - k_y^2)e^{-jk_{z_1}d_1}, \\
z_{51} &= -k_x k_y e^{-jk_{z_1}d_1}, & z_{63} &= (k_1^2 - k_y^2)e^{+jk_{z_1}d_1}, \\
z_{52} &= (k_1^2 - k_x^2)e^{-jk_{z_1}d_1}, & z_{65} &= -(k_0^2 - k_y^2)e^{-jk_{z_0}d_1}. \\
z_{53} &= -k_x k_y e^{+jk_{z_1}d_1},
\end{aligned}
\tag{2.103}
$$

The matrix equation of (2.102) can be reduced into a two equation system in the two desired unknowns I_{ψ_1} and I_{ϕ_1}. Thus the solution for the spectra I_{ψ_1} and I_{ϕ_1} is given by

$$I_{\psi_1} = \frac{V_1 Z_{22} - V_2 Z_{12}}{Z_{11}Z_{22} - Z_{12}^2}, \tag{2.104}$$

$$I_{\phi_1} = \frac{V_2 Z_{11} - V_1 Z_{12}}{Z_{11}Z_{22} - Z_{12}^2}, \tag{2.105}$$

where

$$Z_{11} = (k_1^2 - k_x^2)k_{z_0}\cos(k_{z_1}d_1) + j(k_0^2 - k_x^2)k_{z_1}\sin(k_{z_1}d_1), \tag{2.106}$$

$$Z_{12} = -k_x k_y \left[k_{z_0}\cos(k_{z_1}d_1) + jk_{z_1}\sin(k_{z_1}d_1)\right], \tag{2.107}$$

$$Z_{22} = (k_1^2 - k_y^2)k_{z_0}\cos(k_{z_1}d_1) + j(k_0^2 - k_y^2)k_{z_1}\sin(k_{z_1}d_1), \tag{2.108}$$

$$V_1 = -k_x k_y (k_{z_0} + k_{z_1})\frac{e^{+jk_{z_1}d_1}}{2k_{z_1}}jf, \tag{2.109}$$

$$V_2 = \left[k_{z_0}(k_1^2 - k_y^2) + k_{z_1}(k_0^2 - k_y^2)\right]\frac{e^{+jk_{z_1}d_1}}{2k_{z_1}}jf. \tag{2.110}$$

Note that the substitution of variables in (2.38) and (2.39) is needed in (2.106)-(2.110) for the purposes of computation of the aperture admittance.

2.1.5 One Dielectric Layer - PEC Sheet Backed

Figure 2.7 shows one dielectric layer, PEC sheet backed, on a rectangular aperture groundplane. The width of the single layer is d_1. The incident spectra I_{ψ_1} and I_{ϕ_1}

are determined by the enforcement of the boundary conditions at the two interfaces at $z = 0$ and d_1. The boundary condition enforcement occurs at each set (k_x, k_y) of spectral frequencies. The enforcement of boundary conditions results in a system of linear equations with the spectra as unknowns to be solved. The boundary conditions and resulting equations at $z = 0$ and are the same as for the free space backed case of 2.1.1.

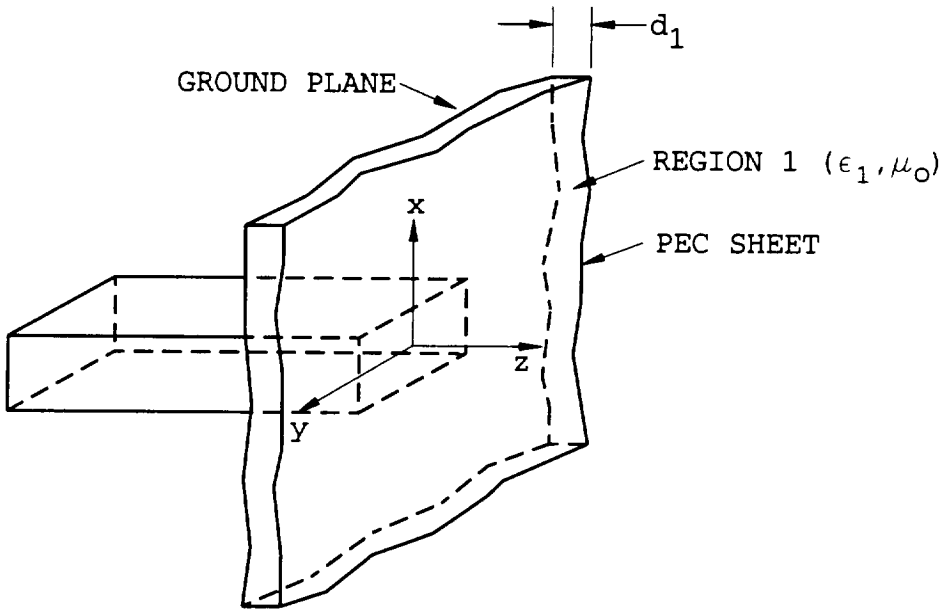

Figure 2.7: One dielectric layer, PEC sheet backed on a rectangular aperture ground-plane.

The boundary condition at $z = d_1$ is that of vanishing tangential electric field, which produces the two equations:

$$-jk_{z_1} I_{\psi_1} e^{-jk_{z_1} d_1} + jk_{z_1} R_{\psi_1} e^{jk_{z_1} d_1} = 0, \tag{2.111}$$

$$jk_{z_1} I_{\phi_1} e^{-jk_{z_1} d_1} - jk_{z_1} R_{\phi_1} e^{jk_{z_1} d_1} = 0. \tag{2.112}$$

(2.43), (2.44), (2.111), and (2.112) form a linear system of four equations in four unknown spectra, given by the matrix equation:

$$\begin{bmatrix} z_{11} & 0 & -z_{11} & 0 \\ 0 & -z_{11} & 0 & z_{11} \\ z_{31} & 0 & z_{33} & 0 \\ 0 & z_{31} & 0 & z_{33} \end{bmatrix} \begin{bmatrix} I_{\psi_1} \\ I_{\phi_1} \\ R_{\psi_1} \\ R_{\phi_1} \end{bmatrix} = \begin{bmatrix} f \\ 0 \\ 0 \\ 0 \end{bmatrix}, \tag{2.113}$$

where

$$\begin{aligned} z_{11} &= -jk_{z_1}, \\ z_{31} &= -jk_{z_1} e^{-jk_{z_1} d_1}, \\ z_{33} &= jk_{z_1} e^{+jk_{z_1} d_1}. \end{aligned} \tag{2.114}$$

The solution of (2.113) for the desired spectra I_{ψ_1} and I_{ϕ_1} is

$$I_{\psi_1} = \frac{e^{+jk_{z_1} d_1} f}{2k_{z_1} \sin(k_{z_1} d_1)}, \tag{2.115}$$

$$I_{\phi_1} = 0. \tag{2.116}$$

Note that the substitution of variables in (2.38) and (2.39) is needed in (2.115) for the purposes of computation of the aperture admittance.

2.2 Coaxial Aperture

The admittance of a coaxial aperture is developed here. The analysis involves representing the fields external to the aperture in terms of the Fourier integral of their plane wave spectra. The aperture admittance is obtained by using a variational assumption for the aperture total field distribution and matching the boundary conditions for the various dielectric slab/resistive sheet configurations under study.

The analysis starts with the representation of the electric vector potential $\mathbf{F}$ in terms of the cylindrical electric scalar potential ψ:

$$\mathbf{F} = \psi\hat{\phi}. \tag{2.117}$$

It will become evident that since the fields in the coaxial aperture are axially symmetric for the purposes of this investigation, only the $\hat{\phi}$ component of $\mathbf{F}$ is required. Referring to Figure 2.8, it can be seen that the potential is a functions of ρ and z, defined only for $z \geq 0$. The subscript 1 refers to Region 1, the dielectric slab in contact with the groundplane. The subscript 2 refers to Region 2, a second dielectric slab which may be on the first dielectric slab. The free space region above the dielectric slab(s) is denoted as Region 0 and all quantities associated with that region possess the subscript 0. The scalar potential is a solution to the scalar wave equation

$$(\nabla^2 + k_{0,1,2}^2)\psi = 0, \tag{2.118}$$

where the wavenumbers $k_{0,1,2}$ are given by

$$k_0^2 = \omega^2\mu_0\epsilon_0, \tag{2.119}$$

for Region 0, and

$$k_{1,2}^2 = \omega^2\mu_0\epsilon_{1,2} = k_0^2\epsilon_{r_{1,2}}, \tag{2.120}$$

for Regions 1 and 2. In general the relative permittivities $\epsilon_{r_{1,2}}$ are complex, representing possible losses in the slabs.

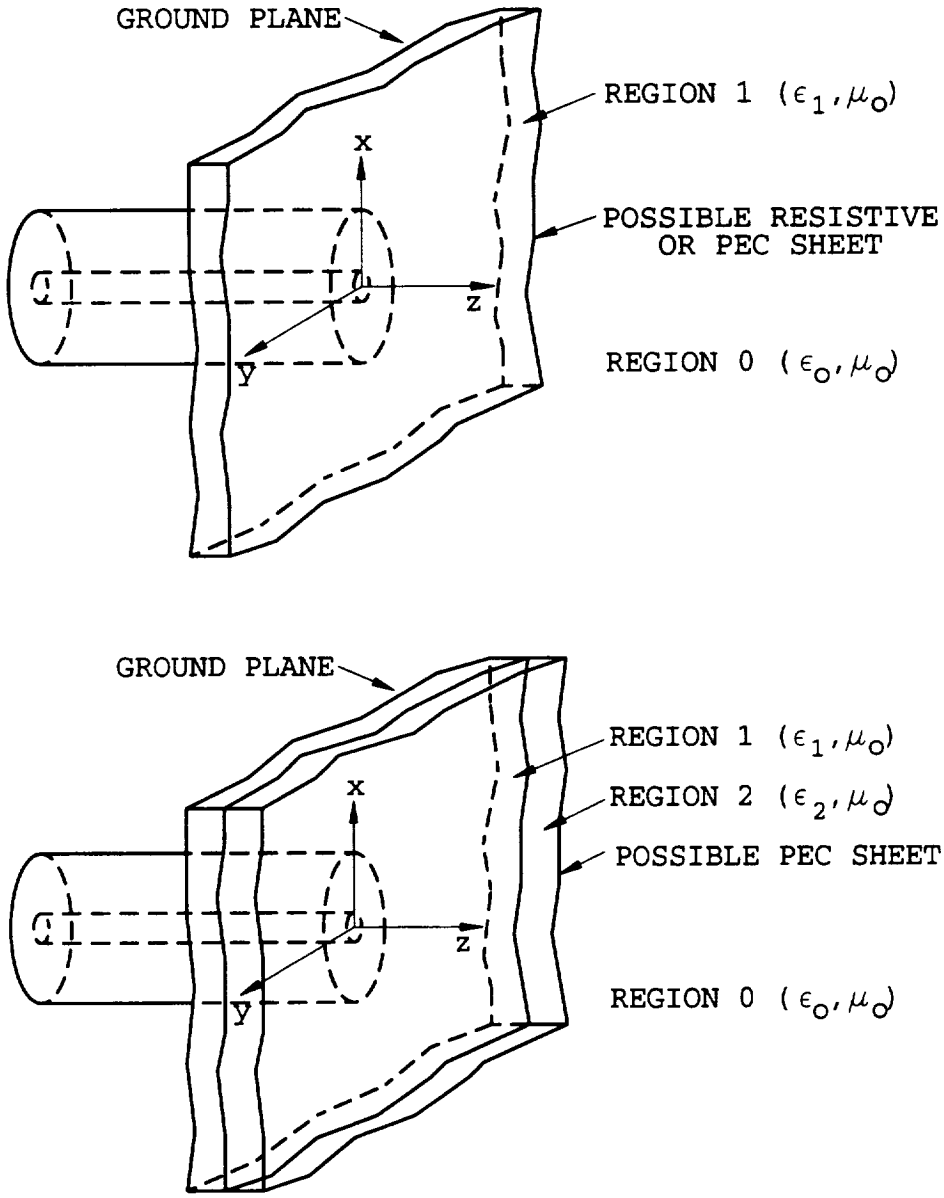

Figure 2.8: Dielectric slab/resistive sheet configurations on coaxial aperture groundplane.

The scalar potential can be expressed in terms of its plane-wave spectra. In Regions 1 and 2, the total spectra is comprised of the incident and reflected spectra, respectively denoted by I and R. In Region 0, the total spectra is comprised of one transmitted spectrum, denoted by T. The plane wave spectral representation chosen for the coaxial geometry involves the Fourier-Bessel transform with Bessel function of order 1. This representation has been chosen because $J_1(\beta\rho) \rightarrow 0$ as $\rho \rightarrow 0$, which is consistent with the fact that the fields vanish in the inner conductor of the coaxial aperture. This spectral representation is also consistent with the coaxial aperture work of Berrie [11]. Thus the plane wave spectral representation of the scalar potential in Region 1 is given by

$$\psi_1(\rho, z) = \int_0^\infty \left[I_{\psi_1}(\beta) e^{-jk_{z_1} z} + R_{\psi_1}(\beta) e^{jk_{z_1} z} \right] J_1(\beta\rho) \beta d\beta; \tag{2.121}$$

in Region 2 by

$$\psi_2(\rho, z) = \int_0^\infty \left[I_{\psi_2}(\beta) e^{-jk_{z_2} z} + R_{\psi_2}(\beta) e^{jk_{z_2} z} \right] J_1(\beta\rho) \beta d\beta; \tag{2.122}$$

and in Region 0 by

$$\psi_0(\rho, z) = \int_0^\infty \left[T_{\psi_0}(\beta) e^{-jk_{z_0} z} \right] J_1(\beta\rho) \beta d\beta. \tag{2.123}$$

The propagation constants are given by

$$k_{z_{0,1,2}} = \pm\sqrt{k_{0,1,2}^2 - \beta^2}, \tag{2.124}$$

where the sign is chosen so that the radiation condition is satisfied. Thus the sign for each propagation constant is chosen so that

$$\Re(k_{z_{0,1,2}}) \geq 0 \tag{2.125}$$

and

$$\Im(k_{z_{0,1,2}}) \leq 0. \tag{2.126}$$

From vector potential theory, the electric and magnetic fields are related to the electric vector potential by

$$\mathbf{E} = -\nabla \times \mathbf{F} = \frac{\partial \psi}{\partial z} \hat{\rho} \tag{2.127}$$

and

$$\mathbf{H} = \frac{1}{j\omega\mu_0}\left[k^2\mathbf{F} + \nabla(\nabla\cdot\mathbf{F})\right] = -j\omega\epsilon\psi\hat{\phi}. \tag{2.128}$$

Therefore the non-zero cylindrical components of the electric and magnetic fields in Region 1 are given by

$$E_{\rho_1}(\rho,z) = \int_0^\infty \left[-jk_{z_1}I_{\psi_1}e^{-jk_{z_1}z} + jk_{z_1}R_{\psi_1}e^{jk_{z_1}z}\right]J_1(\beta\rho)\beta d\beta, \tag{2.129}$$

and

$$H_{\phi_1}(\rho,z) = \int_0^\infty \left[-j\omega\epsilon_1 I_{\psi_1}e^{-jk_{z_1}z} - j\omega\epsilon_1 R_{\psi_1}e^{jk_{z_1}z}\right]J_1(\beta\rho)\beta d\beta; \tag{2.130}$$

in Region 2 by

$$E_{\rho_2}(\rho,z) = \int_0^\infty \left[-jk_{z_2}I_{\psi_2}e^{-jk_{z_2}z} + jk_{z_2}R_{\psi_2}e^{jk_{z_2}z}\right]J_1(\beta\rho)\beta d\beta, \tag{2.131}$$

and

$$H_{\phi_2}(\rho,z) = \int_0^\infty \left[-j\omega\epsilon_2 I_{\psi_2}e^{-jk_{z_2}z} - j\omega\epsilon_2 R_{\psi_2}e^{jk_{z_2}z}\right]J_1(\beta\rho)\beta d\beta; \tag{2.132}$$

and in Region 0 by

$$E_{\rho_0}(\rho,z) = \int_0^\infty \left[-jk_{z_0}T_{\psi_0}e^{-jk_{z_0}z}\right]J_1(\beta\rho)\beta d\beta, \tag{2.133}$$

and

$$H_{\phi_0}(\rho,z) = \int_0^\infty \left[-j\omega\epsilon_0 T_{\psi_0}e^{-jk_{z_0}z}\right]J_1(\beta\rho)\beta d\beta. \tag{2.134}$$

Note that in the above the β functional dependence is dropped from the spectra and is understood.

As in the rectangular aperture case, the solution to the fields can be obtained by satisfying the boundary conditions at the groundplane/dielectric slab interface and other interfaces present in the dielectric slab/resistive sheet configurations, but only if the total fields in the aperture are known. However, the total fields in the aperture are not known, since they consist of an infinite sum of waveguide modes with

unknown coefficients. In order to find the coefficients, a Moment Method solution can be set up in a manner similar to that which has been performed for the coaxial aperture case. For the purposes of this investigation a variational solution will be used [3] and its results compared to the Moment Method solution of Berrie [11]. The variational solution assumption for the coaxial aperture total electric field is of the form of the dominant TEM mode. The importance of higher-order coaxial modes is investigated in Subsection 3.3.2.

Thus the total electric field in the plane $z = 0$ is assumed to be

$$\mathbf{E}(\rho,0) = \mathbf{e}_0 = \begin{cases} \frac{\hat{\rho}}{\sqrt{2\pi \ln(b/a)\rho}} & , \quad \text{in the aperture} \\ 0 & , \quad \text{outside the aperture} \end{cases} , \tag{2.135}$$

where the factor $\frac{1}{\sqrt{2\pi \ln(b/a)}}$ normalizes the electric field so that

$$\int_0^{2\pi} \int_0^{\infty} \mathbf{E}(\rho,0) \cdot \mathbf{E}(\rho,0) \rho d\rho d\phi = 1. \tag{2.136}$$

Referring back to Figure 2.8, it can be seen that a and b are the inner and outer radii of the coaxial waveguide, respectively.

The coaxial waveguide aperture admittance, Y_a, is given by

$$Y_a = \frac{\int_0^{2\pi} \int_0^{\infty} \mathbf{E}(\rho,0) \times \mathbf{H}(\rho,0) \rho d\rho d\phi}{\left| \int_0^{2\pi} \int_0^{\infty} \mathbf{E}(\rho,0) \cdot \mathbf{e}_0 \rho d\rho d\phi \right|^2} = 2\pi \int_0^{\infty} E_{\rho_1}(\rho,0) H_{\phi_1}(\rho,0) \rho d\rho. \tag{2.137}$$

Evaluation of (2.137) is accomplished through the use of Parseval's Theorem in two dimensions in a cylindrical coordinate system independent of ϕ:

$$\int_0^{\infty} E_{\rho_1} H_{\phi_1} \rho d\rho = \int_0^{\infty} \mathcal{E}_{\rho_1} \mathcal{H}_{\phi_1} \beta d\beta, \tag{2.138}$$

where $\mathcal{E}_{\rho_1}$ and $\mathcal{H}_{\phi_1}$ are the Fourier-Bessel transforms of E_{ρ_1} and H_{ϕ_1}, at $z = 0$. These transforms can be found from (2.129) and (2.130) and are given by

$$\mathcal{E}_{\rho_1}(\beta) = jk_{z_1} \left[-I_{\psi_1} + R_{\psi_1} \right] \tag{2.139}$$

and

$$\mathcal{H}_{\phi_1}(\beta) = -j\omega\epsilon_1 \left[I_{\psi_1} + R_{\psi_1} \right]. \tag{2.140}$$

Thus the aperture admittance can be written as

$$Y_a = 2\pi \int_0^\infty \{jk_{z_1}[-I_{\psi_1} + R_{\psi_1}]\}\{-j\omega\epsilon_1[I_{\psi_1} + R_{\psi_1}]\}\beta d\beta. \tag{2.141}$$

The unknown quantities in (2.141) are the incident and reflected spectra of Region 1. The boundary condition of continuous tangential electric field at $z = 0$ for each spectral value β gives the relationship between the Region 1 incident and reflected spectra as

$$jk_{z_1}[-I_{\psi_1} + R_{\psi_1}] = \frac{J_0(\beta a) - J_0(\beta b)}{\sqrt{2\pi \ln(b/a)\beta}} = f, \tag{2.142}$$

where the Fourier-Bessel transform of the aperture electric field is denoted by f for the sake of brevity. Substitution of(2.142) into (2.141) allows the aperture admittance to be written as

$$Y_a = \frac{1}{\ln(b/a)} \int_0^\infty \frac{(-j\omega\epsilon_1[I_{\psi_1} + R_{\psi_1}])}{f} \frac{(J_0(\beta a) - J_0(\beta b))^2}{\beta} d\beta. \tag{2.143}$$

In order to use the aperture admittance in the calculation of the reflection coefficient, it must first be normalized with respect to the dominant mode waveguide admittance:

$$Y_n = \frac{Y_a}{Y_g} = \frac{Y_a}{Y_0\sqrt{\epsilon_{rc}}}, \tag{2.144}$$

where Y_0 is the admittance in the waveguide and ϵ_{rc} is the relative permittivity of the waveguide material. Thus, the reflection coefficient of the coaxial waveguide aperture is given by

$$\Gamma = \frac{1 - Y_n}{1 + Y_n}. \tag{2.145}$$

A few items about the integration in (2.143) must be stated. The β integration is performed along the path in the complex β plane shown in Figure 2.9. The integration path is deformed from the real axis so as to avoid surface wave poles. Surface wave poles can occur on the real axis when there is at least one lossless dielectric layer in any of the five configurations of Figure 2.1. These poles occur

in the interval $k_0 \leq \beta \leq \epsilon_r k_0$, where ϵ_r is the greater of the two real relative permittivities, or is the only real relative permittivity. Loss in the dielectric layer(s) causes the layer(s) surface wave poles to move below the real axis. The integration path starts at $\beta = 0$, goes to $k_0 + j0.4k_0$, then to $|\epsilon_{rg}|k_0 + j0.4k_0$, $2|\epsilon_{rg}|k_0$, and then $\infty + j0$. This integration path was determined experimentally and found to work well. The integration path crosses no poles during its deformation from the real axis, so no residues need to be computed and included in the integral.

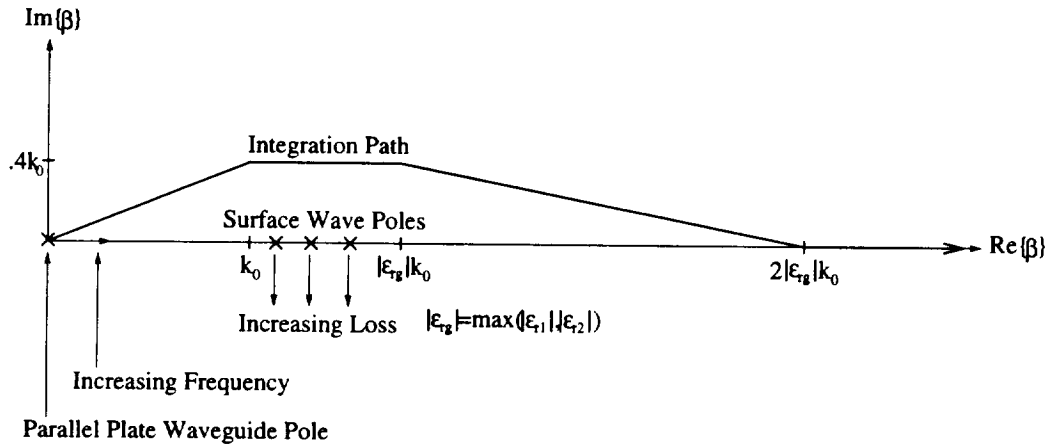

Figure 2.9: Integration path in the complex β plane, with surface wave poles and parallel plate waveguide pole (PEC sheet backed cases only).

If there is a PEC sheet present, an additional complication occurs when the frequency is high enough to excite one or more parallel plate waveguide modes. A mode manifests itself as a pole in the complex β plane by appearing at $\beta = 0$ at the cutoff frequency, and then moves along the positive real axis as the frequency increases. No provision has been included in the codes for this contingency, since the codes are to be used only at frequencies where there are no propagating parallel plate waveguide modes.

However, the solution for the reflection coefficient is by no means complete. The aperture admittance is still dependent on the unknown spectra I_{ψ_1} and R_{ϕ_1}, which are dependent on the boundary conditions given by the particular dielectric slab/resistive or PEC sheet configuration in contact with the aperture ground plane.

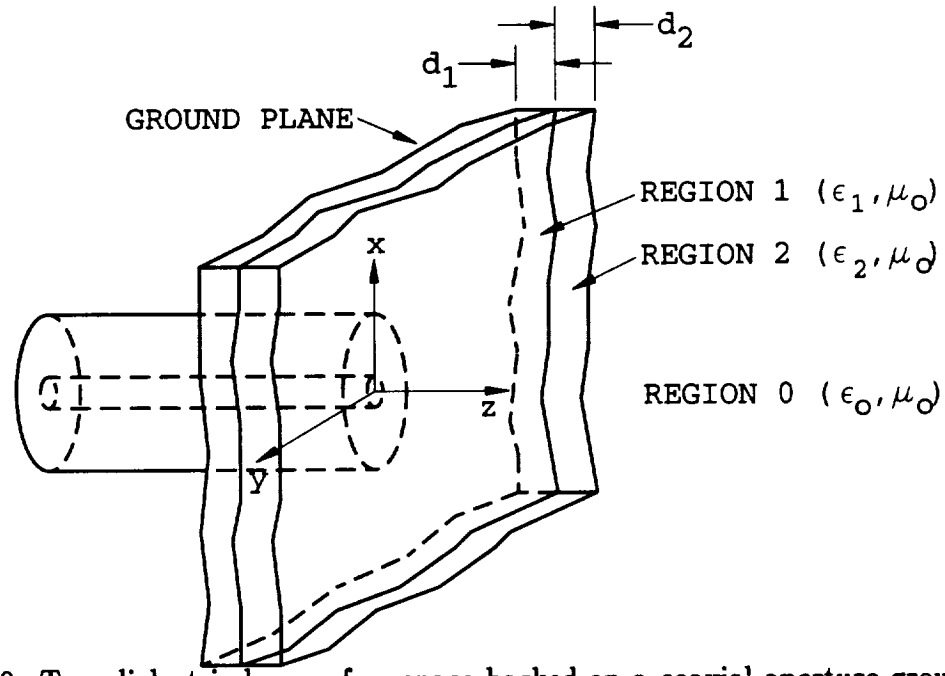

Figure 2.10: Two dielectric layers, free space backed on a coaxial aperture groundplane.

The following subsections give the derivation of I_{ψ_1} and R_{ϕ_1} for the five configurations under investigation.

2.2.1 Two Dielectric Layers - Free Space Backed

Figure 2.10 shows two dielectric layers, free space backed, on a coaxial aperture groundplane. The width of the first layer is d_1, and the width of the second layer is $d_2 - d_1$. The spectra I_{ψ_1} and R_{ψ_1} are determined by the enforcement of the boundary conditions at the three interfaces at $z = 0$, d_1, and d_2. The boundary condition enforcement occurs at every spectral value β. The enforcement of boundary conditions results in a system of linear equations with the spectra as unknowns to be solved. The boundary conditions with their resulting equations are listed here:

The boundary condition of continuous tangential electric field across the interface at $z = 0$ gives the equation:

$$-jk_{z_1} I_{\psi_1} + jk_{z_1} R_{\psi_1} = f. \tag{2.146}$$

The boundary condition of continuous tangential electric field across the interface at $z = d_1$ gives the equation:

$$k_{z_1} I_{\psi_1} e^{-jk_{z_1} d_1} - k_{z_1} R_{\psi_1} e^{jk_{z_1} d_1} = k_{z_2} I_{\psi_2} e^{-jk_{z_2} d_1} - k_{z_2} R_{\psi_2} e^{jk_{z_2} d_1}. \tag{2.147}$$

The boundary condition of continuous tangential magnetic field across the interface at $z = d_1$ gives the equation:

$$\epsilon_{r_1} I_{\psi_1} e^{-jk_{z_1} d_1} + \epsilon_{r_1} R_{\psi_1} e^{jk_{z_1} d_1} = \epsilon_{r_2} I_{\psi_2} e^{-jk_{z_2} d_1} + \epsilon_{r_2} R_{\psi_2} e^{jk_{z_2} d_1}. \tag{2.148}$$

The boundary condition of continuous tangential electric field across the interface at $z = d_2$ gives the equation:

$$k_{z_2} I_{\psi_2} e^{-jk_{z_2} d_2} - k_{z_2} R_{\psi_2} e^{jk_{z_2} d_2} = k_{z_0} T_{\psi_0} e^{-jk_{z_0} d_2}. \tag{2.149}$$

The boundary condition of continuous tangential magnetic field across the interface at $z = d_2$ gives the equation:

$$\epsilon_{r_2} I_{\psi_2} e^{-jk_{z_2} d_2} + \epsilon_{r_2} R_{\psi_2} e^{jk_{z_2} d_2} = T_{\psi_0} e^{-jk_{z_0} d_2}. \tag{2.150}$$

These five linear equations in the five unknown spectra form this matrix equation:

$$\begin{bmatrix} z_{11} & z_{12} & 0 & 0 & 0 \\ z_{21} & z_{22} & z_{23} & z_{24} & 0 \\ z_{31} & z_{32} & z_{33} & z_{34} & 0 \\ 0 & 0 & z_{43} & z_{44} & z_{45} \\ 0 & 0 & z_{53} & z_{54} & z_{55} \end{bmatrix} \begin{bmatrix} I_{\psi_1} \\ R_{\psi_1} \\ I_{\psi_2} \\ R_{\psi_2} \\ T_{\psi_0} \end{bmatrix} = \begin{bmatrix} f \\ 0 \\ 0 \\ 0 \\ 0 \end{bmatrix}, \tag{2.151}$$

where

$$\begin{aligned} z_{11} &= -jk_{z_1}, & z_{33} &= -\epsilon_{r_2} e^{-jk_{z_2} d_1}, \\ z_{12} &= jk_{z_1}, & z_{34} &= -\epsilon_{r_2} e^{+jk_{z_2} d_1}, \\ z_{21} &= k_{z_1} e^{-jk_{z_1} d_1}, & z_{43} &= k_{z_2} e^{-jk_{z_2} d_2}, \\ z_{22} &= -k_{z_1} e^{+jk_{z_1} d_1}, & z_{44} &= -k_{z_2} e^{+jk_{z_2} d_2}, \\ z_{23} &= -k_{z_2} e^{-jk_{z_2} d_1}, & z_{45} &= -k_{z_0} e^{-jk_{z_0} d_2}, \\ z_{24} &= k_{z_2} e^{+jk_{z_2} d_1}, & z_{53} &= \epsilon_{r_2} e^{-jk_{z_2} d_2}, \\ z_{31} &= \epsilon_{r_1} e^{-jk_{z_1} d_1}, & z_{54} &= \epsilon_{r_2} e^{+jk_{z_2} d_2}, \\ z_{32} &= \epsilon_{r_1} e^{+jk_{z_1} d_1}, & z_{55} &= -e^{-jk_{z_0} d_2}. \end{aligned} \tag{2.152}$$

In the code (2.151) is solved numerically for the spectra I_{ψ_1} and R_{ψ_1}.

2.2.2 Two Dielectric Layers - PEC Sheet Backed

Figure 2.11 shows two dielectric layers, PEC sheet backed, on a coaxial aperture groundplane. The width of the first layer is d_1, and the width of the second layer is $d_2 - d_1$. The PEC sheet is located at $z = d_2$. The spectra I_{ψ_1} and R_{ψ_1} are determined by the enforcement of the boundary conditions at the three interfaces at $z = 0$, d_1, and d_2. The boundary condition enforcement occurs at each spectral value β. The enforcement of boundary conditions results in a system of linear equations with the spectra as unknowns to be solved. The boundary conditions and resulting equations at $z = 0$ and $z = d_1$ are the same as for the free space backed case of 2.2.1.

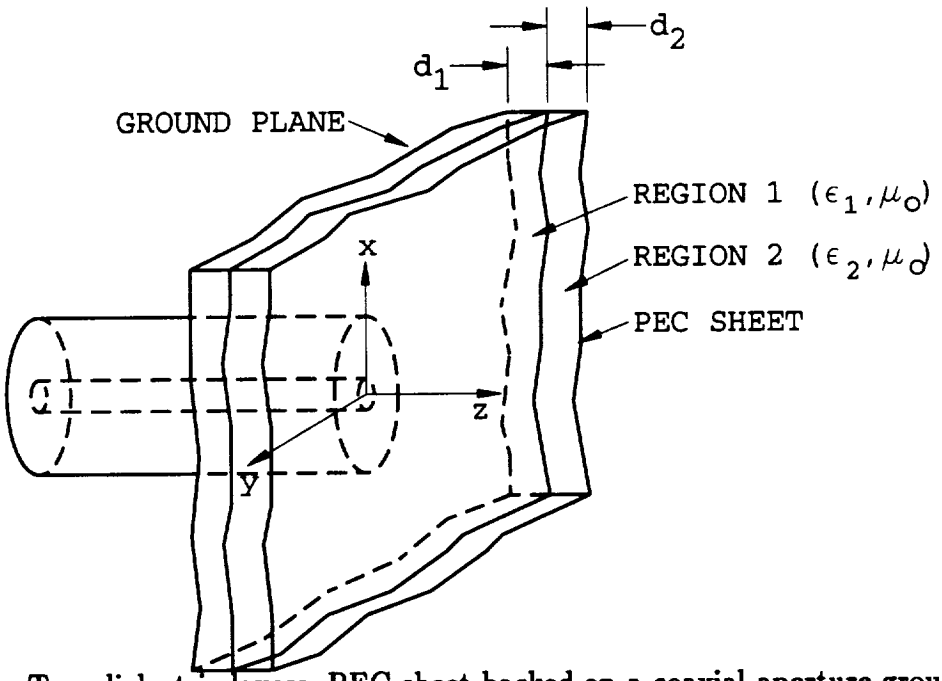

Figure 2.11: Two dielectric layers, PEC sheet backed on a coaxial aperture groundplane.

The boundary condition at $z = d_2$ is that of vanishing tangential electric field, which produces the equation:

$$k_{z_2} I_{\psi_2} e^{-jk_{z_2}d_2} - k_{z_2} R_{\psi_2} e^{jk_{z_2}d_2} = 0. \tag{2.153}$$

(2.146)-(2.148), and (2.153) form a linear system of four equations in four unknown spectra, given by the matrix equation:

$$\begin{bmatrix} z_{11} & z_{12} & 0 & 0 \\ z_{21} & z_{22} & z_{23} & z_{24} \\ z_{31} & z_{32} & z_{33} & z_{34} \\ 0 & 0 & z_{43} & z_{44} \end{bmatrix} \begin{bmatrix} I_{\psi_1} \\ R_{\psi_1} \\ I_{\psi_2} \\ R_{\psi_2} \end{bmatrix} = \begin{bmatrix} f \\ 0 \\ 0 \\ 0 \end{bmatrix}, \tag{2.154}$$

where

$$\begin{aligned} z_{11} &= -jk_{z_1}, & z_{31} &= \epsilon_{r_1} e^{-jk_{z_1}d_1}, \\ z_{12} &= jk_{z_1}, & z_{32} &= \epsilon_{r_1} e^{+jk_{z_1}d_1}, \\ z_{21} &= k_{z_1} e^{-jk_{z_1}d_1}, & z_{33} &= -\epsilon_{r_2} e^{-jk_{z_2}d_1}, \\ z_{22} &= -k_{z_1} e^{+jk_{z_1}d_1}, & z_{34} &= -\epsilon_{r_2} e^{+jk_{z_2}d_1}, \\ z_{23} &= -k_{z_2} e^{-jk_{z_2}d_1}, & z_{43} &= k_{z_2} e^{-jk_{z_2}d_2}, \\ z_{24} &= k_{z_2} e^{+jk_{z_2}d_1}, & z_{44} &= -k_{z_2} e^{+jk_{z_2}d_2}. \end{aligned} \tag{2.155}$$

In the code (2.154) is solved numerically for the spectra I_{ψ_1} and R_{ψ_1}.

2.2.3 One Dielectric Layer - Resistive Sheet Backed

Figure 2.12 shows one dielectric layer, resistive sheet backed, on a coaxial aperture groundplane. The width of the single layer is d_1. The resistive sheet is located at $z = d_1$. The spectra I_{ψ_1} and R_{ψ_1} are determined by the enforcement of the boundary conditions at the two interfaces at $z = 0$ and d_1. The boundary condition enforcement occurs at each spectral value β. The enforcement of boundary conditions results in a system of linear equations with the spectra as unknowns to be solved. The boundary conditions and resulting equations at $z = 0$ and are the same as for the free space backed case of 2.2.1.

The resistive boundary conditions that the electric and magnetic fields obey at $z = d_1$ are

$$\hat{\mathbf{z}} \times (\mathbf{E}_0 - \mathbf{E}_1) = \mathbf{0} \tag{2.156}$$

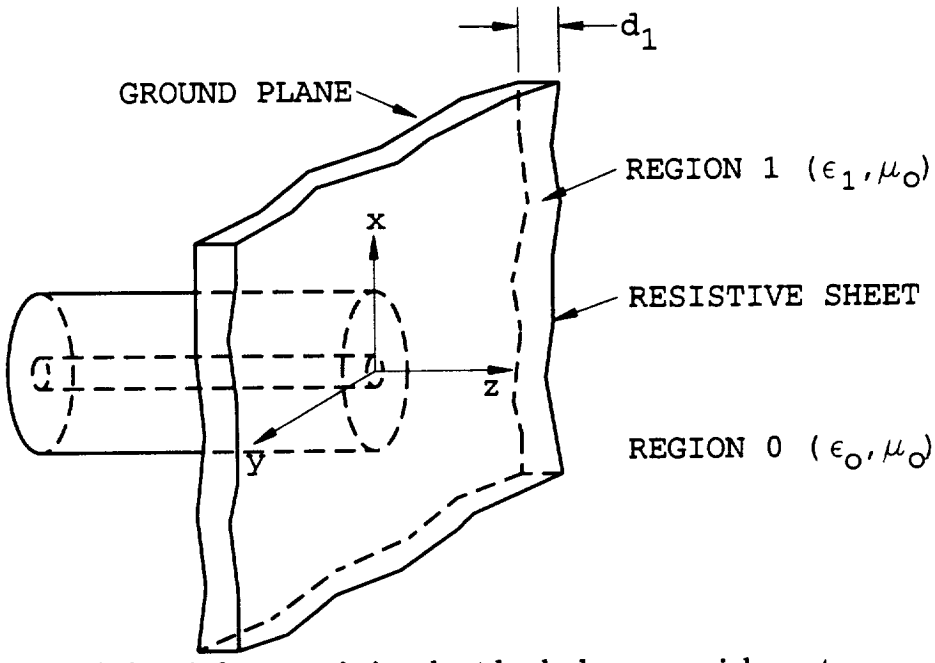

Figure 2.12: One dielectric layer, resistive sheet backed on a coaxial aperture groundplane.

$$\hat{\mathbf{z}} \times \hat{\mathbf{z}} \times \mathbf{E} = -R\hat{\mathbf{z}} \times (\mathbf{H}_0 - \mathbf{H}_1) \tag{2.157}$$

(2.156) gives rise to this equation:

$$k_{z_1} I_{\psi_1} e^{-jk_{z_1}d_1} - k_{z_1} R_{\psi_1} e^{jk_{z_1}d_1} = k_{z_0} T_{\psi_0} e^{-jk_{z_0}d_1}. \tag{2.158}$$

(2.157) gives rise to this equation:

$$\omega\epsilon_1 R I_{\psi_1} e^{-jk_{z_1}d_1} + \omega\epsilon_1 R R_{\psi_1} e^{+jk_{z_1}d_1} = [\omega\epsilon_0 R + k_{z_0}]\, T_{\psi_0} e^{-jk_{z_0}d_1}. \tag{2.159}$$

(2.146), (2.158), and (2.159) form a linear system of three equations in three unknown spectra, given by the matrix equation:

$$\begin{bmatrix} -jk_{z_1} & jk_{z_1} & 0 \\ k_{z_1} e^{-jk_{z_1}d_1} & -k_{z_1} e^{jk_{z_1}d_1} & -k_{z_0} e^{-jk_{z_0}d_1} \\ \omega\epsilon_1 R e^{-jk_{z_1}d_1} & \omega\epsilon_1 R e^{+jk_{z_1}d_1} & -[\omega\epsilon_0 R + k_{z_0}]\, e^{-jk_{z_0}d_1} \end{bmatrix} \begin{bmatrix} I_{\psi_1} \\ R_{\psi_1} \\ T_{\psi_0} \end{bmatrix} = \begin{bmatrix} f \\ 0 \\ 0 \end{bmatrix}. \tag{2.160}$$

In the code (2.160) is solved numerically for the spectra I_{ψ_1} and R_{ψ_1}.

2.2.4 One Dielectric Layer - Free Space Backed

Figure 2.13 shows one dielectric layer, free space backed, on a coaxial aperture groundplane. The width of the single layer is d_1. The matrix equation for the three spectra I_{ψ_1}, R_{ψ_1}, and T_{ψ_0} is readily obtained by letting the resistivity R in (2.160) tend to ∞, giving:

$$\begin{bmatrix} -jk_{z_1} & jk_{z_1} & 0 \\ k_{z_1}e^{-jk_{z_1}d_1} & -k_{z_1}e^{jk_{z_1}d_1} & -k_{z_0}e^{-jk_{z_0}d_1} \\ \epsilon_1 e^{-jk_{z_1}d_1} & \epsilon_1 e^{+jk_{z_1}d_1} & -\epsilon_0 e^{-jk_{z_0}d_1} \end{bmatrix} \begin{bmatrix} I_{\psi_1} \\ R_{\psi_1} \\ T_{\psi_0} \end{bmatrix} = \begin{bmatrix} f \\ 0 \\ 0 \end{bmatrix}. \tag{2.161}$$

In the code (2.161) is solved numerically for the spectra I_{ψ_1} and R_{ψ_1}.

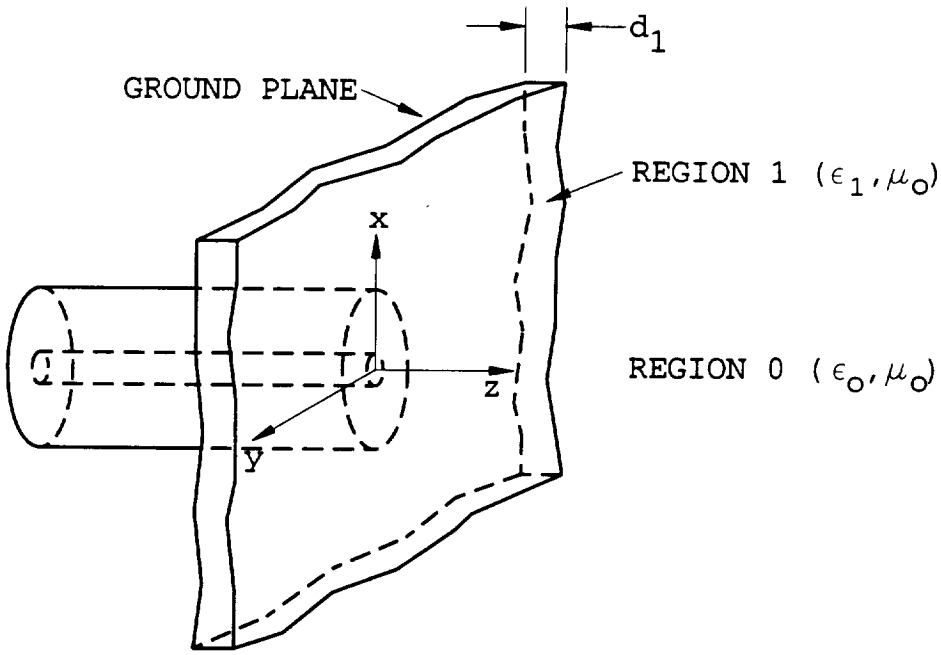

Figure 2.13: One dielectric layer, free space backed on a coaxial aperture groundplane.

2.2.5 One Dielectric Layer - PEC Sheet Backed

Figure 2.14 shows one dielectric layer, PEC sheet backed, on a coaxial aperture groundplane. The width of the single layer is d_1. Since only the sum $I_\psi + R_\psi$ in (2.143) is necessary for the admittance calculation, and is in a compact form readily obtained by letting R go to 0 in (2.160), it is presented here:

$$I_\psi + R_\psi = \frac{f}{k_{z_1} \tan(k_{z_1} d_1)} \tag{2.162}$$

This spectral sum is the expression employed in the code for the single PEC sheet backed dielectric layer case.

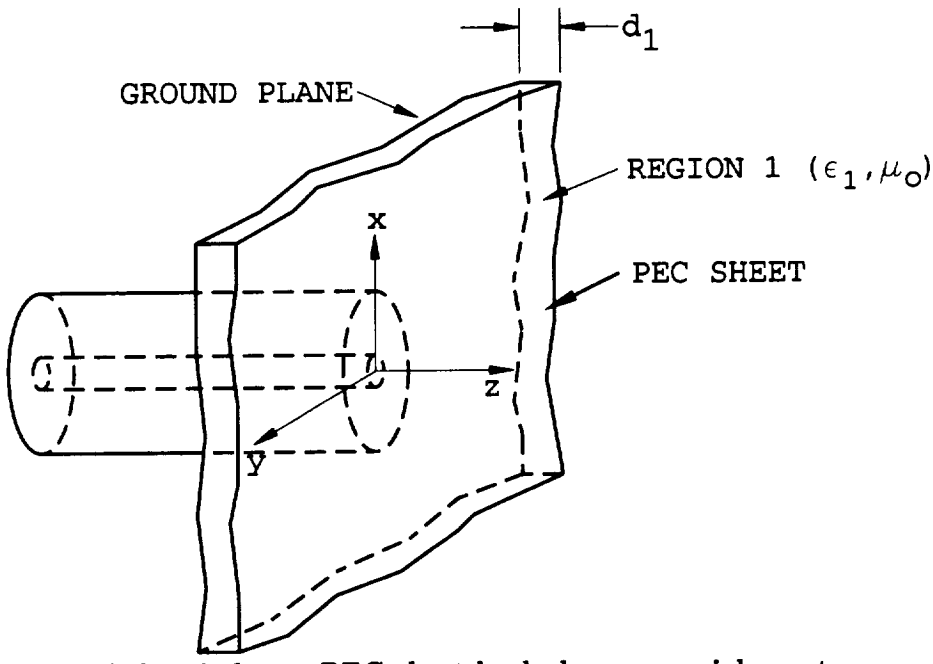

Figure 2.14: One dielectric layer, PEC sheet backed on a coaxial aperture groundplane.

Chapter 3

Parameter Study

A parameter study employing the numerical model of the previous chapter has been conducted. The parameter study focuses on three topics. The first is the behavior of the reflection coefficient for a single free space or PEC sheet backed dielectric layer when permittivity is a parameter fixed over frequency. The second is the validity of the approximation of a thin dielectric layer by a thin resistive sheet. The third is a study of the errors introduced by air gaps and the neglect of higher order modes.

3.1 Single Layer

In this section the single layer geometries of Figures 2.6, 2.7, 2.13, and 2.14 are studied. In all cases the thickness of the dielectric sheet is $d_1 = .2''$. The permittivity parameter ϵ_r is set at either 2, 4, 6, or 8. The rectangular aperture employed is a free space filled X band waveguide aperture with $a = .4''$ and $b = .9''$ at f = 8-12 GHz. The coaxial aperture employed is a Teflon ($\epsilon_r = 2.1$) filled 50Ω coaxial waveguide aperture with $a = .5''$, $b = 1.153''$ at f = .1-2 GHz.

Figure 3.1 shows the reflection coefficient for the rectangular aperture, free space backed case. Figure 3.2 shows the reflection coefficient for the rectangular aperture, PEC sheet backed case. These figures illustrate that the reflection coefficient show a strong dependency upon the permittivity. This is also a very desirable feature since the extraction process will not be as sensitive to measurement noise. The sample

thickness determination is based upon two criteria. The first criterion is to choose a thickness where no nulls are present. The second criterion is to limit the thickness to less than a quarter wavelength in the sample to avoid the generation of surface waves. The presence of surface waves is detrimental for a finite groundplane/sample size. This is due to the surface waves being reflected back to the aperture which changes the aperture impedance from the value for an infinite coated groundplane.

Figure 3.3 shows the reflection coefficient for the coaxial aperture, free space backed case. Figure 3.4 shows the reflection coefficient for the coaxial aperture, PEC sheet backed case. The dependency of the permittivity upon the reflection coefficient is not very strong for the free space back case, at least for this frequency range and coaxial aperture size. More desirable results are obtain when the sample is PEC backed.

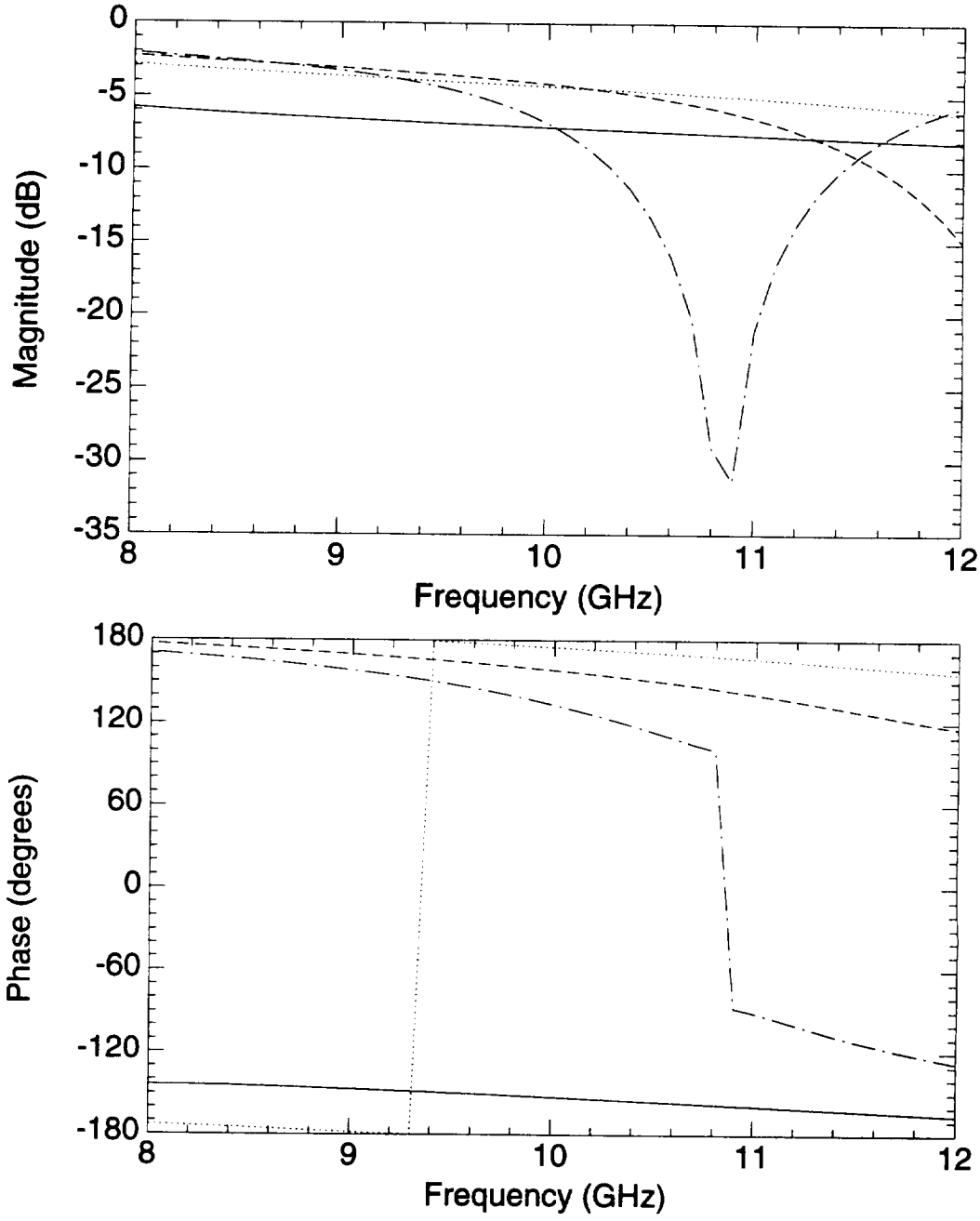

Figure 3.1: Free space filled rectangular X band aperture, .2″ slab, free space backed, ϵ_r = 2-solid, 4-dotted, 6-dashed, 8-dotdashed

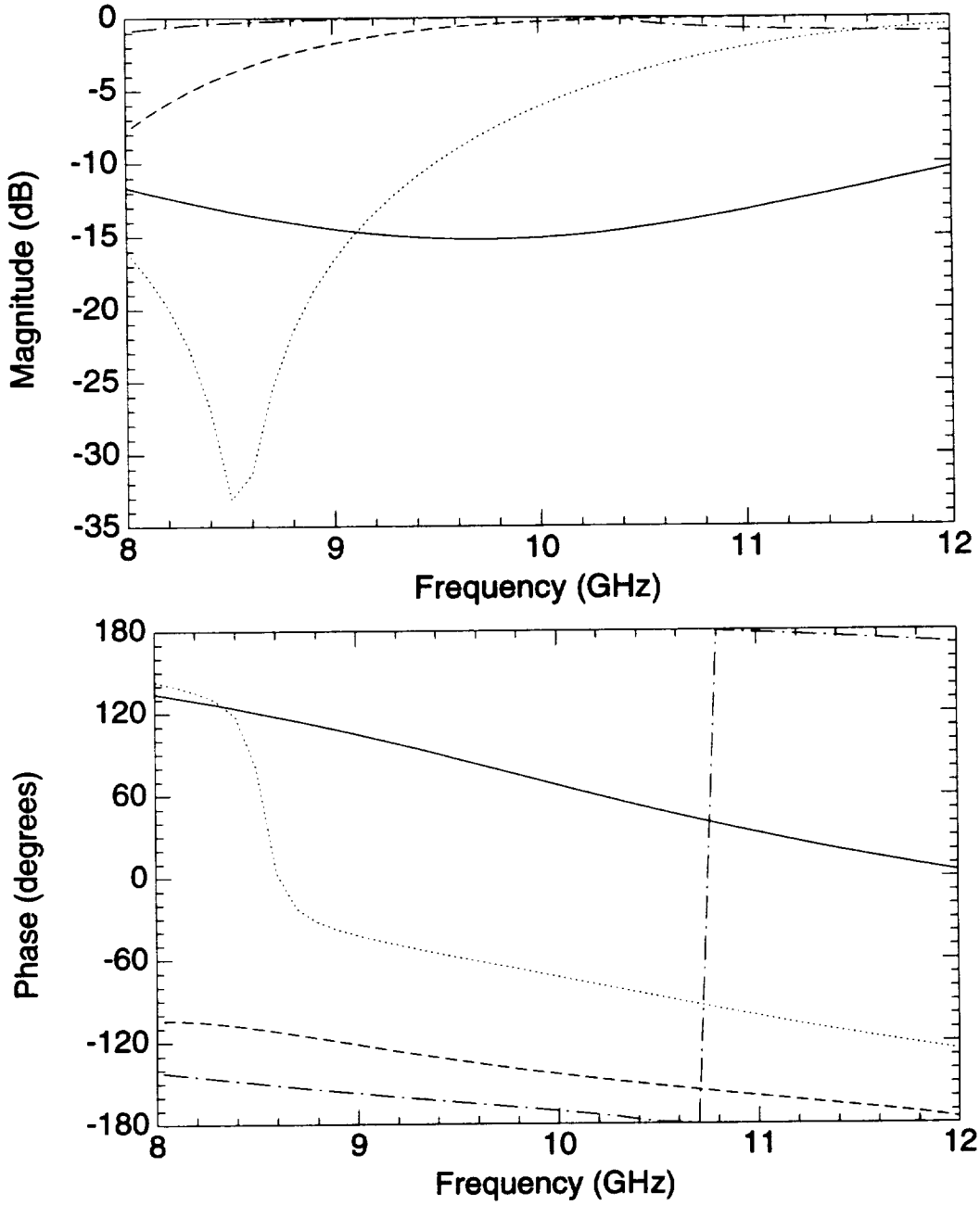

Figure 3.2: Free space filled rectangular X band aperture, .2″ slab, PEC sheet backed, ϵ_r = 2-solid, 4-dotted, 6-dashed, 8-dotdashed

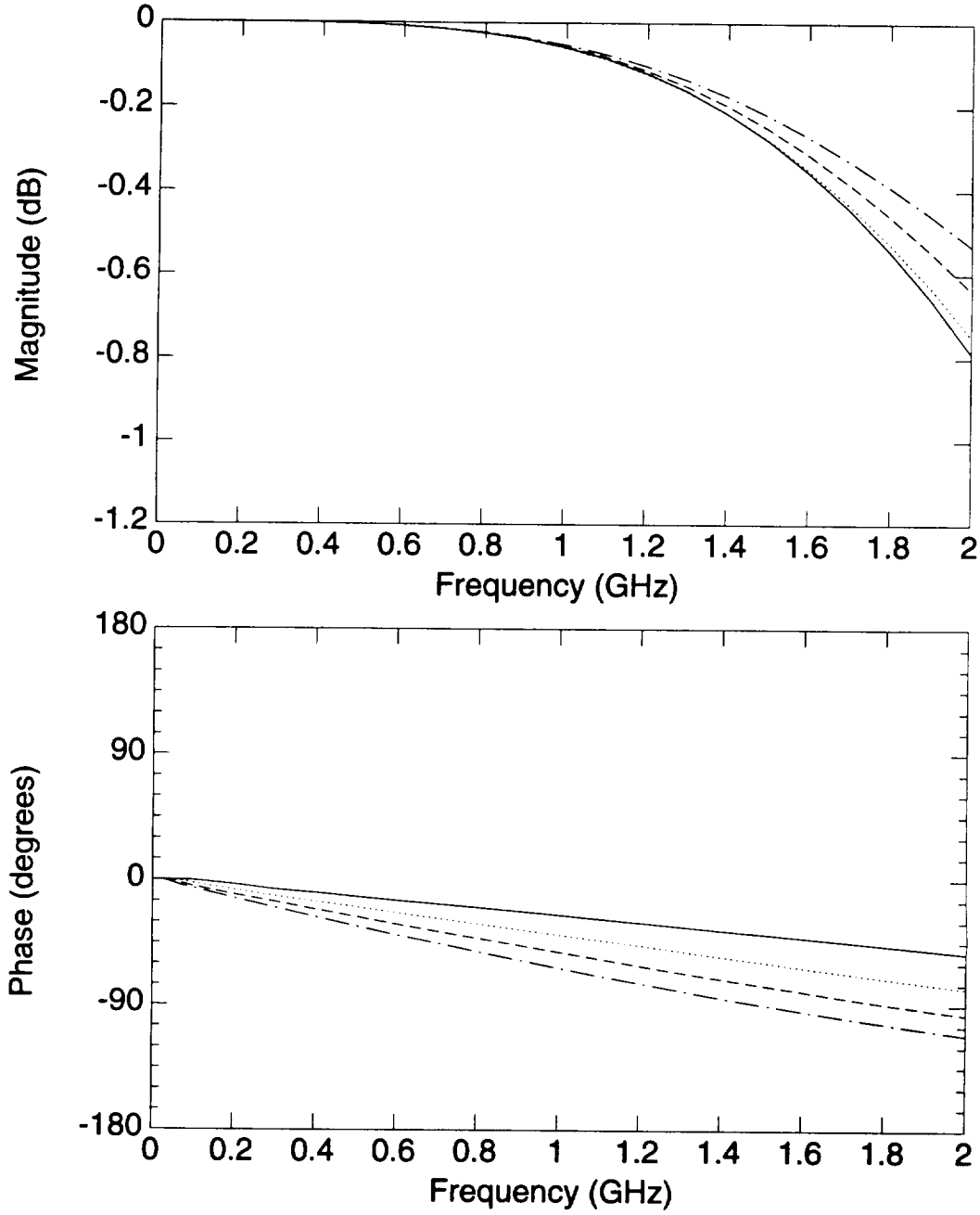

Figure 3.3: Teflon filled 50Ω coaxial aperture, .2″ slab, free space backed, ϵ_r = 2-solid, 4-dotted, 6-dashed, 8-dotdashed

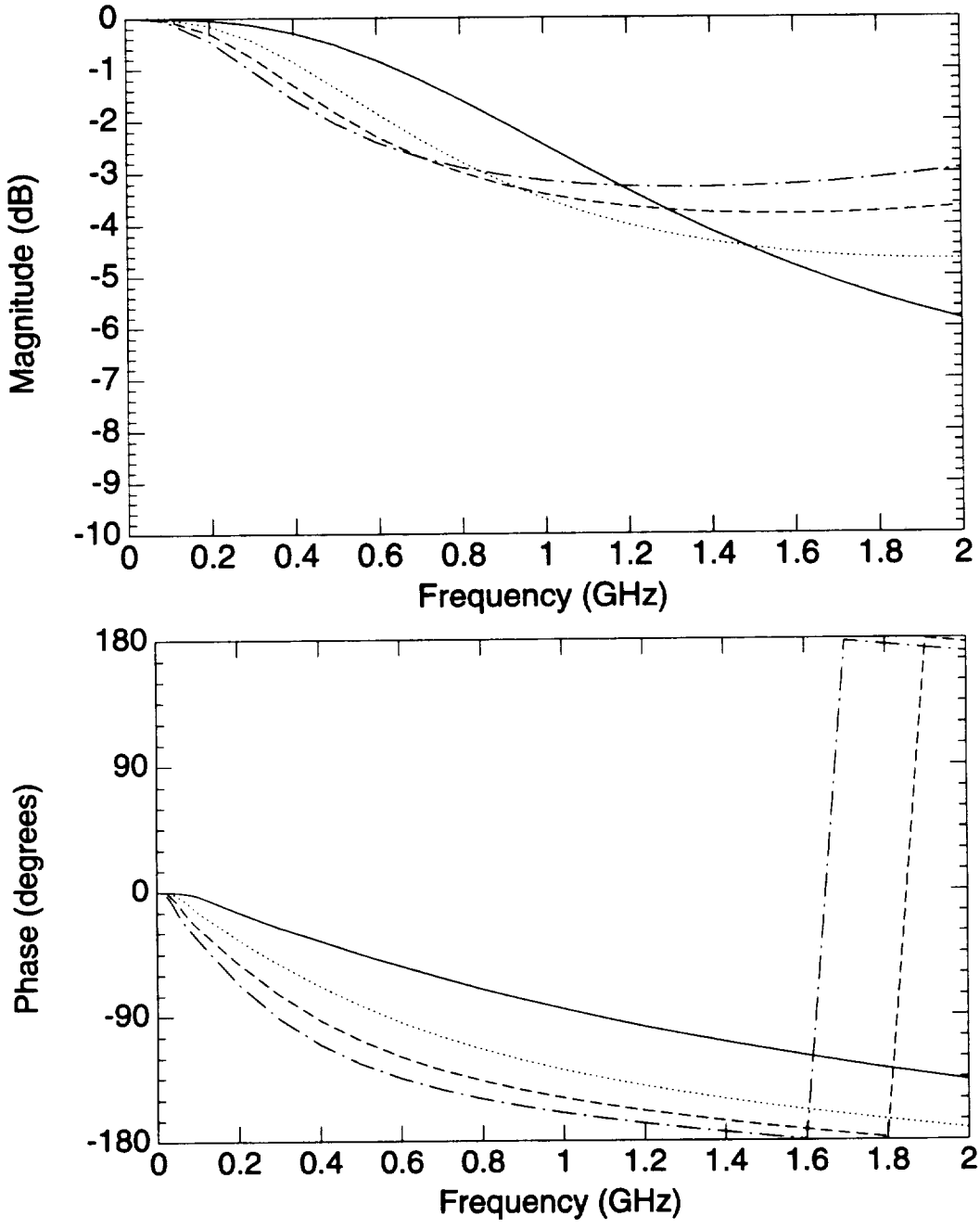

Figure 3.4: Teflon filled 50Ω coaxial aperture, .2″ slab, PEC sheet backed, ϵ_r = 2-solid, 4-dotted, 6-dashed, 8-dotdashed

3.2 Dual Layer

In this section the resistive sheet backed single layer geometry of Figure 2.5 is compared with the free space backed dual layer geometry of Figure 2.3. The aperture employed is a free space filled X band rectangular waveguide aperture with $a = .4''$ and $b = .9''$. The frequency range is f = 8-12 GHz. The dielectric layer in contact with the groundplane has a thickness of $.2''$ and a relative permittivity of $\epsilon_r = 4$. The frequency range is f = 8-12 GHz. The resistive sheet in contact with the single dielectric layer has a resistivity of $R = 10^3\Omega/\square$, $10^4\Omega/\square$, or $10^5\Omega/\square$. The second dielectric layer in the dual layer structure is made of conducting material only;, i.e.,

$$\epsilon_r = 1 - \frac{j\sigma}{2\pi f \epsilon_0}, \tag{3.1}$$

where σ is the conductivity of the material in Siemens (Ω^{-1}). The thickness of the second layer is $t = .002''$. The conductivity of the second layer is chosen to satisfy the resistive sheet approximation to the thin material slab, utilizing the resistivity of the resistive sheet in the single layer configuration:

$$\sigma = \frac{1}{tR}, \tag{3.2}$$

which holds as long as t satisfies the condition [13]

$$|kt/2| = k_0\sqrt{|\epsilon_r|}\frac{t}{2} \ll 1. \tag{3.3}$$

Thus the three values of σ corresponding in order to the respective R values above are 19.7 Ω^{-1}, 1.97 Ω^{-1}, and .197 Ω^{-1}. The quantity $|kt/2|$ for each of the three values of σ is plotted versus frequency in Figure 3.5.

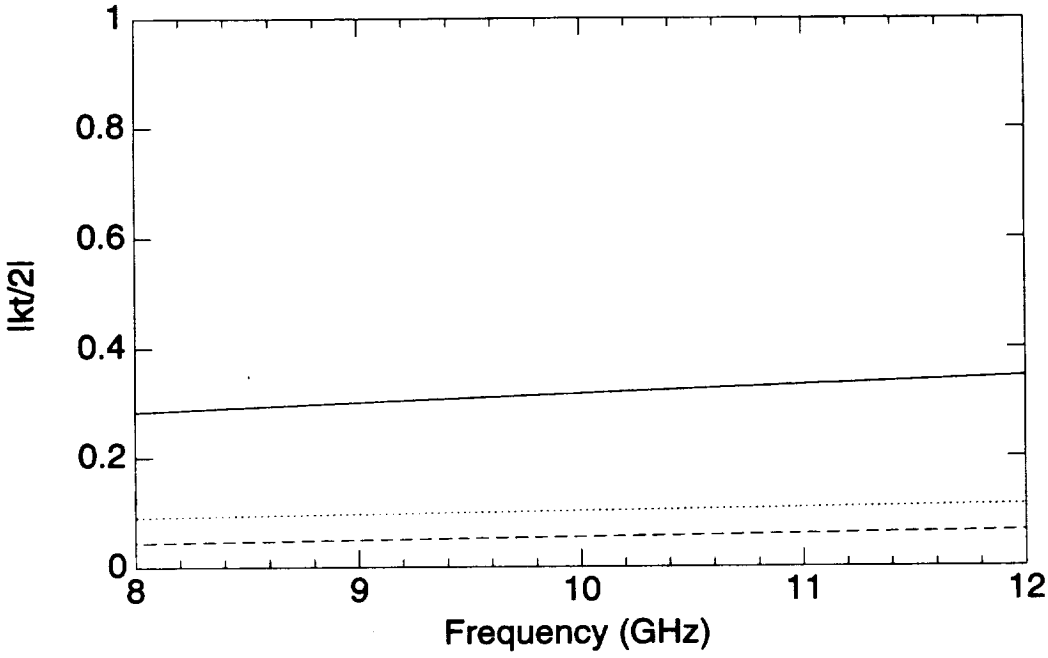

Figure 3.5: $|kt/2|$ versus frequency - $\sigma = 19.7\Omega^{-1}$ - solid, $\sigma = 1.97\Omega^{-1}$ - dotted, $\sigma = .197\Omega^{-1}$ - dashed.

Figure 3.6 shows the reflection coefficient for the single layer, resistive sheet backed cases. Figure 3.7 shows the reflection coefficient for the corresponding dual layer cases. Note that for the case where $|kt/2|$ is the smallest, ($\sigma = .197\Omega^{-1}$) the thin sheet approximation holds. The thin sheet approximation also performs well for the middle σ value, but not well for the largest σ value, where $|kt/2|$ is the largest, on the order of 0.3. This demonstrates the necessity of satisfying the condition that $|kt/2|$ must be much less than 1 in order for the thin sheet approximation to be applicable. Note for a thicker sample, say .02″ thick, the range of R values can vary from $R = 10^2$ to $10^4\Omega/\square$ to have the same performance as the shown cases.

The dependency of the reflection coefficient upon the resistivity of a resistive sheet is demonstrated in Figure 3.8. The resistive sheet varies in resistivity from $0\Omega/\square$ to $3000\Omega/\square$, and is in contact with a .2″ thick dielectric sheet with $\epsilon_r = 4$. The dielectric sheet rests on an X-band rectangular waveguide aperture with a dominant mode excitation of 10 GHz.

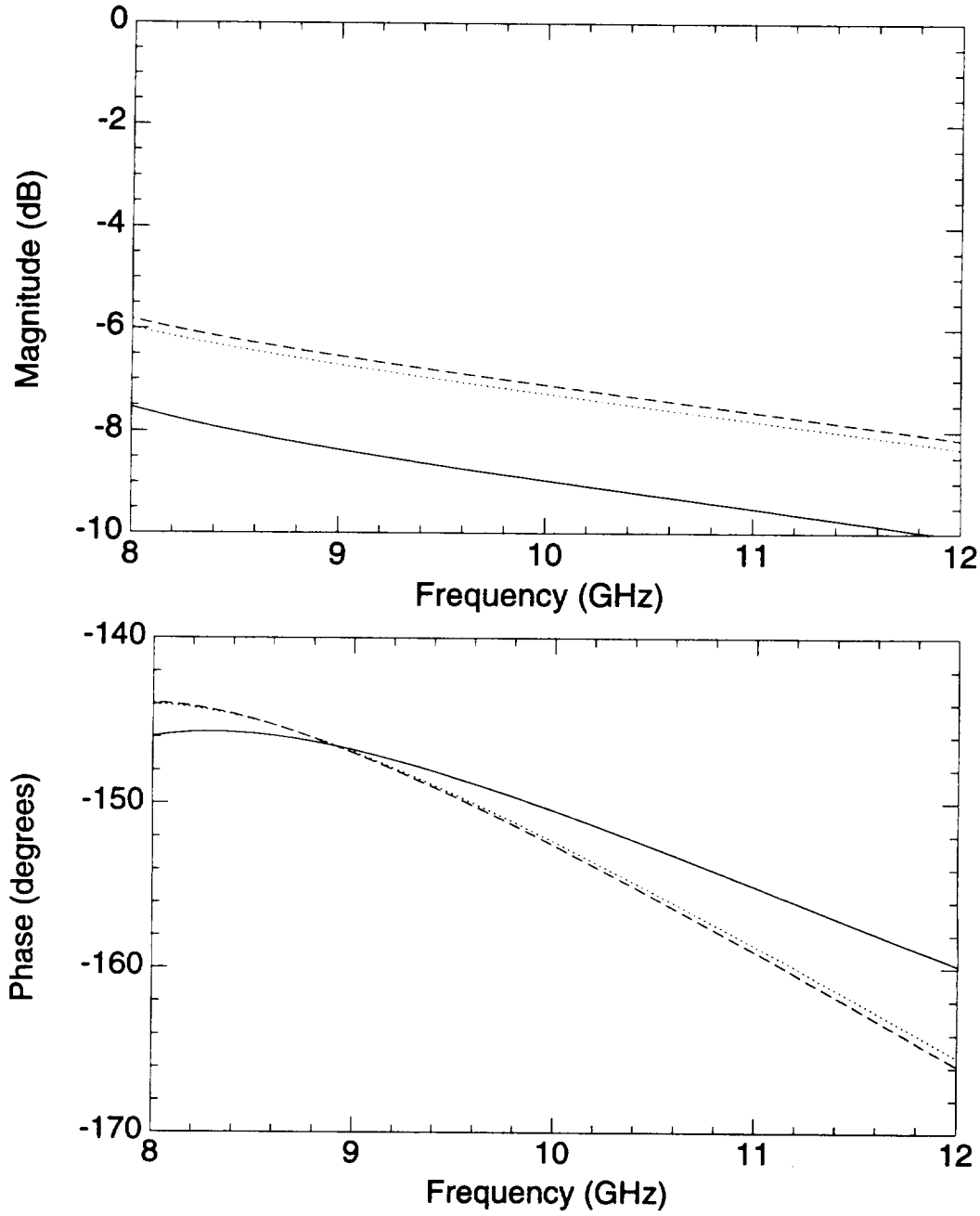

Figure 3.6: Free space filled rectangular X band aperture, Resistive sheet backed, .2″ slab with $\epsilon_r = 4$, $R = 10^3\Omega/\square$ - solid, $R = 10^4\Omega/\square$ - dotted, $R = 10^5\Omega/\square$ - dashed.

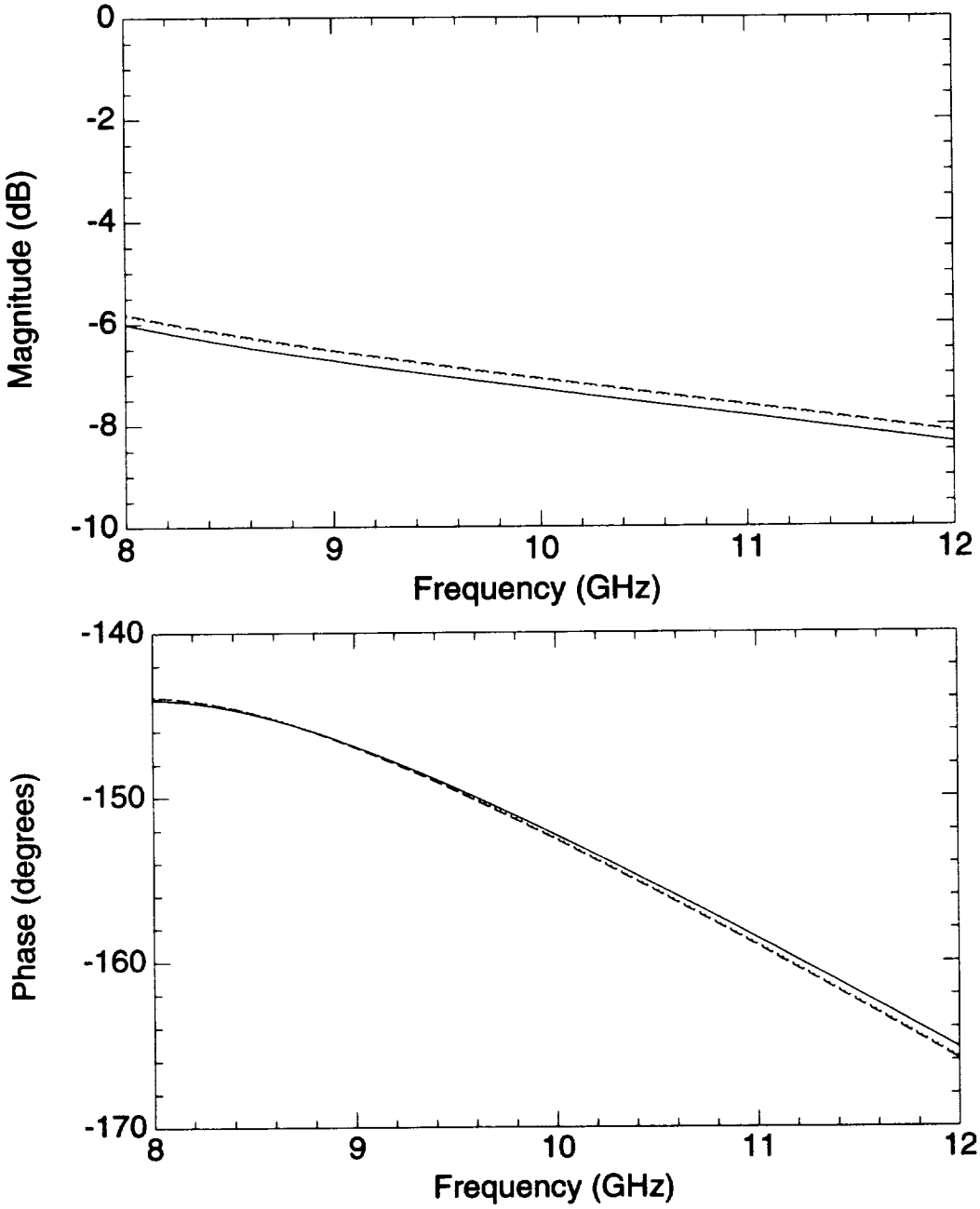

Figure 3.7: Free space filled rectangular X band aperture, .002″ sheet backed, .2″ slab with $\epsilon_r = 4$, $\sigma = 19.7\Omega^{-1}$ - solid, $\sigma = 1.97\Omega^{-1}$ - dotted, $\sigma = .197\Omega^{-1}$ - dashed.

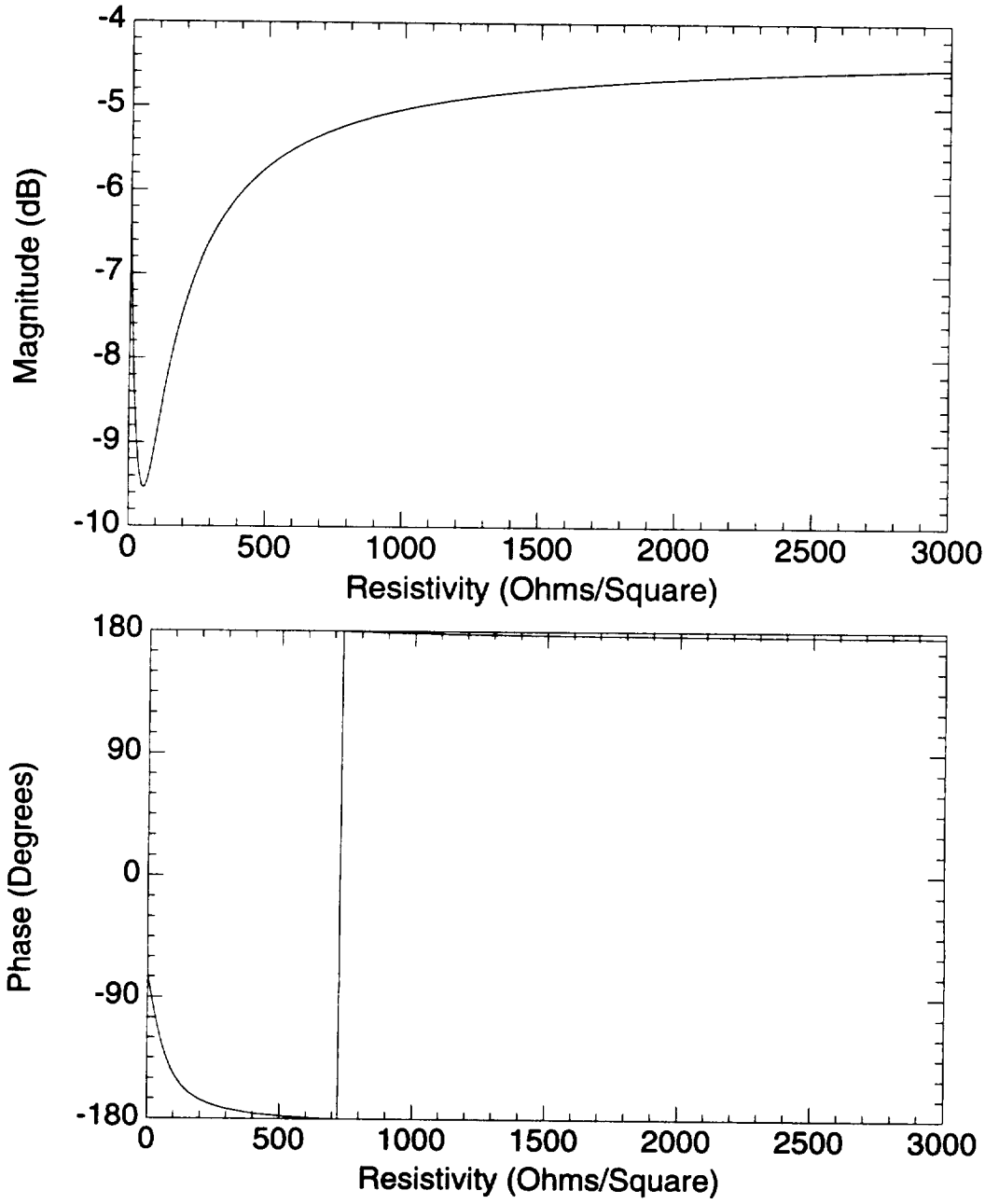

Figure 3.8: Reflection coefficient dependency on resistivity at 10 GHz for a resistive sheet backed .2″ thick dielectric sheet with $\epsilon_r = 4$ on an X-band rectangular waveguide aperture.

3.3 Errors

In this section the errors introduced by air gaps and the neglect of higher order modes are studied. The studies of these two error sources are of practical value. The air gap study will examine the sensitivity of the reflection coefficient measurement to uniform air gaps between the groundplane and the dielectric layer that should be flush with the groundplane. The higher order mode study will examine the limits in frequency where the lowest order mode approximation is valid.

3.3.1 Air Gaps

The air gap study involves the single layer free space backed rectangular aperture geometry of Figure 2.6. The rectangular aperture employed is a free space filled rectangular X band waveguide aperture with $a = .4''$ and $b = .9''$ at f = 8-12 GHz. The coaxial aperture employed is a Teflon filled 50Ω coaxial waveguide aperture with $a = .5''$, $b = 1.153''$ at f = .1-2 GHz. The dielectric sheet has a thickness of $d_1 = .2''$ and relative permittivity of either $\epsilon_r = 4$ or 8.

The reflection coefficient for the rectangular aperture case is shown in Figures 3.9 and 3.10 for $\epsilon_r = 4$ and 8 respectively. The reflection coefficient with no air gap is compared against the reflection coefficients for gaps .05% and .10% the thickness of the dielectric layer. Note that in Figure 3.10 magnitude information near the null is not shown since the null does not contain any useful information. The permittivities extracted from the reflection coefficient for the gap cases assuming there is no gap are shown in Figures 3.11 and 3.12 for $\epsilon_r = 4$ and 8 respectively. It can be seen that as the gap width is increased the extraction becomes more inaccurate. Also, the gap has a greater effect for higher permittivities. Therefore, a higher permittivity sample requires more care in the prevention of air gaps to ensure an accurate permittivity extraction.

The reflection coefficient for the coaxial aperture case is shown for $\epsilon_r = 4$ and 8 in Figures 3.13 and 3.14, respectively. The reflection coefficient with no air gap is

compared against the reflection coefficients for gaps .05% and .10% the thickness of the dielectric layer. The permittivities extracted from the reflection coefficient for the gap cases assuming there is no gap are shown in Figures 3.15 and 3.16 for $\epsilon_r = 4$ and 8 respectively. Note that the errors due to the air gap are not manifested in the real part of the permittivity, but in the imaginary part. As the gap width increases, the error increases. The error is greater for the greater permittivity. Note that great care must be taken to avoid air gaps for the coaxial measurement configuration for even low permittivity samples, since even small gaps produce a significant extraction error.

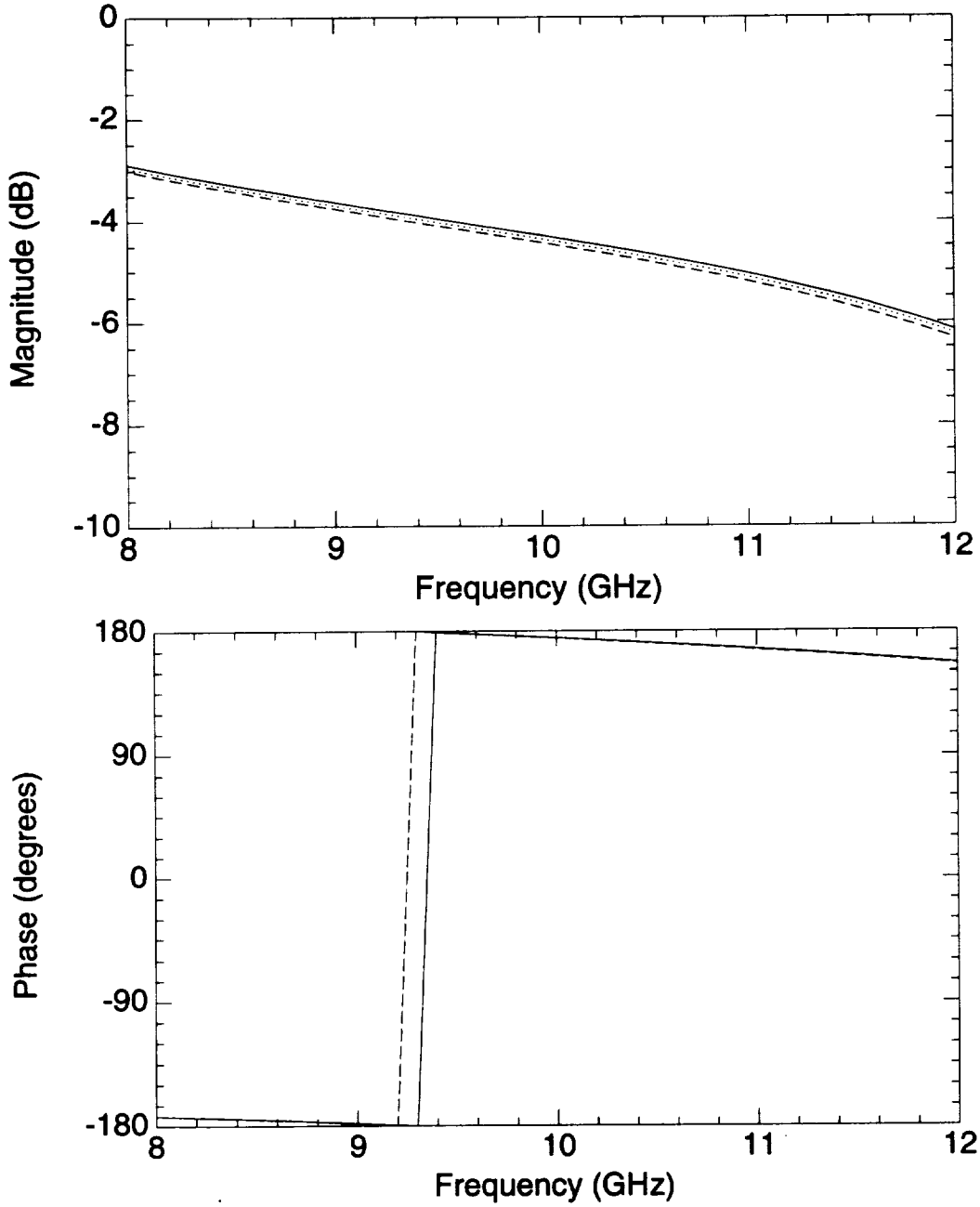

Figure 3.9: Air gap study, X band, .2", $\epsilon_r = 4$. No gap-solid, .05% gap-dotted, .10% gap-dashed.

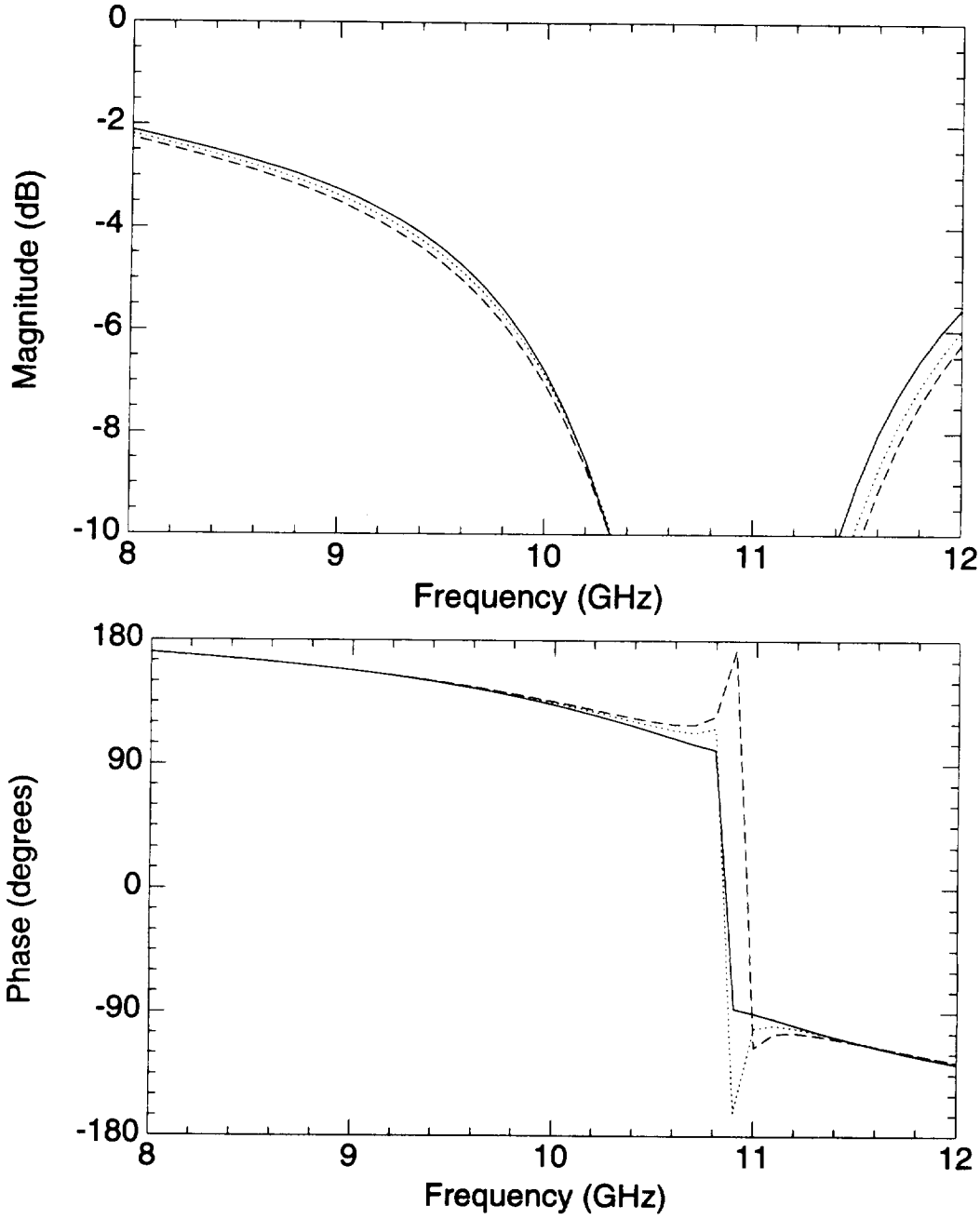

Figure 3.10: Air gap study, X band, .2″, $\epsilon_r = 8$. No gap-solid, .05% gap-dotted, .10% gap-dashed.

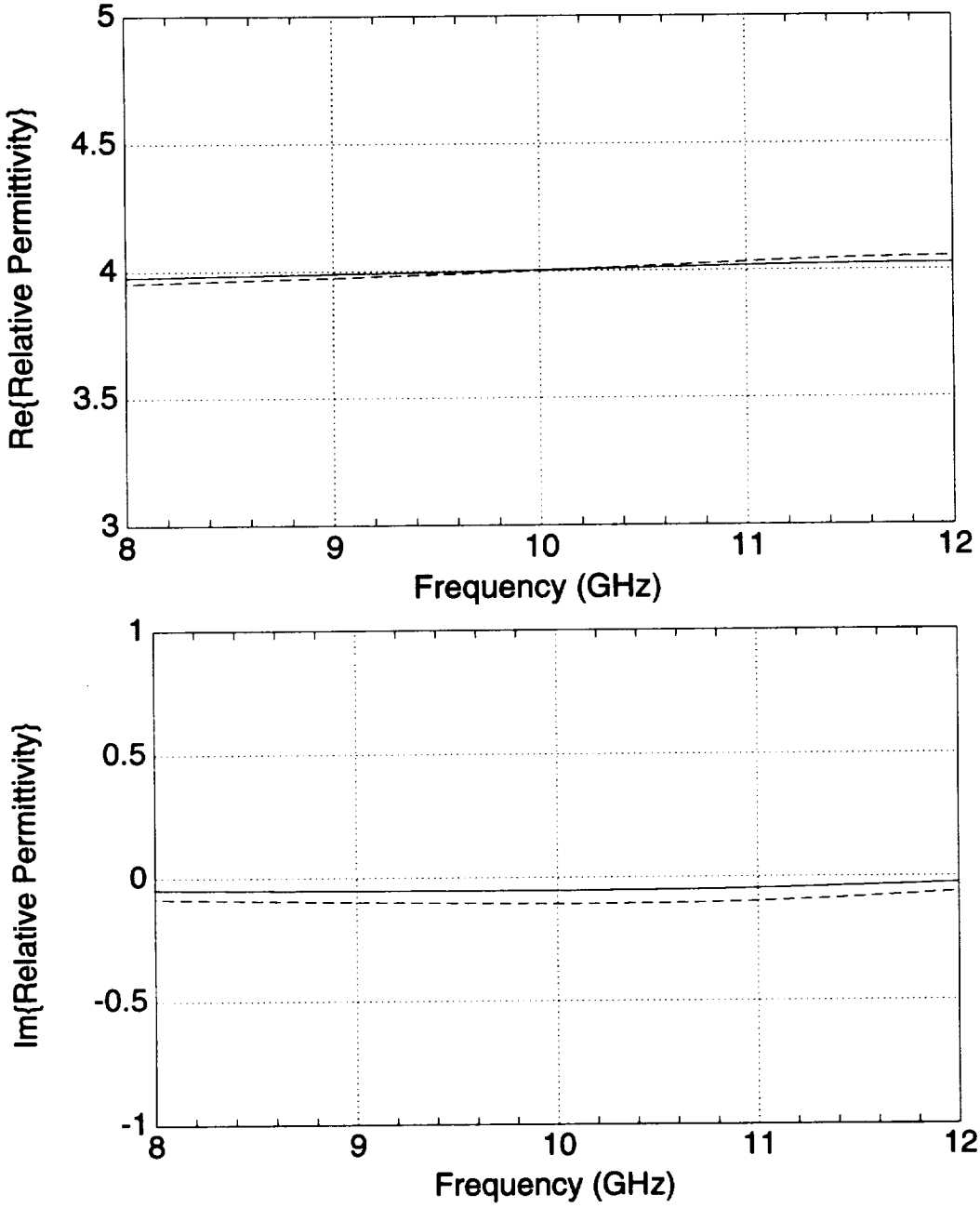

Figure 3.11: Permittivity extraction, X band, .2″, $\epsilon_r = 4$. No gap-solid, .05% gap-dotted, .10% gap-dashed.

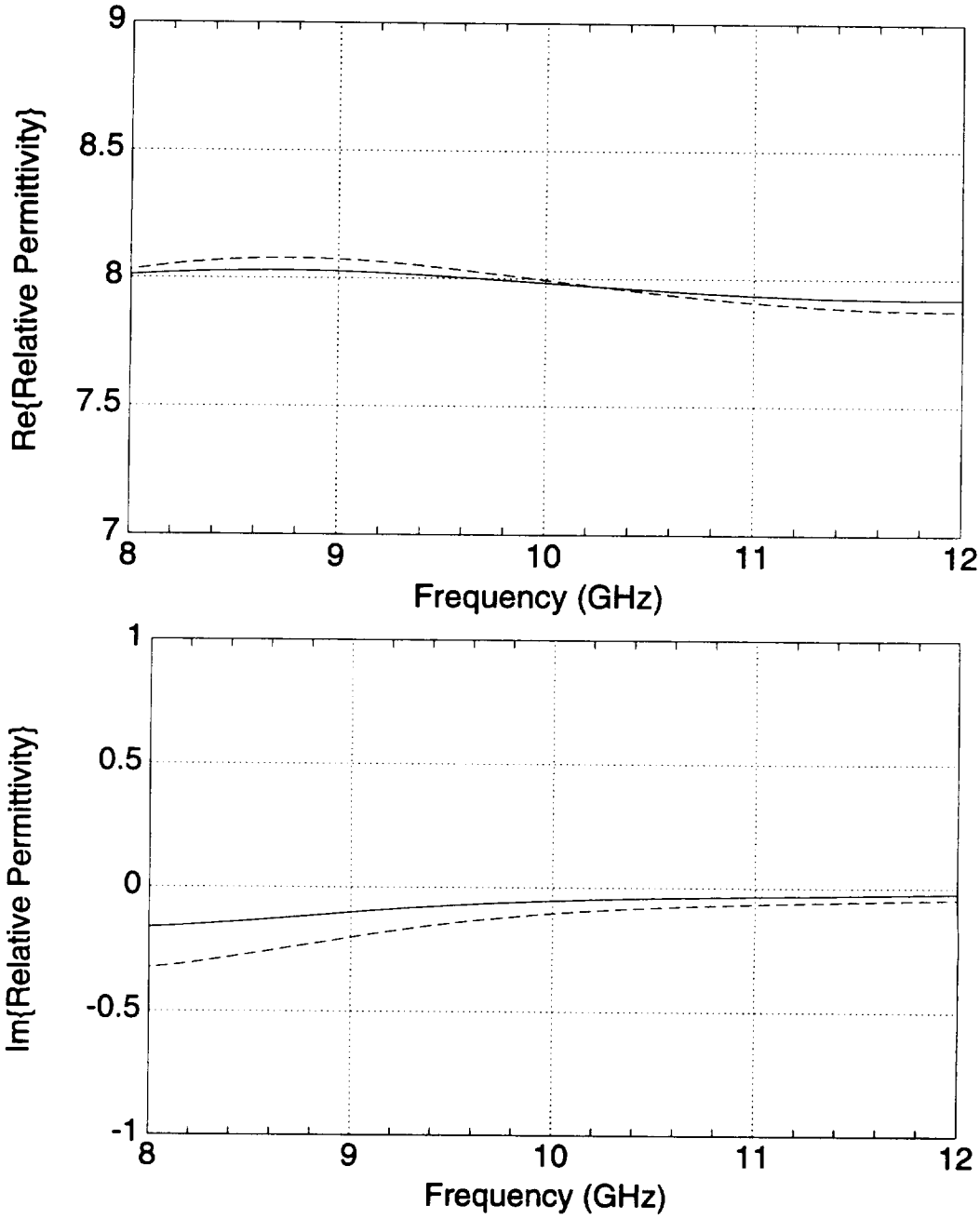

Figure 3.12: Permittivity extraction, X band, .2″, $\epsilon_r = 8$. No gap-solid, .05% gap-dotted, .10% gap-dashed.

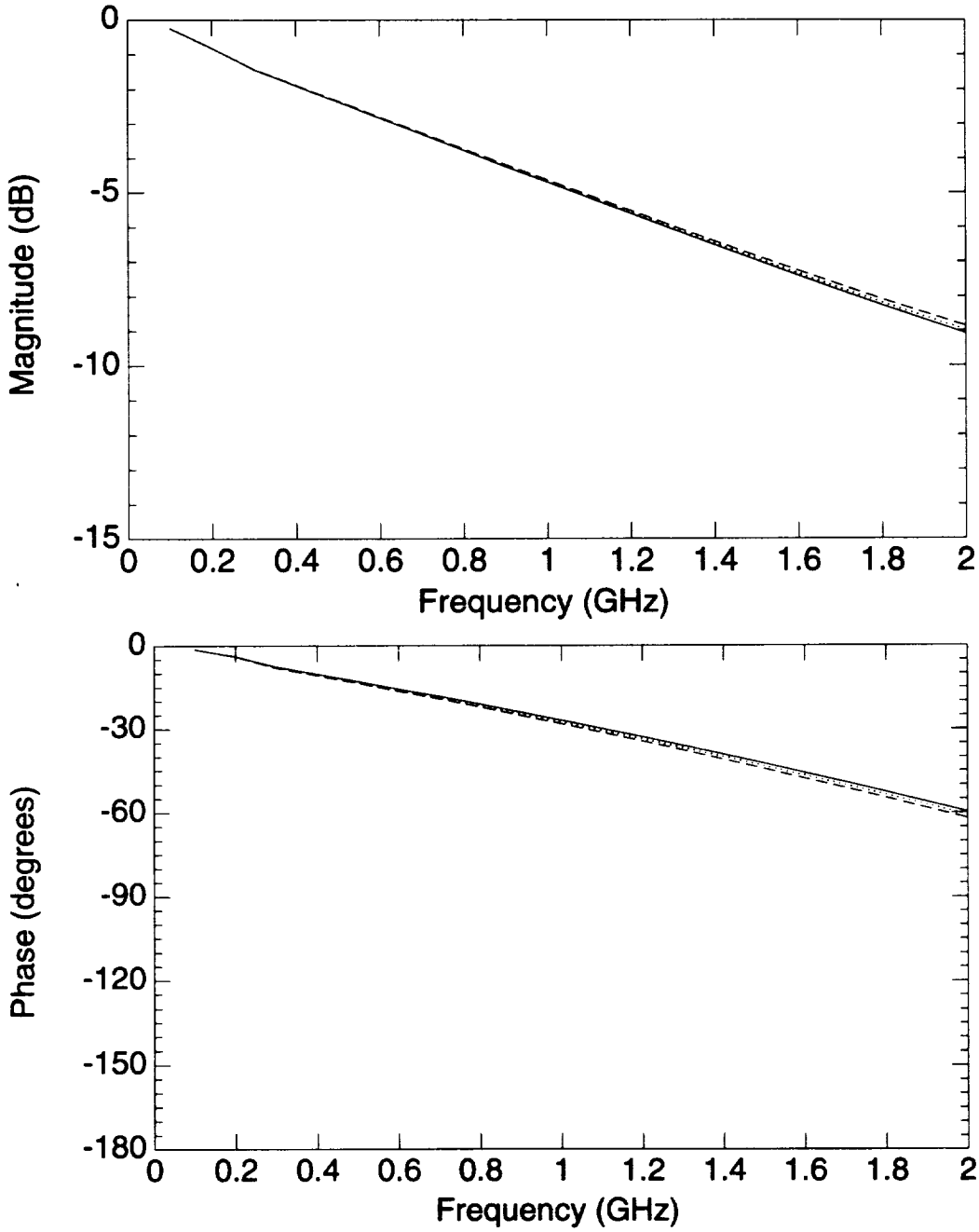

Figure 3.13: Air gap study, coaxial, .2″, $\epsilon_r = 4$. No gap-solid, .05% gap-dotted, .10% gap-dashed.

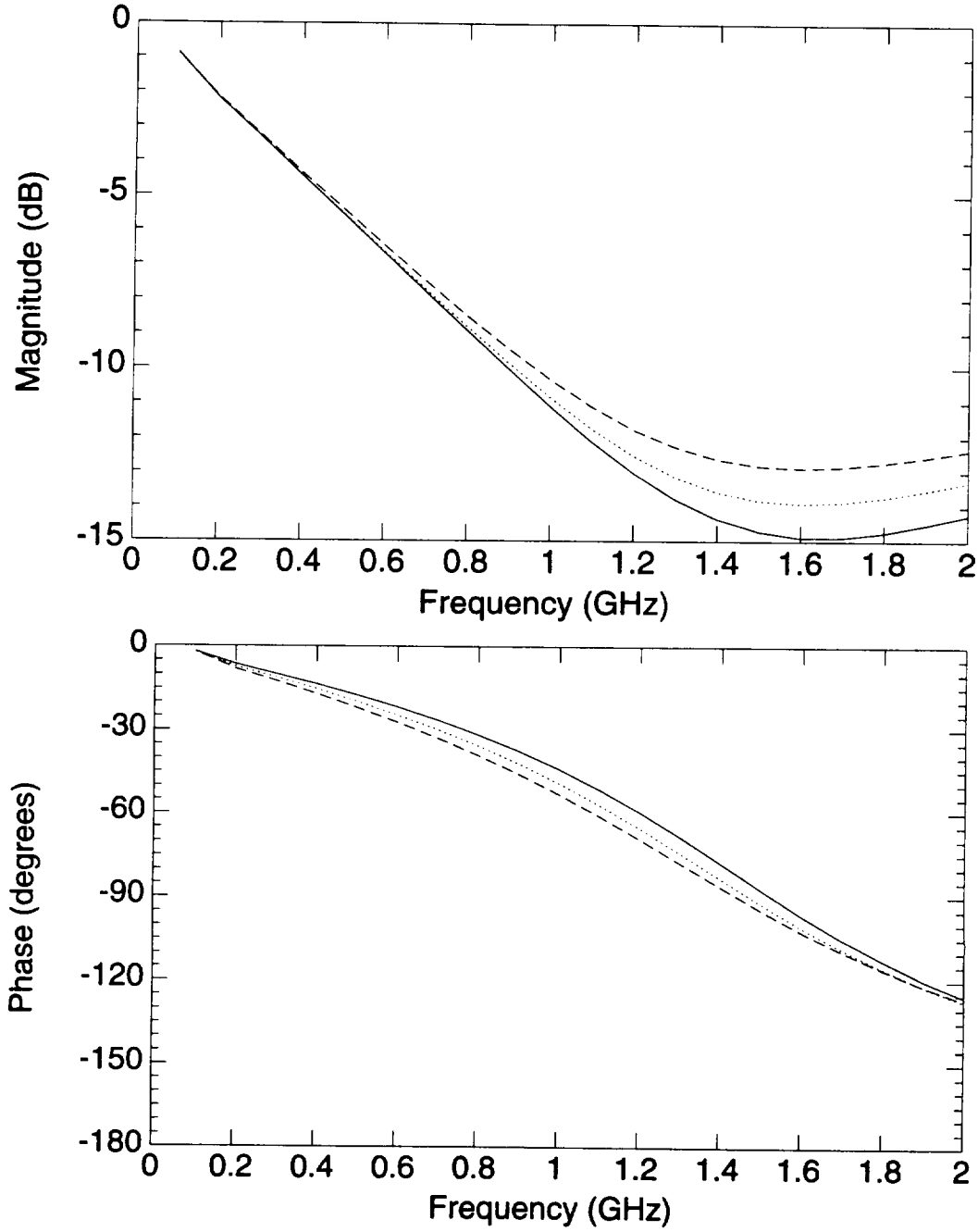

Figure 3.14: Air gap study, X band, .2″, $\epsilon_r = 8$. No gap-solid, .05% gap-dotted, .10% gap-dashed.

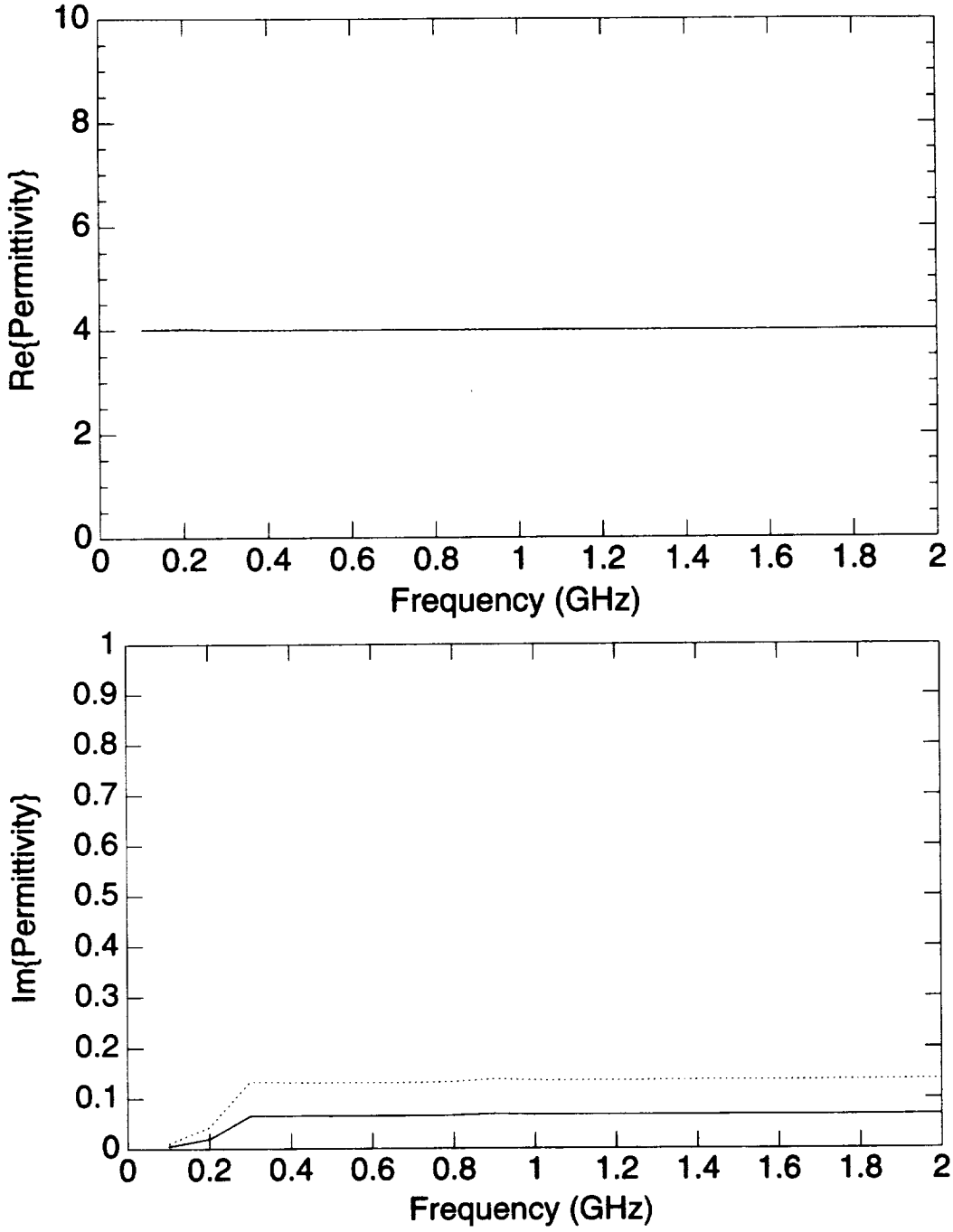

Figure 3.15: Permittivity extraction, coaxial, .2″, $\epsilon_r = 4$. No gap-solid, .05% gap-dotted, .10% gap-dashed.

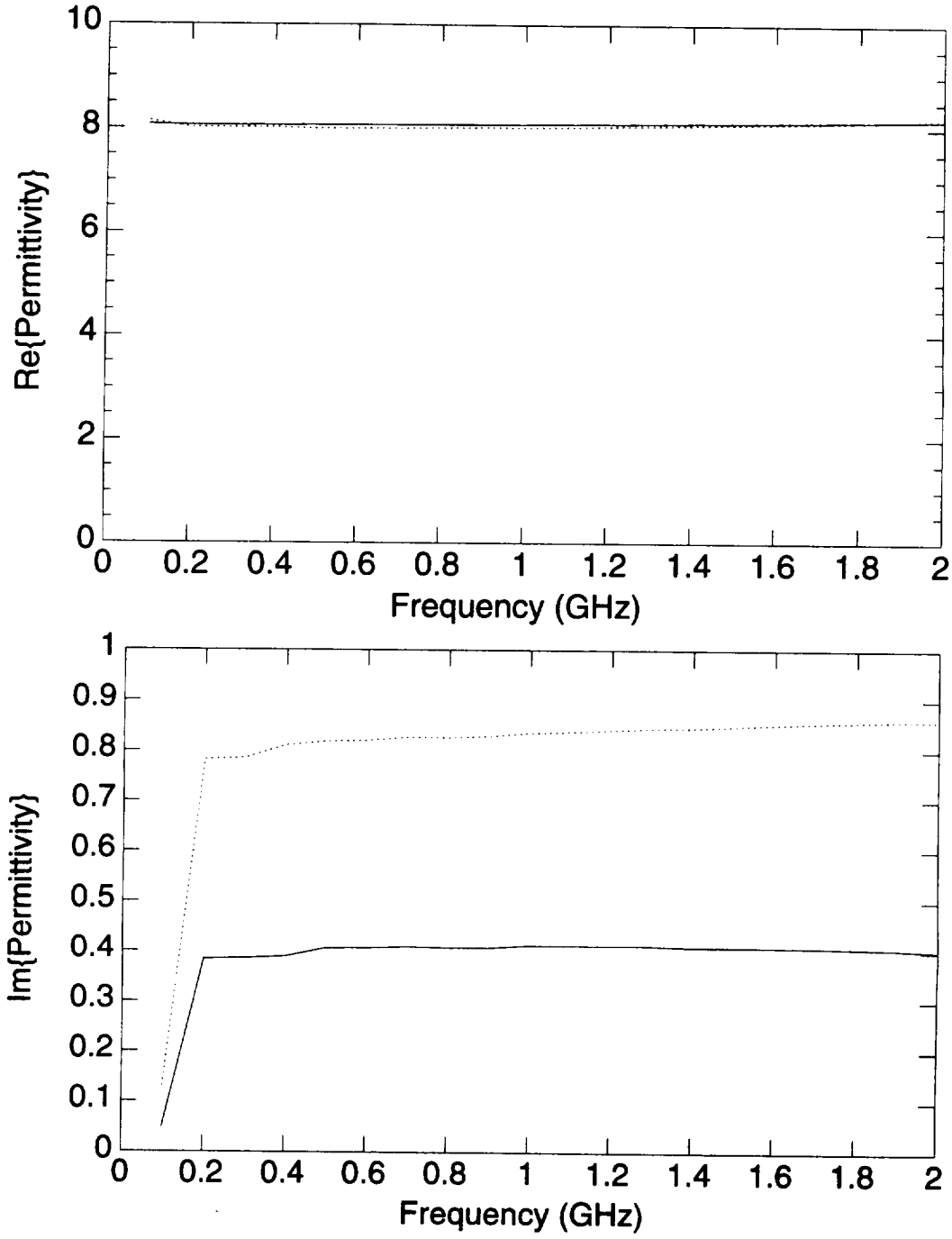

Figure 3.16: Permittivity extraction, coaxial, .2″, $\epsilon_r = 8$. No gap-solid, .05% gap-dotted, .10% gap-dashed.

3.3.2 Higher Order Modes

The existence of higher order modes can occur for both the rectangular and coaxial apertures. Their effect was observed during the calibration of the measured data for the rectangular guide. Generally, three measurements are required to calibrate data. The three measurements originally taken were a short, open and matched load at the aperture. The resulting calibrated data typically had an oscillation which was not explainable. A potential source of error existed in the calibration due to the "exact" reference used for the open measurement. The exact reference value assumed only a TE_{10} in the waveguide at the aperture. The approximation is very reasonable and sufficiently accurate for many applications. However, for inverse problems (such as material parameter determination), this may not be sufficient as shown in the following figures.

The calculated (single mode only) and measured reflection coefficient in the X-band is shown in Figure 3.17. Note that the measured response is offset and lower than the calculated response by approximately 1 dB. An additional calculation using a hybrid FEM/BEM code for an aperture in an infinite groundplane at 10 GHz yielded a reflection coefficient of -12.8 dB which is in agreement with the measurement. The calibration of the measured reflection coefficient for the open aperture used three calibration standards of a short, an offset short and a matched load. Figure 3.18 illustrates the effect of calibrating the measured reflection coefficient for a dielectric (lossy foam, thickness = .595 in.) covered aperture with two sets of calibration standards. One standard set uses a short, an offset short and a matched load where the other standard replaces the offset short with an open aperture (free space) measurement. It is clearly seen that the calibration with the open aperture measurement has a non-physical oscillation. This oscillation can be directly attributed to using only one expansion mode in the waveguide for the exact reference value for the open aperture measurement.

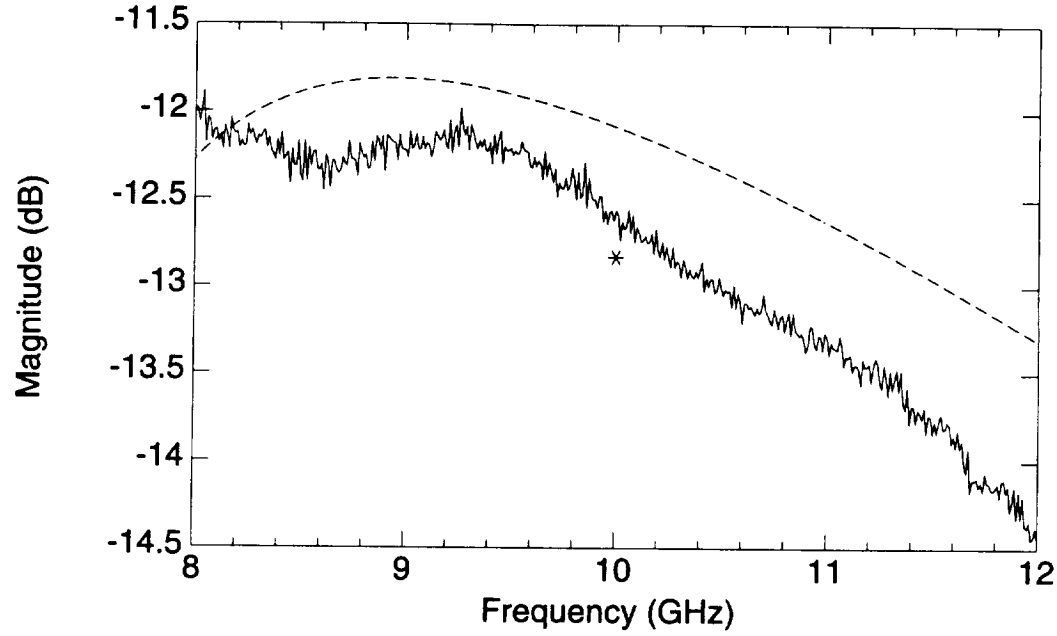

Figure 3.17: Reflection coefficient for a X-band aperture. Measured - solid, calculation (single mode expansion) - dashed, hybrid FEM/BEM calculation - star.

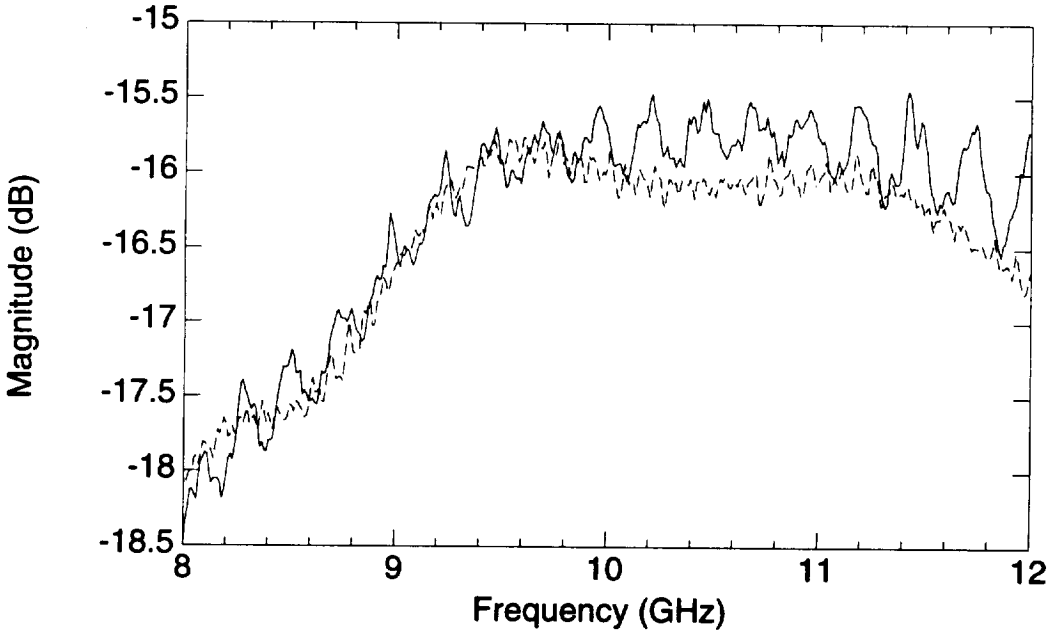

Figure 3.18: Comparison for calibration standards using (solid) and not using (dashed) an open measurement on a lossy foam sample.

The necessity of higher order modes in the analytical solution is very apparent. Most references pertaining to this technique ignore the effect of higher order modes. Of two references that discuss the effect of higher order modes for rectangular apertures, only one has results that demonstrate their importance [8], especially when the aperture has a material covering. The other reference does not consider them to be very important [12]. It should be noted that the formulation and computer software for the coaxial aperture does include the effect of the higher order modes.

Chapter 4

Measurements

The measurement procedure and some results are presented in this chapter. In the first section, a brief discussion of the measurement configuration and calibration is given. In the second section, the Newton-Raphson extraction procedure is described. In the third section, some measured results are presented along with a comparison against the numerical model.

4.1 Measurement Configuration and Calibration

The measurement configuration consists of a Hewlett-Packard 8510B network analyzer with a groundplane fixture having a rectangular aperture in the center of the groundplane. The groundplane measures 9″ square to simulate an infinite groundplane in the 8 to 12 GHz band (X-band). These dimensions allow the separation between the aperture to the groundplane edge to be several wavelengths. Additionally, the perimeters of the aperture and the groundplane are rotated 45 degrees to minimize any direct surface wave/edge diffraction back into the aperture.

The reflection coefficient data must be calibrated before de-embedding of the permittivity can be performed. There are three types of linear errors in reflection coefficient measurements: directivity, frequency response, and source match, represented respectively by the dimensionless quantities E_D, E_R and E_S. All three error terms are complex and frequency dependent, and ideally E_D and E_S are 0 and

E_R is 1. The effect of these three linear errors on the actual reflection coefficient S_{11_a}, which produces the measured reflection coefficient S_{11_m}, can be modeled as the two-port error adapter of Figure 4.1.

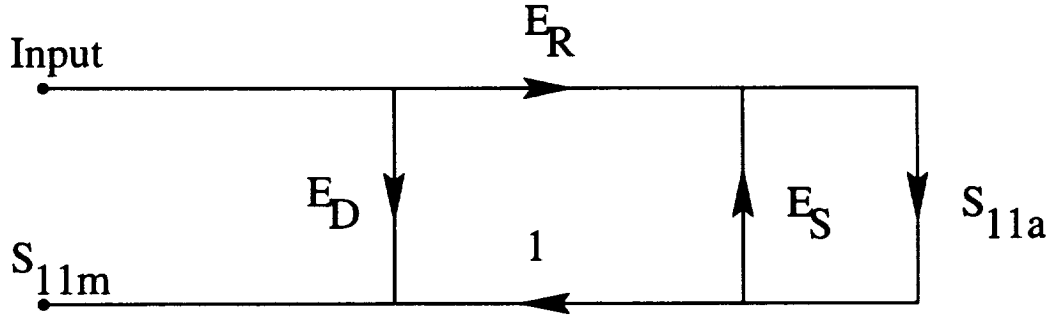

Figure 4.1: One port error model

The values of E_D, E_R, and E_S must be determined for each frequency so that the data can be calibrated. S_{11_a} is related to S_{11_m} through this equation:

$$E_D + \frac{E_R S_{11_a}}{1 - E_S S_{11_a}} = S_{11_m} \tag{4.1}$$

Three such equations as in (4.1) are required for solution of the three unknowns E_D, E_R, and E_S. These are formed by taking three reflection coefficient measurements for which S_{11_a} is known. The three reflection coefficient measurements employed in the calibration code developed are the short circuit, offset short circuit, and matched load. The short circuit is formed by placing a metal plate against the waveguide aperture. The metal plate is typically aluminum and considered PEC so that $S_{11_a} = -1$. The offset short circuit is formed by extending the waveguide 1.2 cm through the use of a material sample holder and shorting the open end. In this case $S_{11_a} = -e^{-jk2d}$ where $d = .012$ m. The matched load is formed by attaching to the aperture a lossy waveguide termination, with an assumed reflection coefficient $S_{11_a} = 0$. With the error terms determined, they are used in the solution of (4.1) for S_{11_a}:

$$S_{11_a} = \frac{S_{11_m} - E_D}{E_S(S_{11_m} - E_D) + E_R}. \tag{4.2}$$

This completes the calibration of the reflection coefficient data.

4.2 Newton-Raphson Extraction Procedure

The permittivity of a material sample is extracted from its calibrated reflection coefficient data via the Newton-Raphson iterative procedure for finding roots of transcendental equations [15]. The general form of the iterative Newton-Raphson equations are

$$f(x) = 0, \tag{4.3}$$

and

$$x_{n+1} = x_n - \frac{f(x_n)}{f'(x_n)}, \tag{4.4}$$

where f is a function of x. It is desired to find an x that satisfies (4.3), which is called a root. The Newton-Raphson procedure is initiated with a guess of the root, called x_0. x_0 is inserted into (4.4), which produces x_1. The process by which x_n is obtained is called the n^{th} iteration. If the function is properly behaved, the x_n's would converge to a zero of (4.3). A convergence criterion on x_n is employed to terminate the Newton-Raphson method when the desired level of accuracy for the zero is achieved.

The permittivity of the material sample is defined to be the zero of this functional:

$$f(\epsilon_h) = \Gamma(\epsilon = \epsilon_h) - \Gamma(\epsilon = \epsilon_s) \tag{4.5}$$

where Γ is the reflection coefficient of the aperture at a certain frequency, which is covered by a dielectric slab of permittivity ϵ and the thickness of the material sample slab. ϵ_h is the permittivity of a homogeneous slab of the same thickness as the sample slab of unknown permittivity ϵ_s.

The use of Γ can be incorporated in one of three ways in (4.5). The first is just to use the magnitude of Γ which is appropriate for a lossless dielectric. The phase of Γ can also be used when the dielectric is lossless. However, when the dielectric is lossy, then the complex value of Γ is required.

A ϵ_h is sought via the Newton-Raphson procedure so that

$$f(\epsilon_h) = 0 \tag{4.6}$$

is true. In order to apply the Newton-Raphson procedure to (4.6), the derivative of $f(\epsilon_h)$, $f'(\epsilon_h)$ must be computed. It is impractical to compute $f'(\epsilon_h)$ exactly, however, a simple approximation to $f'(\epsilon_h)$ is given by the following central difference formula:

$$f'(\epsilon_h) \approx \frac{f(\epsilon_h + \Delta\epsilon) - f(\epsilon_h - \Delta\epsilon)}{2\Delta\epsilon}, \tag{4.7}$$

where $\Delta\epsilon$ is a differential parameter such that $|\Delta\epsilon| \ll 1$.

The convergence criterion of the Newton-Raphson procedure is given by

$$|f(\epsilon_h)| \leq \varepsilon \tag{4.8}$$

where ε is the convergence criterion constant, a small real number such that $|\varepsilon| \ll 1$. At the end of the first iteration when the convergence criterion is met, the Newton-Raphson procedure is terminated and ϵ_h is called the permittivity of the sample material.

4.3 Examples

The permittivity of three samples were extracted from calibrated reflection measurements in the X-band. Prior to de-embedding, the calibrated data was smoothed using a moving average to minimize the effect of noise. The samples were acrylic, epoxy resin, and a carbon loaded foam. The dimensions of the samples are shown in Table 4.1. It should be noted that the accuracy of the material value de-embedding is limited due to the use of a single waveguide mode expansion.

The first example is that of the permittivity extraction of a .111 in. thick acrylic plexiglass sheet. A nominal relative permittivity value for plexiglass at 10 GHz is $\epsilon_r = 2.59 - j0.017$ [14], and varies insignificantly from this value throughout the X band. The raw and calibrated reflection coefficient data is presented in Figure 4.2, along with a comparison against the reference solution for a dielectric sheet of

the same thickness and permittivity. Note that a significant difference occurs in the magnitude between the calibrated and calculated (using the nominal permittivity value) reflection coefficient. One source of error can be due to an air gap between the sample and the groundplane. However, the influence of higher order modes can also account for this and has been shown to be important.

The de-embedded relative permittivity is shown in Figure 4.3 where the complex reflection coefficient was used to obtain both the real and imaginary part of the permittivity. The average de-embedded relative permittivity is approximately 2.3 - j0.1. The discrepancy between the de-embedded and nominal relative permittivities is most likely due to the neglect of higher order modes.

The second example is that of the permittivity extraction from a .256 in. thick epoxy resin sample. Figure 4.4 shows the epoxy's calibrated reflection coefficient data compared against reference curves of the reflection coefficient for a dielectric slab .256 in. with permittivity $\epsilon_r = 8.5$. Note that the calibrated reflection coefficient is corrupted in the region 8-9 GHz, where there is a minimum in the magnitude of the reflection coefficient. The extracted permittivity of the epoxy is shown in Figure 4.5. The permittivity for frequencies below 8.5 GHz were not calculated due to the difficulties introduced by the corruption. Note that the epoxy is found to be basically lossless with a relative permittivity ranging from 9.5 at 8.5 GHz down to 8.0 at 12 GHz. Note that the imaginary component of the dielectric constant is positive for some frequencies. This behavior can be attributed to error introduced when higher order modes are ignored in the aperture. The effect of these the higher order modes become more apparent for electrically thick material coatings [8].

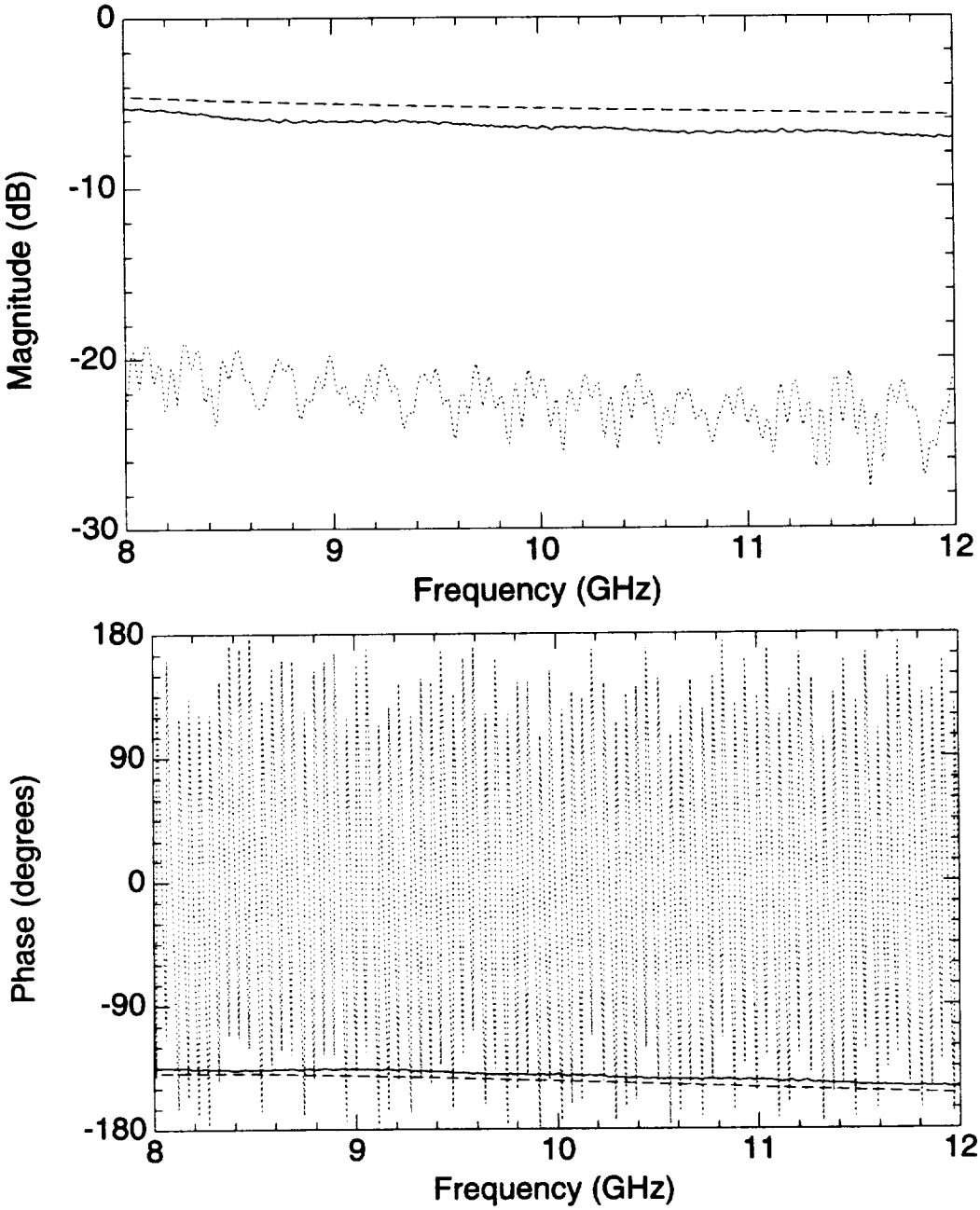

Figure 4.2: Reflection coefficient data for an X band rectangular aperture reflection measurement of a plexiglass sheet .111 in. thick. (Raw - solid, calibrated - dotted, reference - dashed.)

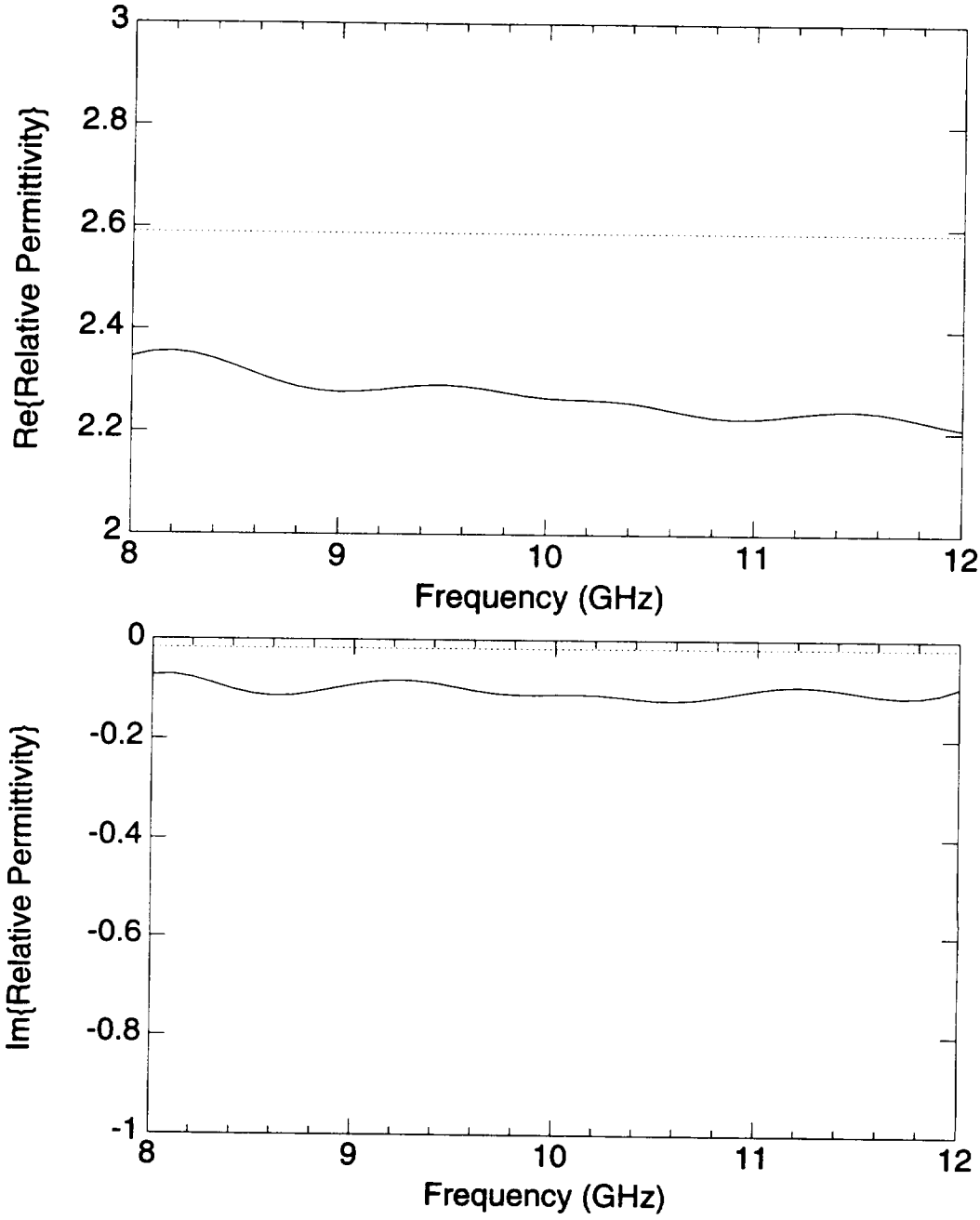

Figure 4.3: De-embedded (solid) and actual (dashed) relative permittivity of the plexiglass sample.

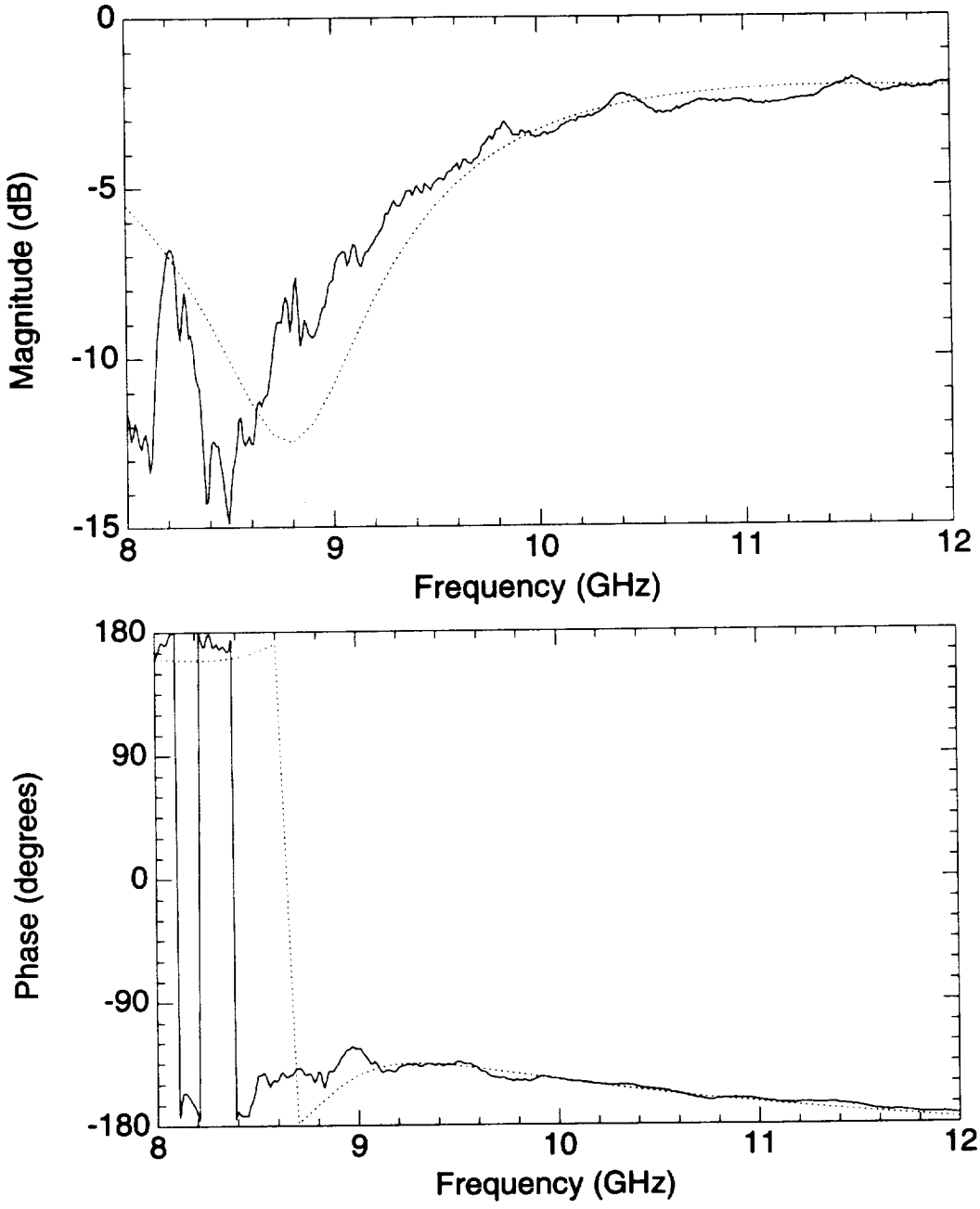

Figure 4.4: Reflection coefficient data for an X band rectangular aperture reflection measurement of an epoxy resin sheet .256 in. thick. (Raw - solid, reference - dotted.)

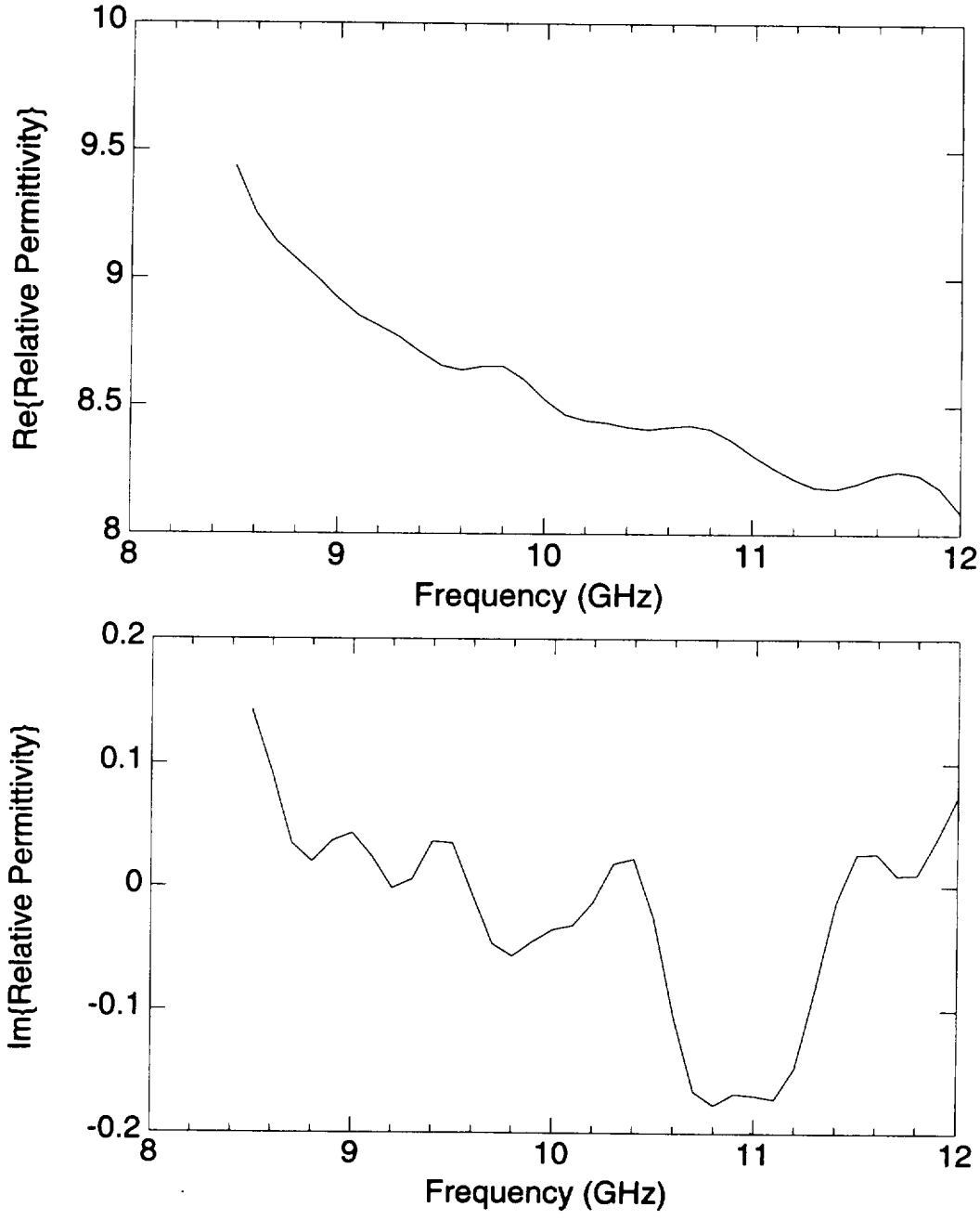

Figure 4.5: De-embedded relative permittivity of the epoxy resin sample.

Table 4.1: Material Sample Dimensions

Material	Thickness (inches)	Sides (inches)
Acrylic	0.111	9.1 x 9.1
Epoxy	0.256	4.9 x 5.0
Lossy Foam 1	0.595	12 x 14
Lossy Foam 2	0.886	12 x 14

The third example is that of the permittivity extraction from two samples of a commercially available lossy foam (anechoic chamber foam), one .595 in. thick, the other .886 in. thick. The relative permittivity of the lossy foam obtained via slotted line is approximately $\epsilon_r = 1.2 - j0.38$. This value is extrapolated from measurements between .1 to 6 GHz. Figure 4.6 shows the calibrated reflection coefficient data for the lossy foam samples and Figure 4.7 shows the permittivities extracted from the complex reflection coefficient of the lossy foam samples. Similar de-embedded permittivity values were obtained for both sample thicknesses. The average de-embedded relative permittivity is approximately 1.05 - j0.175. The discrepancy between the de-embedded and slotted line method relative permittivities is most likely due to the neglect of higher order modes.

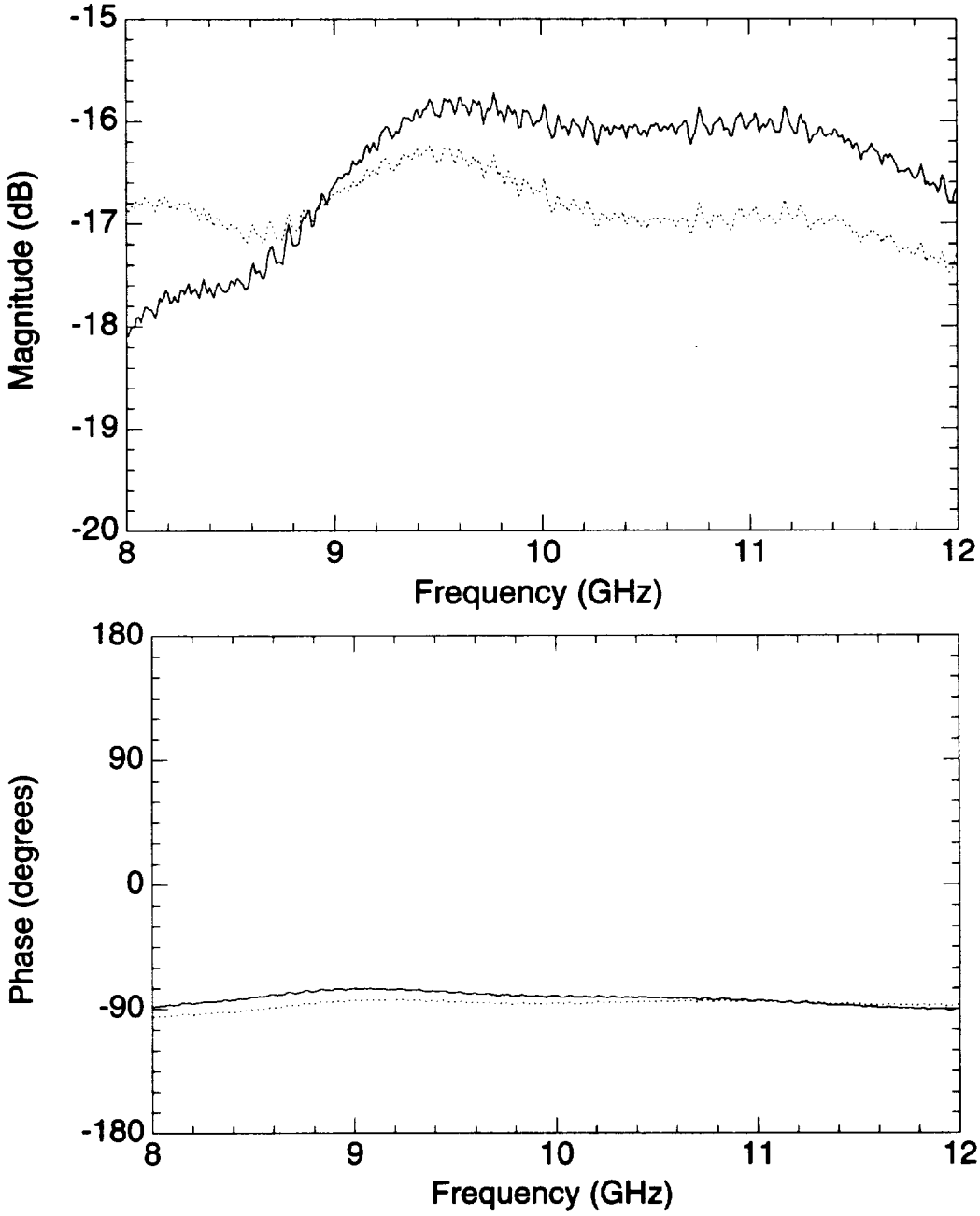

Figure 4.6: Reflection coefficient data for an X band rectangular aperture reflection measurement of lossy foam sheets. (.595 in. thick - solid, .886 in. thick - dotted.)

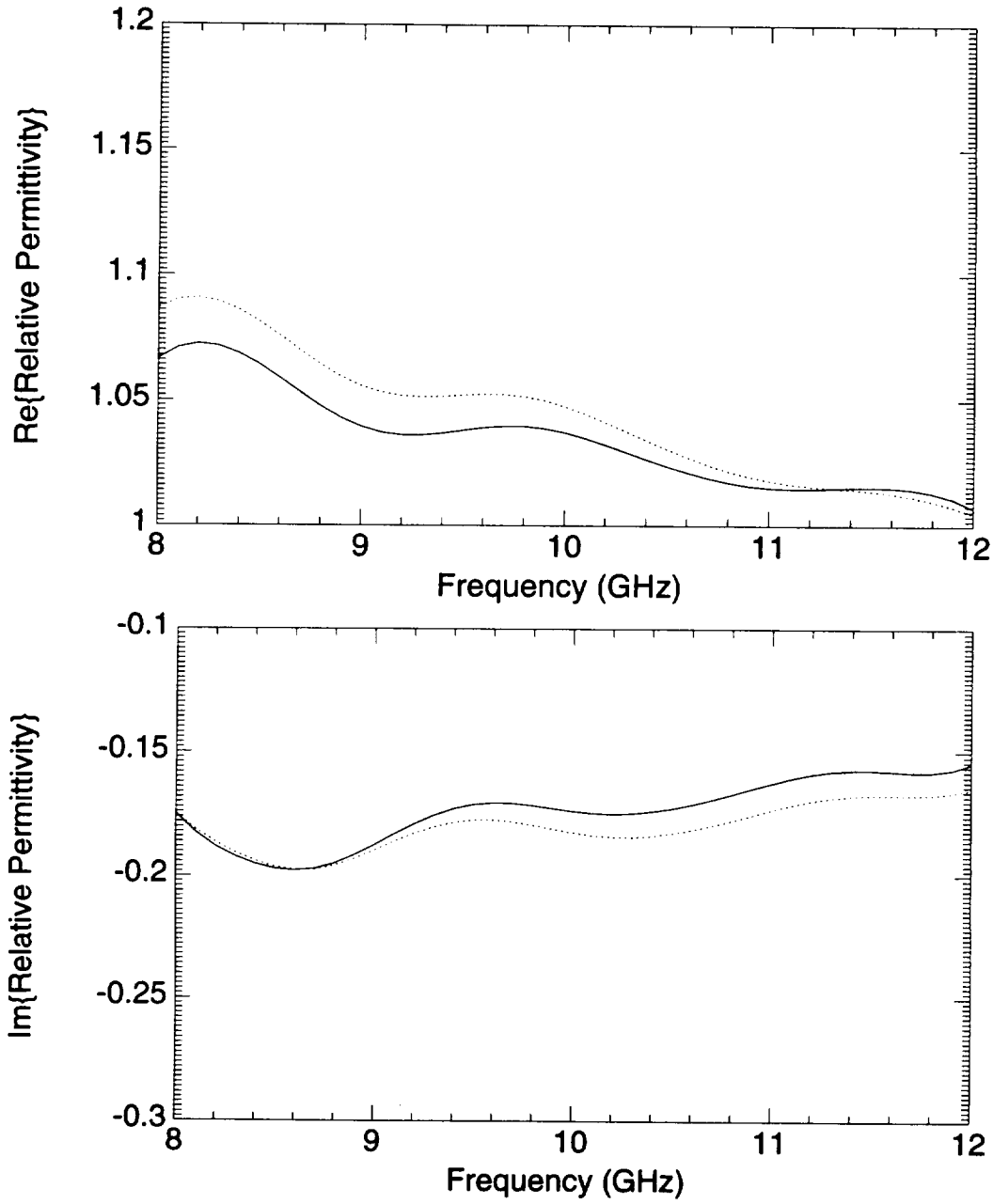

Figure 4.7: Permittivity extraction from two lossy foam sheets via X-Band rectangular aperture. (.595 in. thick - solid, .886 in. thick - dotted.)

Chapter 5

Conclusions

A variety of analytical reflection coefficient solutions were presented for material loaded rectangular apertures in an infinite groundplane. These solutions provide an analytical reference in a Newton-Raphson based technique to extract the material value from the material. The analytical solutions, for simplicity, involved only the dominate TE_{10} mode in the waveguide. The restriction limits the accuracy of the resulting extracted values. The inclusion of the higher order modes decreases the attractiveness of this general approach do to a significant computational requirement.

However, some useful material value results are still possible considering the simplicity of the Newton-Raphson technique and its non-destructive nature to planar material samples.

Bibliography

[1] H. Bussey, "Measurement of RF Properties of Material A Survey," Proceedings of the IEEE, Vol. 55, No. 6, pp. 1046-1053, June 1967.

[2] M. Afsar, J. Birch and R. Clarke, "The Measurement of the Properties of Materials," Proceedings of the IEEE, Vol. 74, No. 1, pp. 183-199, June 1986.

[3] R. Compton, "The Admittance of Aperture Antennas Radiating into Lossy Media," Report 1691-5, Antenna Laboratory, The Ohio State University, March 1964.

[4] W. Croswell, R. Rudduck and D. Hatcher, "The Admittance of a Rectangular Waveguide Radiating into a Dielectric Slab," IEEE Trans. on Antennas and Propagation, Vol. AP-15, No. 5, pp. 627-633, September 1967.

[5] R. Rudduck and C. Yu, "Circular Waveguide Method for Measuring Reflection Properties of Absorber Panels," IEEE Trans. on Antennas and Propagation, Vol. AP-22, No. 2, pp. 251-256, March 1974.

[6] S. Bakhtiari, S. Ganchev, and R. Zoughi, "Open-Ended Rectangular Waveguide for Nondestructive Thickness Measurement and Variation Detection of Lossy Dielectric Slabs Backed by a Conducting Plate,"*IEEE Transactions on Instrumentation and Measurement.*,vol. 42, pp. 19-24, February 1993.

[7] M. Decreton, and F. Gardiol, "Simple Nondestructive Method for the Measurement of Complex Permittivity,"*IEEE Transactions on Instrumentation and Measurement*,vol. 23, pp 434-438, December 1974.

[8] V. Teodoridis, T. Sphicopoulos, and F. Gardiol, "The Reflection from an Open-Ended Rectangular Waveguide Terminated by a Layered Dielectric Medium,"*IEEE Transactions on Microwave Theory and Techniques.*,vol. 33, pp. 359-366, May 1985.

[9] HP Product Note 8510-3, "Measure Dielectric Constant with the HP 8510 Network Analyzer," Hewlett-Packard Company.

[10] HP 85075A Dielectric Probe, Hewlett-Packard Company.

[11] J. Berrie and A. Dominek, "Measurement of Electrical Parameters for Planar Materials," Report No. 720946-16, ElectroScience Laboratory, The Ohio State University, January 1992; Prepared under Grant No. NAG3-1000 for the NASA Lewis Research Center, Cleveland, OH.

[12] R. Rudduck, "The Admittance of a Rectangular Waveguide Aperture Covered by a Lossless Dielectric Slab," Report 1691-22, ElectroScience Laboratory, The Ohio State University, May 1967.

[13] S. Gilmore and A. Dominek, "Electromagnetic Scattering by an Inhomogeneous Penetrable Material with an Embedded Resistive Sheet," Report No. 721929-50, ElectroScience Laboratory, The Ohio State University, August 1992; Prepared under Grant No. NSG-1613 for the NASA Langley Research Center, Hampton, VA.

[14] Moreno, T., *Microwave Transmission Design Data* , Dover Publications Inc., New York, 1958.

[15] Kuo, S., *Computer Applications of Numerical Methods* , Addison Wesley, Reading, Massachusetts, 1972.

731507-1, "Material Measurements Using Groundplane Apertures," Komisarek, Dominek and Wang, October 1995